การพัฒนาสารประกอบเบนโซพอร์ไฟรินเป็นตัวเร่งปฏิกิริยาเชิงไฟฟ้าสำหรับรีดักชันคาร์บอนไดออกไซด์

นางสาวพิชญดา จินตนาเลิศ

วิทยานิพนธ์นี้เป็นส่วนหนึ่งของการศึกษาตามหลักสูตรปริญญาวิทยาศาสตรมหาบัณฑิต
สาขาวิชาเคมี ภาควิชาเคมี
คณะวิทยาศาสตร์ จุฬาลงกรณ์มหาวิทยาลัย
ปีการศึกษา 2557

DEVELOPMENT OF BENZOPORPHYRINIC COMPOUNDS AS ELECTROCATALYSTS FOR CARBON DIOXIDE REDUCTION

Miss Pichayada Jintanalert

A Thesis Submitted in Partial Fulfillment of the Requirements
for the Degree of Master of Science Program in Chemistry
Department of Chemistry
Faculty of Science
Chulalongkorn University
Academic Year 2014

Thesis Title	DEVELOPMENT OF BENZOPORPHYRINIC COMPOUNDS AS ELECTROCATALYSTS FOR CARBON DIOXIDE REDUCTION
By	Miss Pichayada Jintanalert
Field of Study	Chemistry
Thesis Advisor	Associate Professor Patchanita Thamyongkit, Dr.rer.nat.
Thesis Co-Advisor	Dr. Parichatr Vanalabhpatana, Ph.D.

Accepted by the Faculty of Science, Chulalongkorn University in Partial Fulfillment of the Requirements for the Master's Degree

.....Dean of the Faculty of Science
(Professor Supot Hannongbua, Dr.rer.nat.)

THESIS COMMITTEE

.....Chairman
(Assistant Professor Warinthorn Chavasiri, Ph.D.)

.....Thesis Advisor
(Associate Professor Patchanita Thamyongkit, Dr.rer.nat.)

.....Thesis Co-Advisor
(Dr. Parichatr Vanalabhpatana, Ph.D.)

.....Examiner
(Assistant Professor Rojrit Rojanathanes, Ph.D.)

.....External Examiner
(Dr.Cheewita Suwanchawalit, Ph.D.)

พิชญดา จินตนาเลิศ : การพัฒนาสารประกอบเบนโซพอร์ไฟรินเป็นตัวเร่งปฏิกิริยาเชิงไฟฟ้าสำหรับรีดักชันคาร์บอนไดออกไซด์ (DEVELOPMENT OF BENZOPORPHYRINIC COMPOUNDS AS ELECTROCATALYSTS FOR CARBON DIOXIDE REDUCTION) อ.ที่ปรึกษาวิทยานิพนธ์หลัก: รศ. ดร. พัชณิตา ธรรมยงค์กิจ, อ.ที่ปรึกษาวิทยานิพนธ์ร่วม: อ. ดร. ปาริฉัตร วนลาภพัฒนา, 100 หน้า.

งานวิจัยนี้ศึกษาปฏิกิริยารีดักชันเชิงเคมีไฟฟ้าของคาร์บอนไดออกไซด์โดยใช้อนุพันธ์เบนโซพอร์ไฟรินเป็นตัวเร่งปฏิกิริยาในเชิงไฟฟ้า อนุพันธ์เบนโซพอร์ไฟรินมีหมู่เฟนิลบนตำแหน่งมีโซและเชื่อมต่อกับวงเบนซีนแบบหลอมรวมบนตำแหน่งบีต้าเพื่อขยายระบบคอนจูเกต ในงานนี้โลหะกลางสารประกอบอนุพันธ์เบนโซพอร์ไฟรินที่สนใจ คือ โคบอลต์(II), ทองแดง(II), นิกเกิล(II), ดีบุก(IV) และ สังกะสี(II) ยืนยันอนุพันธ์เบนโซพอร์ไฟรินที่สังเคราะห์ด้วยเทคนิคทางสเปกโทรสโกปี และได้ศึกษาการเร่งเชิงไฟฟ้าสำหรับรีดักชันของคาร์บอนไดออกไซด์โดยเทคนิคไซคลิกโวลแทมเมตรี การทดลองไซคลิกโวลแทมเมตรีดำเนินในภาวะที่อิ่มตัวด้วยไนโตรเจนและคาร์บอนไดออกไซด์และในภาวะที่มีและไม่มีแสงจากหลอดไฟแฮโลเจน จากผลการทดลองด้วยไซคลิกโวลแทมเมตรี ลิแกนด์อิสระของสารประกอบเบนโซพอร์ไฟรินและสารประกอบเชิงซ้อนของเบนโซพอร์ไฟรินกับโลหะมีผลต่อการเร่งปฏิกิริยารีดักชันเชิงเคมีไฟฟ้าของคาร์บอนไดออกไซด์ จากการพิจารณาจากค่าความต่างของศักย์ไฟฟ้ารีดักชันและค่ากระแสไฟฟ้าที่เพิ่มขึ้นพบว่าสารประกอบคอปเปอร์ (II) เททระเบนโซพอร์ไฟรินแสดงผลในการเร่งปฏิกิริยารีดักชันของคาร์บอนไดออกไซด์ที่ดีที่สุดโดยมีค่ากระแสไฟฟ้าที่เปลี่ยนแปลงในปฏิกิริยารีดักชันที่สองคิดเป็นร้อยละ 154 ในขณะที่สารประกอบทิน (IV) เททระเบนโซพอร์ไฟรินมีประสิทธิภาพในการเป็นตัวเร่งปฏิกิริยาน้อยที่สุดสำหรับรีดักชันของคาร์บอนไดออกไซด์

ภาควิชา เคมี	ลายมือชื่อนิสิต .....
สาขาวิชา เคมี	ลายมือชื่อ อ.ที่ปรึกษาหลัก .....
ปีการศึกษา 2557	ลายมือชื่อ อ.ที่ปรึกษาร่วม .....

5472052223 : MAJOR CHEMISTRY

KEYWORDS: TETRABENZOPORPHYRIN / REDUCTION OF CARBON DIOXIDE / CYCLIC VOLTTAMMETRY / ELECTROCATALYST

PICHAYADA JINTANALERT: DEVELOPMENT OF BENZOPORPHYRINIC COMPOUNDS AS ELECTROCATALYSTS FOR CARBON DIOXIDE REDUCTION. ADVISOR: ASSOC. PROF. PATCHANITA THAMYONGKIT, Dr.rer.nat., CO-ADVISOR: DR. PARICHATR VANALABHPATANA, Ph.D., 100 pp.

This research studies on an electrochemical reduction of carbon dioxide (CO_2) by using metallobenzoporphyrin derivatives as electrocatalysts. The benzoporphyrin derivatives have phenyl groups at meso positions and fused with benzo rings at β-positions of the pyrrolic units in order to extend the conjugated system. In this study, the central metals of the benzoporphyrin derivatives of interest are cobalt(II), copper(II), nickel(II), tin(IV) and zinc(II). The formation of the benzoporphyrin derivatives were confirmed by spectroscopic techniques and their electrocatalytic activity for the reduction of CO_2 was studied by means of cyclic voltammetry. The cyclic voltammetric experiments were performed under saturated nitrogen and saturated CO_2 conditions, and with and without radiation by a tungsten-halogen lamp. Based on cyclic voltammatric results, free base and the metallated benzoporphyrin derivatives exhibited catalytic effect on electrochemical reduction of CO_2. Considering the reduction potential and the current enhancement, it was found that copper(II)-tetraphenyltetrabenzoporphyrin exhibited the highest catalytic activity with the current enhancement at the second reduction of 154%, while tin(IV)-tetraphenyltetrabenzoporphyrin showed the least catalytic activity for the reduction of CO_2.

Department:	Chemistry	Student's Signature	.....
Field of Study:	Chemistry	Advisor's Signature	.....
Academic Year:	2014	Co-Advisor's Signature	.....

ACKNOWLEDGEMENTS

I would like to begin by thanking Associate Professor Dr. Patchanita Thamyongkit and Dr. Parichatr Vanalabhpatana for being the best advisors anyone could ever ask for. There are no words that can express the depth of gratitude that I have toward them. They have supported me in everything that I set out to improve the synthetic and the electrochemical skills, believe in me even at the moment of my life when I was down and help me to get back on my feet.

I am also grateful to Assistant Professor Dr. Warinthorn Chavasiri, for serving as the chairman, Assistant Professor Dr. Rojrit Rojanathanes and Dr. Cheewita Suwanchawarit for serving as the members of my thesis committee, respectively, for their valuable suggestion and comments.

I would like to thank the 90th Anniversary of Chulalongkorn University Fund (Ratchadaphiseksomphot Endowment Fund) and Graduate School of Chulalongkorn university for partial financial support of this research.

Finally, I am grateful to my family and my friends for their love, understanding and great encouragement throughout the entire course of my study.

CONTENTS

Page

Page

LIST OF FIGURES

Page

Page

Page

Page

Page

Page

LIST OF TABLES

Page

LIST OF SCHEMES

Page

LIST OF ABBREVIATIONS

^{o}C	: degree Celcius
calcd	: calculated
$CDCl_3$	: deuterated chloroform
CO_2	: carbon dioxide
^{13}C-NMR	: carbon nuclear magnetic resonance spectroscopy
d	: day(s)
DMF	: *N*,*N*'-dimethylformamide
d	: doublet (NMR)
dd	: doublet of doublet (NMR)
ESI-HRMS	: electrospray ionization-high resolution mass spectrometry
equiv	: equivalent(s)
g	: gram(s)
h	: hour(s)
^{1}H-NMR	: proton nuclear magnetic resonance spectroscopy
J	: coupling constant
m/z	: mass per charge ratio
MALDI-MS	: matrix-assisted laser desorption ionization-mass spectrometry
MeOH	: methanol
CH_2Cl_2	: methylene chloride
ε	: molar absorptivity
m	: multiplet (NMR)
mmol	: millimole(s)

mg	: milligram(s)
mV	: millivolt(s)
MHz	: megahertz(s)
mL	: milliliter(s)
nm	: nanometer(s)
N_2	: nitrogen
obsd	: observed
ppm	: part per million
rt	: room temperature
s	: singlet (NMR)
s	: second(s)
t	: triplet (NMR)
$TBAPF_6$	: tetrabutylammonium hexafluorophosphate
TEA	: triethylamine
THF	: tetrahydrofuran
vs.	: versus
UV-Vis	: ultraviolet and visible spectroscopy
λ	: wavelength
λ_{ex}	: excitation wavelength
λ_{abs}	: absorption wavelength
λ_{em}	: emission wavelength
μA	: microampere(s)
WE	: working electrode
RE	: reference electrode

CE	: counter electrode
Ag/AgCl	: silver/silver chloride
Ag/Ag^{+}	: silver/silver ion
SCE	: saturated calomel electrode

CHAPTER I

INTRODUCTION

In the recent years, the increase of carbon dioxide (CO_2) in the atmosphere has become a global environmental problem. The current global energy supply is mainly based on fossil fuels like coal, oil and gas [1]. In addition, the combustion of fossil fuels leads to the emission of CO_2 [2]. The electroreduction of CO_2 can give several useful products such as formic acid, formaldehyde, methanol, and methane [3]. For the electrochemical reduction of CO_2 reaction pathways also generate the various products which have the potential values as shown in below:

$CO_2 + 2H^+ + 2e^- \rightarrow HCOOH$ $\quad E^0 = -0.61$ V

$CO_2 + 2H^+ + 2e^- \rightarrow CO + H_2O$ $\quad E^0 = -0.52$ V

$CO_2 + 4H^+ + 4e^- \rightarrow HCHO + H_2O$ $\quad E^0 = -0.48$ V

$CO_2 + 6H^+ + 6e^- \rightarrow CH_3OH + H_2O$ $\quad E^0 = -0.38$ V

$CO_2 + 8H^+ + 8e^- \rightarrow CH_4 + 2H_2O$ $\quad E^\circ = -0.24$ V

Among all organic electrocatalysts, porphyrinic compounds have been in spotlight in recent years as photoactive compounds for optoelectronic applications [4] due to their extremely high absorption coefficients [5], high thermal and photostablities [6]. Moreover, their electrochemical and photophysical properties can be varied by changing the metal center and substituents at the macrocycle peripheral position [7]. Certain transition metal complexes act as electron transfer mediators for photochemical and electrochemical reduction of CO_2 as means of energy storages [selected publications: [8-10]**]**. Grodkowski *et al.* reported that Fe(III)-phthalocyanines and Co(II)-phthalocyanines exhibited electrocatalysis for the reduction of CO_2. Catalytic formation of CO and formate was confirmed by photochemical, and radiation chemical methods [11]. Hammouche *et al.* reported that iron and Co(II)-porphyrins are effective homogeneous catalysts for the electrochemical reduction of CO_2 to CO and formic acid [12]. However, the previous researches showed that the porphyrin derivatives exhibited moderate catalytic activity in reduction of CO_2. Tetrabenzoporphyrins are another interesting group of porphyrin derivatives as in these macracycles, the combination of electronic and structural factors, such as an extension of the π-system, *meso*-substitution, and highly distorted

macrocycle core, cause a red shift and intensification of the Q-band absorption, compared with other porphyrins [13]. These compounds have been found a diverse array of applications in various fields, photodynamic therapy [14] and optoelectronic devices [15]. The structures of porphyrin and benzoporphyrin are shown in **Figure 1–1**.

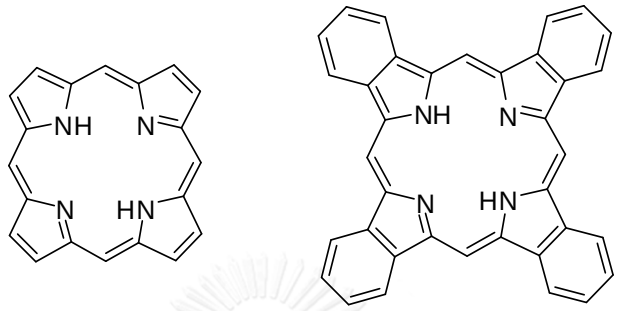

Figure 1–1: Structures of porphyrin and tetrabenzoporphyrin

In this work, metal-free and metal tetraphenyltetrabenzoporphyrins were synthesized, characterized and investigated their potential use as electrocatalysts for reduction of CO_2. The catalytic efficiency in reduction of CO_2 of all target molecules were compared. We hypothesize that there compounds will exhibit a good catalytic activity of reduction of CO_2. Moreover, metallation of tetraphenyltetrabenzoporphyrin with various central metals are expected to catalytically promote the electrochemical reduction of CO_2.

1.1 Objective of Research

The objective of this research is to synthesize metal-free and metal benzoporphyrin derivatives. The efficiency of electrocatalalytic activity in the reduction of CO_2 of each compound are studied by means of cyclic voltammetry under the N_2 saturated and CO_2 saturated condition in ambient light and under radiation.

1.2 Scope of Research

The scope of this research covers the synthesis of metallobenzoporphyrin derivatives bearing the phenyl *meso*-substituents and various central metals *i.e.*, copper (Cu(II)), cobalt (Co(II)), nickel (Ni(II)), tin (Sn(IV)) or zinc (Zn(II)) as shown in **Figure 1–2**. Free base benzoporphyrin will be also investigated to determine the catalytic activity for reduction of CO_2 of the benzoporphyrin ligand and to study the

effect of the central metal on the catalytic efficiency. All compounds will be fully characterized by spectroscopic techniques, *i.e.*, mass spectrometry, and ^{1}H-NMR and ^{13}C-NMR spectroscopy. Photophysical properties were investigated by UV-Vis spectrophotometry and fluorescent spectrophotometry. Electrochemical studies of benzoporphyric compounds were investigated by cyclic voltammetry. The catalytic activity of each compounds are compared to reach out the best electrocatalyst for the reduction of CO_2.

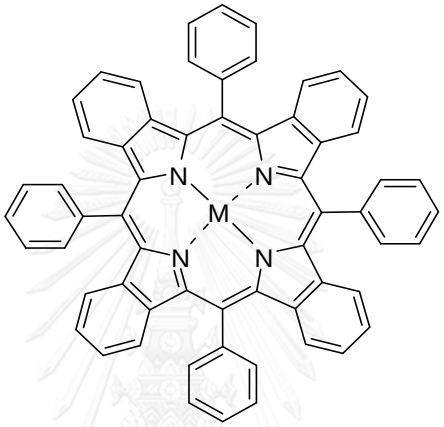

M = H, H (**1**), Co(**Co-1**), Cu (**Cu-1**),
Ni (**Ni-1**), $Sn(OH)_2$ (**$Sn(OH)_2$-1**) and Zn (**Zn-1**)

Figure 1–2: General structure of the target metallobenzoporphyrinic derivatives

CHAPTER II
THEORY AND LITERATURE REVIEWS

2.1 Porphyrins

The Greek word of porphyrin called '*porphura'* meaning purple [13]. Porphyrins (without any substituent, called porphine) and its derivatives consist of four pyrrole rings joined by four interpyrrolic methane bridges to give a highly conjugated macrocycle. The structure of porphine is shown in **Figure 2–1** [16].

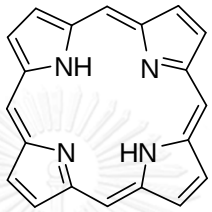

Figure 2–1: The structure of porphyrin (porphine)

The aromaticity of porphyrins has been well known both by its chemical and physical properties. These tetrapyrrolic systems have a closed loop of edgewise overlapping *p*-orbitals which interact favorably to stabilize the olefins: the 22π-electrons inside the porphyrin macrocycle, only 18 electrons are found to actually participate in delocalization pathway, which is consistent with Hückel's [4n+2] rule for aromaticity, where n = 4 [selected publications: [17, 18]]. A free base porphyrin in which metal is inserted in its cavity is called *metalloporphyrin*. Several metalloporphyrins play important roles in many biological systems, for example, magnesium complexes in chlorophylls found in green plants serve as photosynthetic reaction centers which convert light energy into chemical reaction [19], and iron complexes are found in heme B and cytochrome C which are responsible for oxygen transport and a single electron transporter in a redox catalytic reaction, respectively [20]. Porphyrin and their derivatives are highly colored absorbing strongly in the visible region near 400 nm (molar extinction coefficients are about 10^5 $Mol^{-1}{\cdot}L$) also known as Soret band or B-band and several weaker absorption bands known as Q-band between 450–700 nm as shown in **Figure 2–2** [21]. A variation in the peripheral substituents of the porphyrin ring normally results in change in the intensity and wavelength of the absorption bands. The disruption of porphyrin

macrocycles affects to Soret band disappearance [22]. The absorbance energy intensities vary with chelation, pH, and differences in the structure of peripheral substituents. However, as long as the main 18π electron conjugation system still exists, the Soret band is the major characteristic band of the absorption spectra [23].

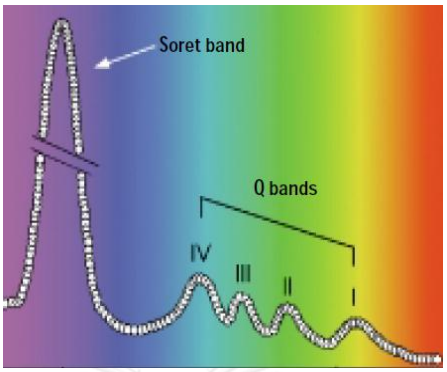

Figure 2–2: Typical UV-Vis absorption spectrum of the porphyrin derivatives

2.2 Structural Modifications of Porphyrins

In the recent years, several kinds of porphyrins have been investigated for their electrochemical properties. The main objectives of the structural modification of the porphyrin are listed below:

1) To adjust the physical properties (*e.g.* solubility and chemical, thermal, and electrical stability)

2) To develop photophysical (*e.g.* absorption and emission wavelength) and electrochemical properties (*e.g.* redox potentials)

The substituents can be inserted at the *meso* and *beta* positions of the porphyrin ring as shown in **Figure 2–3**.

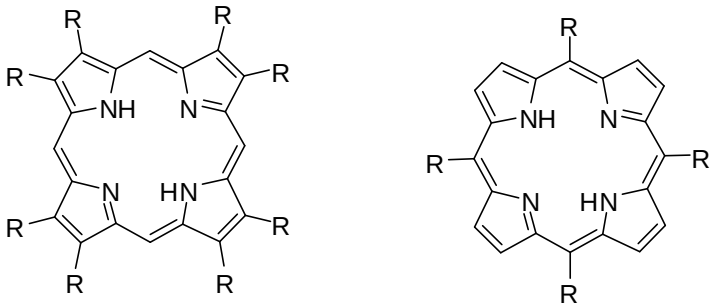

β-substituted porphyrin *meso*-substituted porphyrin

Figure 2–3: Structures of β- and *meso*-substituted porphyrins

Moreover, the structural modification of the porphyrins can be achieved by the coordination of various metal ions at the center of macrocycle. The pyrrole nitrogen groups enable the N-metal σ-bond formation as shown in **Figure 2–4**.

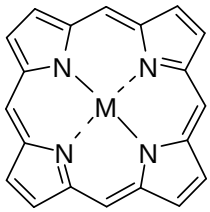

Figure 2–4: Structure of metalloporphyrin

2.3 Uses and Applications of Porphyrin Derivatives

There are a lot of interesting applications of porphyrins in chemical, biochemical and biomedical research, for example:

1) Optoelectronic devices such as solar cells [selected publications: [24-26]]

2) Organic light emitting diodes [selected publications: [27-29]]

3) Dyes for food, cloth and printing [selected publications: [30-32]]

4) Electrochemistry and photocatalysts [selected publications: [33-35]]

5) Optical sensors [selected publications: [36-38]]

6) Photodynamic therapy [selected publications: [39-41]]

2.4 Benzoporphyrins

Tetrabenzoporphyrin (TBP) is one of the most well-known porphyrin derivatives that have aromatic subunits fused directly onto the β-substituted position of porphyrin as shown in **Figure 1–1**. In 1966, tetrabenzoporphyrins were discovered in some petroleum and related deposit [42]. Benzoporphyrins have interesting physical, chemical and spectroscopic properties that are significantly different from porphyrins. Because of the larger conjugation system, Benzoporphyrins are more chemically stable than porphyrin and perform a red shift in absorption and emission spectra to the infrared region that is commonly useful for biomedical applications such as photodynamic therapy [selected publications: [14, 43, 44]]. Moreover, tetrabenzoporphyrins can also be used as electrocatalysts [45], nonlinear optical materials [46] and photovoltaic cells [selected publications: [47-49]].

2.5 Electrochemical Techniques [50]

Electrochemical techniques are concerned with the interplay between electricity and chemistry. These methods deal with the measurements of electrical quantities such as current, potential and charge related to chemical parameters. Electrochemical methods have some general advantages over other types of analytical techniques. Firstly, electrochemical measurements are often specific for a particular oxidation state of an element. Secondly, the instrument of electrochemical methods is relatively inexpensive. Thirdly, the method is simple and does not require highly skillful analysts. Noteworthy, the features of electrochemical methods provide information about activities rather than concentrations of species.

2.5.1 Electrochemical Cells [50]

Three-electrode cell as shown in **Figure 2–5** is commonly used in voltammetric measurements. The cell is usually a covered beaker of 5–50 mL volume and contains three electrodes, working, reference, and counter electrodes, which are immersed in the sample solution. While the working electrode (WE) (such as glassy carbon) is the electrode at which the reaction of interest occurs, the reference electrode (RE) provides a stable and reproducible potential, against which the potential of the WE is compared. The commonly used silver/silver chloride (Ag/AgCl) serves as reference electrodes for the experiments in aqueous solution. For non-aqueous condition, silver/silver ion (Ag/Ag+) in acetonitrile, *N,N'*dimethylformamide (DMF) or dimethyl sulfoxide (DMSO) is widely used. To minimize contamination of the sample solution, the RE may be insulated from the sample through a salt bridge. The counter electrode (CE) is an electrode which an electrical current is expected to flow. The CE is usually inert conducting material such as platinum wire or graphite rod. The complete system, integrating the three-electrode cell and built-in gas control, is available commercially available.

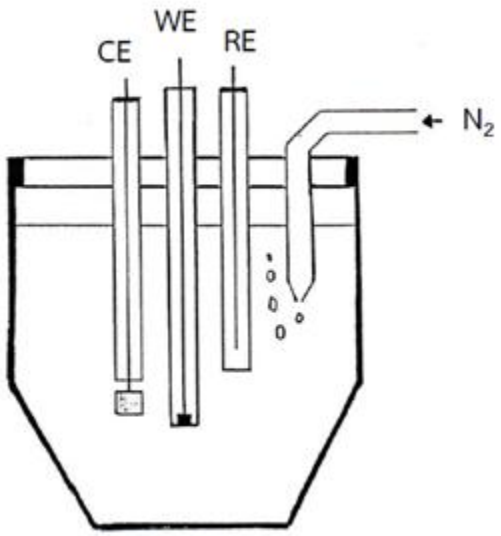

Figure 2–5: Cell for voltammetric measurements: working electrode (WE); reference electrode (RE); and counter electrode (CE). Electrodes and gas bubbling tube are inserted through holes in the cell cover [51]

2.5.2 Solvents and Supporting Electrolytes [52]

Electrochemical measurements are commonly carried out in a medium that consists of solvent containing a supporting electrolyte. The choice of the solvent is primarily dictated by the solubility of the analyte and its redox activity and by solvent properties such as the electrical conductivity, electrochemical activity and chemical reactivity. The solvent should not react with the analyte and should not undergo electrochemical reactions over a wide potential range. While water has been used as a solvent more than any other media, non-aqueous solvent (*e.g.*, acetonitrile, DMF, dichloromethane or DMSO) has also frequently been used. Mixed solvents may also be considered for certain applications.

Supporting electrolytes are required in electrochemical experiments to decrease the resistance of the solution, to eliminate migration effect and to maintain a constant ionic strength. The inert supporting electrolyte may be an inorganic salt, a mineral acid or a buffer. While potassium chloride, sodium hydroxide or hydrochloric acid is widely used when using water as a solvent, tetraalkylammonium salts are often employed in organic media. Buffer system (such as acetate, phosphate or citrate buffer solution) is used when pH control is essential. The supporting electrolyte should be prepared from highly purified reagent, and should not be easily

oxidized or reduced. The usual electrolyte concentration range is 0.1–1.0 M, in other case, in large excess of the concentration of all electroactive species.

2.6 Cyclic Voltammetry [52]

Cyclic voltammetry is one of the most commonly used electrochemical techniques to probe the electrocatalytic ability of the analyte since it can give both the qualitative and quantitative information about the analyte electrochemical reactions. Cyclic voltammetry consists of the linearity of scanning potential with a triangular waveform, sweeping through a potential range and reversing the direction of the sweep in a cyclic wave (**Figure 2–6**). The resulting plot of the current *vs*. the applied potential is called a cyclic voltammogram. Note that the scan direction may be either in the positive or negative direction, depending on whether a reductive or oxidative process is studied. The potential is measured between the RE and the WE whereas the current is measured between the WE and the CE. For this waveform in **Figure 2–6**, the forward scan produces a cathodic current for any analyte that can be reduced through the range of the scanned potential. On the contrary, the reverse scan yields an anodic current for the product of the forward scan being reoxidized. Thus, there are reduction and oxidation peaks observed for a reversible reaction as shown in **Figure 2.7**. Significant parameters in a cyclic voltammogram are cathodic peak potential (E_{pc}), anodic peak potential (E_{pa}), cathodic peak current (i_{pc}) and anodic peak current (i_{pa}).

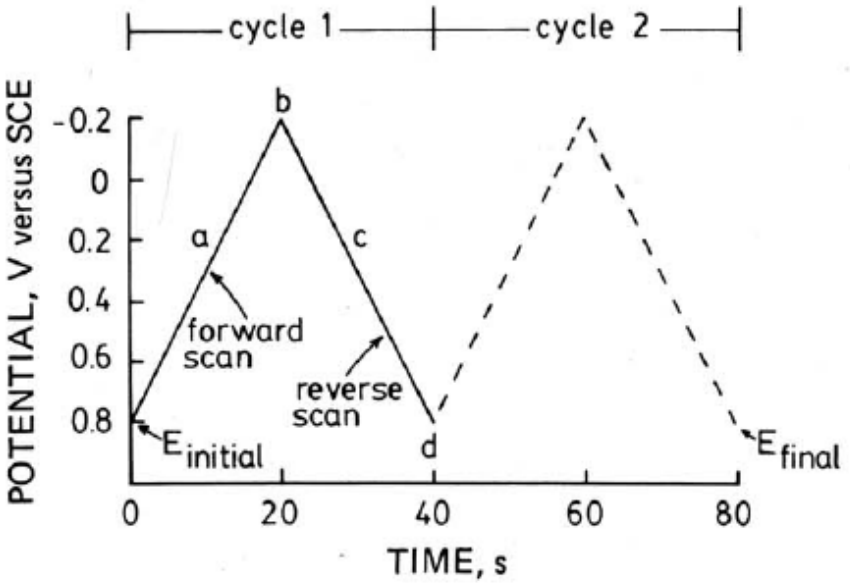

Figure 2–6: Typical waveform for cyclic voltammetry [52]

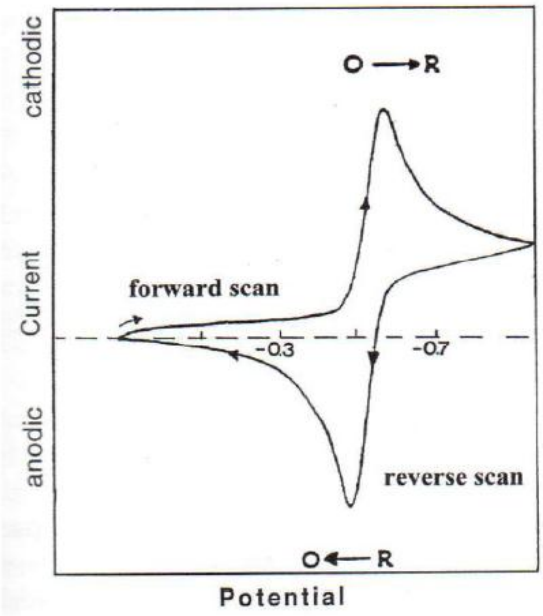

Figure 2–7: Typical cyclic voltammogram for a reversible redox couple [51]

Figure 2–7 illustrates the expected response of a reversible redox couple during a single potential cycle. It is assumed that only the oxidized form from oxidation is present initially. Thus, a negative-going potential scan is chosen for the first half cycle, starting from a value where no reduction occurs. As the applied potential approaches the character of E^0 for the redox process, a cathodic current

begins to increase until a peak is reached. After traversing the potential region in which the reduction process takes place (at least 90/*n* mV beyond the peak), the direction of the potential sweep is reversed. During the reverse scan, the reduction form (generated in the forward half-cycle and accumulated near electrode surface) is reoxidized back *via* oxidation, resulting in an anodic current.

2.6.1 Types of Cyclic Voltammograms [52]

Cyclic voltammograms can be classified as reversible, quasireversible and irreversible voltammograms depending on the nature of the electrochemical reactions of electroactive species.

1) Reversible Cyclic Voltammograms

Reversible cyclic voltammograms can be obtained when the oxidized or reduced species are reduced or oxidized, respectively, back to the starting species in the reverse scan. This is represented by the forward wave which is followed by a corresponding reverse wave upon changing the scan direction.

2) Irreversible Cyclic Voltammograms

Irreversible cyclic voltammograms are often characterized by a single oxidation or reduction wave without reverse wave, indicating non-regeneration of the starting electroactive species. This may arise from the formation of an electroinactive reduction or oxidation product in the forward scan.

3) Quasireversible Cyclic Voltammograms

For the quasireversible reactions, the current is controlled by both mass transport and charge transfer, the standard rate constant of kinetic parameter (k^0) in the range of 10^{-5} and 10^{-1} cm·s^{-1}. In general, quasireversible voltammograms are more extended and exhibit a large peak potential separation, ΔE_p, compared to those reversible systems. For quasireversible reactions, peak current (i_p) is not proportional to the square root of the scan rate.

2.7 Electrocatalysis [53]

The redox reactions of organic compounds are frequently limited by slow kinetics, thus high overpotentials are required to proceed the redox reactions at the reasonable rates. To solve this problem, a catalyst can be used to provide an

alternative reaction pathway, allowing the reaction to occur close to the reversible potential with the increased current density.

A catalyst is a substance that increases the rates of the chemical reactions, without itself undergoing any chemical change. This means that a catalyst enters as a reactant, undergoes chemical transformation, but it is ultimately regenerated so that its concentration remains undiminished. Therefore, it is apparent that a catalyst can only increase the rate of a process which is thermodynamically feasible. A catalyst may participate in multiple chemical transformations. Substances that increase the reaction rates are called positive catalysts. Substances that interact with catalysts to slow the reaction are called inhibitors (or negative catalysts). Substances that increase the activity of catalysts are called promoters and substances that deactivate catalysts are called catalytic poisons.

There are two modes of catalysts in the electrochemical reactions: heterogeneous and homogeneous catalysts [54].

2.7.1 Heterogeneous Catalyst [55]

A heterogeneous catalyst has in a different phase as the reactants. Typically heterogeneous electrocatalysts involve a solid catalyst with the reactants as either liquid or gaseous. The reactants are adsorbed on to a surface of the catalyst at active sites, *via* the formation of chemical bonds. After the reaction, the product molecules are desorbed from the surface area and break away. This leaves the active site for a new reactant molecule to attach and react. Frequently, the transport of reactants and products from one phase to another plays a dominant role in limiting the reaction rate. For solid heterogeneous catalysts, an active site is a part of surface which is particularly good at adsorbing things and helping them to react. The catalysts with large surface area such as mesoporous silicates, having the surface areas of 1000 $m^2 \cdot g^{-1}$, are widely used. Alternatively, the catalyst is dispersed on a second material that enhances the effectiveness or minimizes their cost. Frequently, the interaction between support and the catalyst affects to the catalytic reaction. Generally porous materials, such as alumina or various kind of carbon, were used as the supports because of the high surface area.

2.7.2 Homogeneous Catalyst [56]

In homogeneous catalysis, the catalyst and the substrate for a reaction are brought together in one phase, most often the liquid phase. Examples of homogeneous catalysis involve the influence of hydrogen on the esterification of ester, e.g. methyl acetate from acetic acid and methanol.

2.8 Electrochemical Reduction of Carbon Dioxide

The electrochemical reduction of CO_2 has attracted considerable attention as a possible source of carbon for the synthesis of organic molecules and possible means of energy storage by considering its products. CO_2 is a low energy molecule and its electrochemical reduction into anion radical requires a quite negative potential. The electrocatalysts for the reduction of CO_2 can convert CO_2 to several useful products such as formic acid, formaldehyde, methanol, and methane. The electrochemical reduction of CO_2 reaction pathways can produce the variety products on the potential values as shown in the equations on page 2 [57]. The nature of the reduction products has a strong efficiency on thermodynamic accessibility form CO_2. Particularly important factor is the number of electrons involved in the reduction processes. The redox potentials become less and less negative as the reaction involves multielectronic pathways. However, the monoelectron reduction mechanism of $CO_2/CO_2^{-}\cdot$ requires –2.21 V *vs.* SCE, which is a highly critical value [selected publications: [58, 59]].

The reaction products pathways comprise a mixture of various substances. Moreover, the reduction of CO_2 in aqueous solutions in the cathodic potential region is always accompanied by hydrogen evolution. Hence, an important criterion that describes the reaction selectivity is the Faradaic field (η_k) for each individual k^{th} organic reaction product [60].

Behar, D. *et al.* [61] studied the electrocatalytic reduction of CO_2 by cyclic voltammetry. Co(II)-porphyrin was reduced to Co(I)-porphyrin and Co(0)-porphyrin by radiation-chemical, photochemical and electrochemical methods in aqueous and organic solvent. One-electron reduction of Co(I)-porphyrin leads to the formation of a species that is observed as a transient intermediate by pulse radiolysis in aqueous solutions and as a stable product following the reduction by sodium in tetrahydrofuran solutions. The products were found to be CO and formate ion which were confirmed

by cyclic voltammetric experiments in acetonitrile and butyronitrile solvent containing triethylamine as a reductive quencher. The product was determined by gas chromatography (GC).

Neta, P. *et al.* [11] studied the electrocatalytic reduction of CO_2 to CO by Fe(III)-porphyrins in the presence of homogeneous catalysts. The porphyrin structures were derived from spectrophotometric measurements and the formation of CO was confirmed by GC. The studies showed that Fe(III)-porphyrins were reduced by photoreduction in the presence of CO_2 to stable Fe(II)-porphyrins products and then to Fe(I)-porphyrins in organic solvents and in aqueous solutions. Fe(II)-porphyrins are readily reduced to $[\text{Fe-porphyrin}]^-$, which does not react with CO_2. The species that reduced CO_2 to CO was Fe(0)-porphyrins. The yield of free CO increases with time of photolysis and reaches turnover numbers of 70 molecules of CO per porphyrin molecule.

Wang, Z. *et al.* [35] studied photocatalysis of nanotubes containing a Sn(IV)-porphyrins. The results showed that the nanotubes containing Sn(IV)-porphyrin can reduce the metal ion in Au(I) thiourea or thiosulfate in the presence of ascorbic acid as an electron donor (ED). Cyclic reaction of photocatalytic reduction of Au(I) complex is shown below:

$$\text{SnP} + h\nu \rightarrow \text{SnP}^*$$

$$\text{SnP}^* + \text{ED} \rightarrow \text{SnP}^{\cdot -} + \text{ED}_{ox}$$

$$\text{SnP}^{\cdot -} + \text{Au}^+ \rightarrow \text{SnP} + \text{Au}^o$$

Sonoyama, N. *et al.* [62] described the catalytic activity of metallated *meso*-tetraphenylporphyrin (M-TPP) supported on gas diffusion electrodes (GDEs) for electrochemical reduction of CO_2. Co(II)-TPP and Fe(III)-TPPCl showed high activity for electrochemical reaction of CO_2, Cu(II)-TPP and Zn(II)-TPP exhibited moderate activity, and H_2TPP gave catalytic activity for reduction of CO_2. CO can be observed as a main product, except that the Cu(II)-TPP catalyst gave formic acid as main product. According to high performance liquid chromatography (HPLC) technique, the reduction of CO_2 was preceded *via* electron transfer from TPP ring that was reduced, and its central metals served as the adsorption sites of CO_2.

Hammouche, M. *et al.* [63] studied that homogenous catalysis for the electrochemical reduction of CO_2 was reduced Fe(0)-porphyrins. The Fe(III)-porphyrins alone showed three reversible waves corresponding to the following redox couple; $Fe(III)^{+}/Fe(II)$, $Fe(II)/Fe(I)^{-}$ and $Fe(I)^{-}/Fe(0)$. When CO_2 was present, the current was increased in height and the reduction process become irreversible. The main product observed was CO by GC technique.

Ramirez, G. *et al.* [64] studied a supramolecular electrode made of stacked Co(II)-tetrabenzoporphyrin. The stack was held together by π–π interactions and the first layer of the porphyrin complex was anchored to the glassy carbon surface through a porphyrin 4-aminopyridine group. The electrode formed by Co(II)-tetrabenzoporphyrin adsorbed on the glassy carbon surface was inactive towards the reduction of CO_2. Moreover, a home-made photoreactor designed for this study is shown in **Figure 2–8**. The remaining of Co(II)-tetrabenzoporphyrin catalyst on the supramolecular electrode could be detected before and after reaction by atomic force microscopy and electrochemical impedance spectroscopy. Based on GC, the main product was found to be CO.

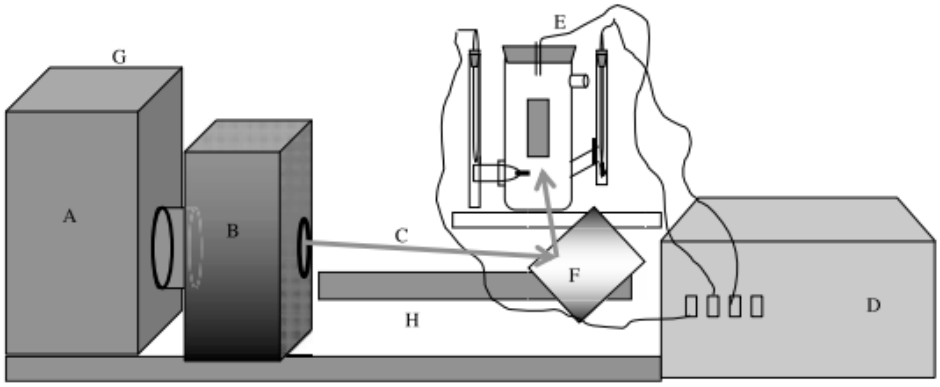

Figure 2–8: Ramirez's home-made photoreactor consisting of (A) halogen lamp (in it black box), (B) monochromator, (C) light beam, (D) potentiostat, (E) electrochemical cell, (F) mirror, (G) position of PC-cooling fan and (H) optical line.

CHAPTER III
EXPERIMENTAL

3.1 Chemicals

All chemicals were purchased from commercial sources and used as received without further purification, unless noted otherwise.

Benzaldehyde (C_6H_5CHO) : Merck

Boron trifluoride diethyletherate ($BF_3 \cdot Et_2O$) : Fluka

Cobalt acetate tetrahydrate ($Co(OAc)_2 \cdot 4H_2O$) : Sigma-Aldrich

Copper acetate monohydrate ($Cu(OAc)_2 \cdot H_2O$) : Sigma-Aldrich

Deuterated chloroform ($CDCl_3$) : Cambridge isotope

Chloroform ($CHCl_3$) : RCI Lab-scan

1,8-Diazabicyclo[5,4,0]undec-7-ene (DBU) : Sigma-Aldrich

2,3-Dichloro-5,6-dicyano-1,4-benzoquinone (DDQ): Sigma-Aldrich

Diethyl ether : Merck

N,*N*-Dimethylformamide (DMF) : RCI Lab-scan

Ethyl isocyanoacetate ($C_2H_5OCOCH_2CN$) : Sigma-Aldrich

Ethylene glycol ($HOCH_2CH_2OH$) : Merck

Hexane : Distilled from commercial grade

Hydrochloric acid (HCl) : Merck

Anhydrous magnesium sulfate ($MgSO_4$) : Merck

Methanol (CH_3OH) : Distilled from commercial grade

Methylene chloride (CH_2Cl_2) : Distilled from commercial grade

Nickel acetate tetrahydrate ($Ni(OAc)_2 \cdot 4H_2O$) : Sigma-Aldrich

1-Nitrocyclohexene : Sigma-Aldrich

Potassium hydroxide (KOH) : Merck

Silica gel 60 particle size : Merck

Anhydrous sodium sulfate (Na_2SO_4) : Merck

Sodium sulfite (Na_2SO_3) : Merck

Sodium hydrogencarbonate ($NaHCO_3$) : Merck

Sodium chloride (NaCl)	: Merck
Sulfuric acid (H_2SO_4)	: Merck
Tin chloride dihydrate ($SnCl_2 \cdot 2H_2O$)	: Sigma-Aldrich
Tetrabutylammonium hexafluorophosphate ($TBAPF_6$)	: Sigma-Aldrich
Tetrahydrofuran (THF)	: RCI Lab-scan
Toluene	: RCI Lab-scan
Triethylamine (TEA)	: Fluka
Zinc acetate dihydrate ($Zn(OAc)_2 \cdot 2H_2O$)	: Merck

3.2 Analytical Instruments

Proton nuclear magnetic resonance spectroscopic (^{1}H-NMR) and carbon-13 nuclear magnetic resonance spectroscopic (^{13}C-NMR) spectra were obtained in $CDCl_3$ at 400 MHz for ^{1}H nuclei and 100 MHz for ^{13}C nuclei (Varian Company, USA). Chemical shift were reported in parts per million (ppm) relative to the residual $CHCl_3$ peak (7.26 ppm for ^{1}H-NMR and 77.0 ppm for ^{13}C-NMR). Coupling constant (*J*) are reported in Hertz (Hz). Mass spectra were obtained using high resolution electrospray ionization (HR-ESI), and matrix-assisted laser desorption ionization (MALDI) mass spectrometry with dithranol as a matrix. Absorption spectra were recorded in toluene by a Hewlett-Packard 8453 spectrophotometer and absorption extinction coefficient (ε) were reported in $L \cdot (mol \cdot cm)^{-1}$. Fluorescence spectra were measured in toluene using a Perkin-Elmer LS45 luminescence spectrophotometer. Cyclic voltammograms were recorded with a potentiostat/galvanostat (Autolab PGSTAT101, Eco Chemie, The Netherlands) at room temperature. A conventional three-electrode system consisting of a glassy carbon electrode (BAS, USA) as a working electrode, a platinum wire as a counter electrode, and a silver/silver ion (Ag/Ag^+) in acetonitrile served as a reference electrodes was applied. The Ag/Ag^+ electrode have a potential of +0.296 V *vs.* saturated calomel electrode (SCE) at 25°C [65]. A schematic setup of an electrochemical cell for cyclic voltammetric measurement is shown in **Figure 3–1** [52]. Prior to use the glassy carbon electrode was polished with an aqueous suspension of alumina powder and rinsed with milli-Q water. The light source of this research was a tungsten-halogen lamp at 75 Watt giving a light wavelength in a range

between 400–1000 nm [66]. The distance from the light source to the experiment set up was 70 cm

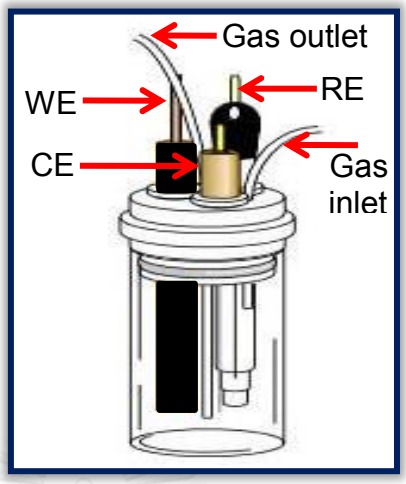

Figure 3–1: A schematic set up of an electrochemical cell for cyclic voltammetric experiment

3.3 Experimental Procedures

3.3.1 Synthesis of Benzoporphyrin Derivatives

3.3.1.1 Synthesis of 2H-Isoindole-4,5,6,7-tetrahydro-1-carboxylic acid ethyl ester (2)

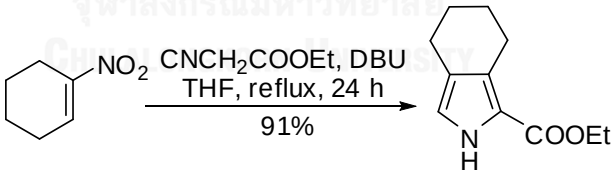

2

Following a previously published procedure [67], a solution of 1-nitrocyclohexene (4.40 mL, 39.2 mmol) and ethyl isocyanoacetate (4.31 mL, 39.2 mmol) dissolved in THF (100 mL) was placed in a 3-neck-round bottom flask equipped with a condenser under N_2 atmosphere. After that, DBU (5.54 mL, 39.2 mmol) was slowly added and the reaction was refluxed for 24 h. The solvent was removed under reduced pressure and the crude product was purified by column chromatography (silica gel, CH_2Cl_2) to afford **2** as pale yellow solid (6.85 g, 91%). ^{1}H-NMR: δ_H 1.33 (t, J = 6.8 Hz, 3H), 1.67–1.79 (m, 4H) 2.54 (t, J = 5.6 Hz, 2H), 2.80 (t, J = 5.6 Hz, 2H), 4.29 (q, J = 7.2 Hz, 2H), 6.63 (s, 1H), 8.80 (br s, 1H)

(**Figure A-1**). Other spectroscopic data were consistent with those described in the literature.

3.3.1.2 Synthesis of 4,5,6,7-tetrahydroisoindole (3)

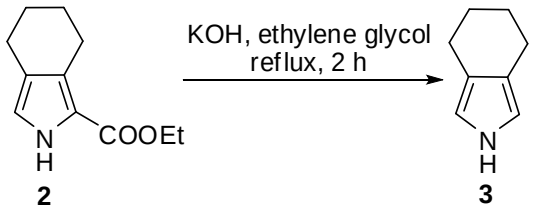

Following a previously published procedure [67], a mixture of compound **2** (3.00 g, 15.5 mmol), KOH (12.5 g, 223 mmol) in ethylene glycol (120 mL) was refluxed for 2 h until the homogenous solution turned black. Then, the mixture was cooled rapidly by using an ice bath and CH_2Cl_2 was added. The organic phase was washed several times with water and the aqueous phase was washed with CH_2Cl_2. The collected organic phase was concentrated to dryness, affording a black solid containing **3** (1.88 g) which was used in the next step without further purification. ^{1}H-NMR: δ_H 1.79–1.93 (m, 4H), 2.67–2.80 (m, 4H), 6.57 (s, 2H), 7.98 (br s, 1H) (**Figure A-2**). Other spectroscopic data were consistent with those described in the literature.

3.3.1.3 meso-Tetraphenylcyclohexanoporphyrin (4)

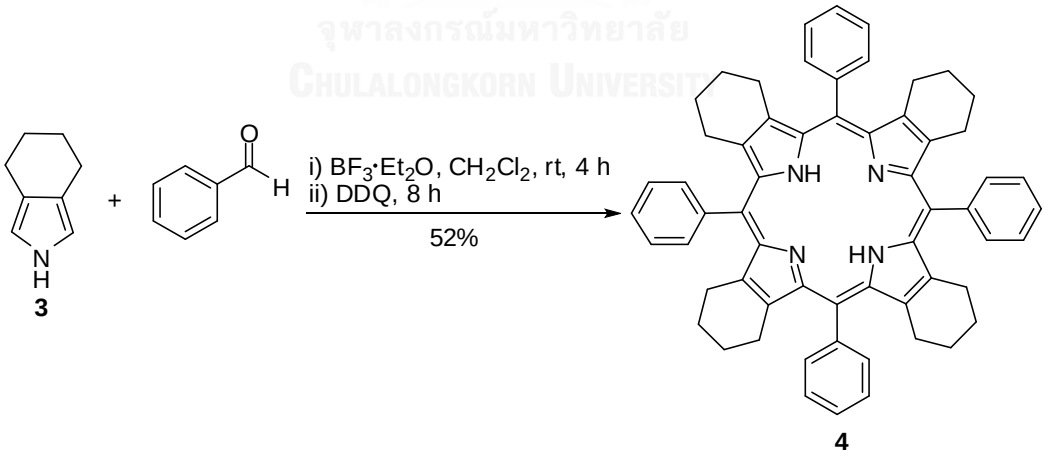

Following a previously published procedure [67], CH_2Cl_2 (575 mL) was degassed with N_2 gas in a 1 L two-neck-round bottom flask equipped with a condenser for 30 min. The entire apparatus was shielded from light with air, and a crude containing compound **3** (0.497 g) and benzaldehyde (0.414 mL, 4.10 mmol) was then added. After the mixture was stirred at the room temperature for 20 min.

$BF_3 \cdot Et_2O$ (0.112 mL, 0.821 mmol) was added in one portion and the reaction was continued for additional 4 h. Then, DDQ (0.175 g, 1.44 mmol) was added and the mixture was stirred at room temperature for 8 h. The resulting dark green solution was washed with 10% aqueous Na_2SO_3 and 5% aqueous HCl. The organic phase was separated and dried over anhydrous Na_2SO_4. Subsequently, the solvent was removed under reduced pressure and the crude product was purified by column chromatography (silica gel, $CHCl_3$) to afford **4** as blue green solid (0.407 g, 52% from **2**). ^{1}H-NMR: δ_H 1.18–2.73 (m, 32H), 6.69–7.51 (m, 8H), 7.51–7.88 (m, 4H), 7.88–8.50 (m, 8H) (**Figure A-3**). MALDI-TOF-MS m/z obsd 831.200 [M^+], calcd 831.098 [M = $C_{60}H_{54}N_4$] (**Figure A-4**), $\lambda_{abs}(\varepsilon)$ 462(1.3×10^5), 610, 665 nm (**Figure B-1**, **Figure B-2**). Other spectroscopic data were consistent with those described in the literature.

3.3.1.4 meso-Tetraphenylcyclohexanoporphyrinatonickel (Ni-4)

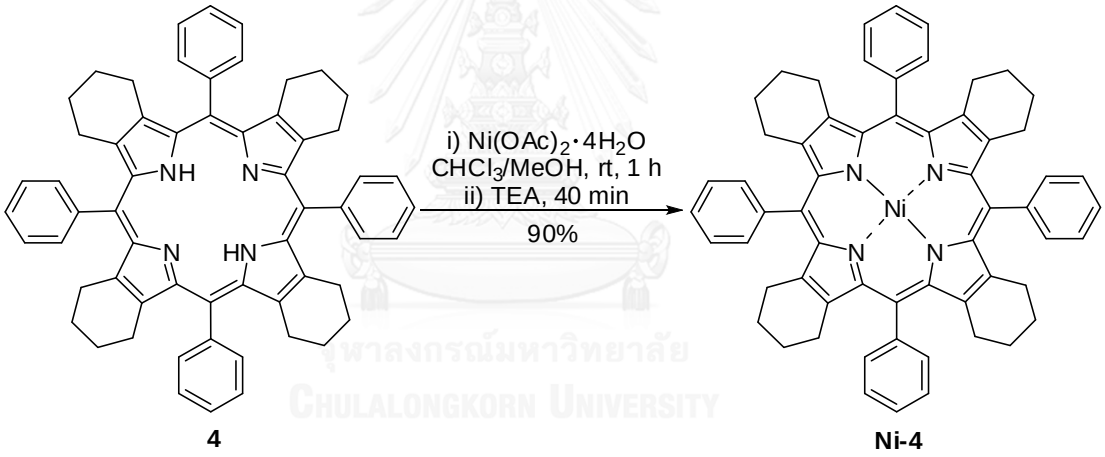

4 **Ni-4**

Following a previously published procedure [68], a solution of **4** (0.112 g, 0.135 mmol) in chloroform (100 mL) was reacted with a solution of $Ni(OAc)_2 \cdot H_2O$ (0.119 g, 0.675 mmol) in methanol (12 mL) at room temperature for 1 h. TEA (0.09 mL, 0.6 mmol) was added and the mixture was stirred for additional 40 min. The mixture was washed with 10% acetic acid and then 10% $NaHCO_3$. The organic phase was separated and dried over anhydrous Na_2SO_4. The solvent was removed by rotary evaporation and the crude was purified by column chromatography (silica gel, CH_2Cl_2/hexane (1:1)) to afford **Ni-4** as purple red solid (0.108 g, 90%). MALDI-TOF-MS m/z obsd 885.627 [M^+], calcd 887.775 [M = $C_{60}H_{52}N_4Ni$] (**Figure**

A-5), $\lambda_{abs}(\varepsilon)$ 425(5.8×10^4), 545, 581 nm (**Figure B-3**, **Figure B-4**). Other spectroscopic data were consistent with those described in the literature.

3.3.1.5 meso-Tetraphenyltetrabenzoporphyrinatonickel (Ni-1)

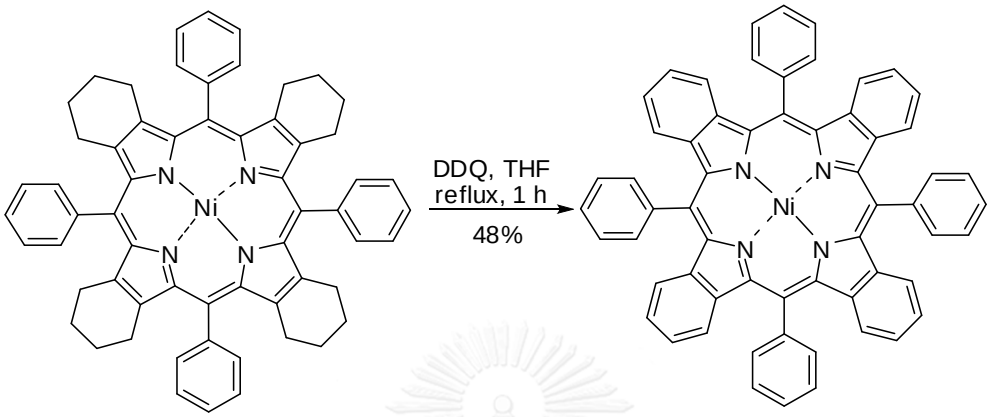

Ni-4 **Ni-1**

Following a previously published procedure [68], a solution of **Ni-4** (0.048 g, 0.054 mmol) and DDQ (0.191 g, 0.841 mmol) in THF (150 mL) was refluxed for 1 h under N_2 atmosphere. The resulting deep green mixture was washed with 10% Na_2SO_3, water and brine. The organic phase was separated and dried over anhydrous Na_2SO_4. The solvent was removed by rotary evaporator and the crude was purified by column chromatography (silica gel, CH_2Cl_2/hexanes (1:1)) to afford **Ni-1** as bright green crystal (0.0226 g, 48%). MALDI-TOF-MS m/z obsd 869.622 [M^+], calcd 871.648 [M = $C_{60}H_{36}N_4Ni$] (**Figure A-6**); $\lambda_{abs}(\varepsilon)$ 449 (2.2×10^5), 644 (9.3×10^4) nm (**Figure B-5**, **Figure B-6**, **Figure B-7**); Upon excitation at 449 nm, no emission peak was observed (**Figure B-8**). Other spectroscopic data were consistent with those described in the literature.

3.3.1.6 meso-Tetraphenylcyclohexanoporphyrinatocopper (Cu-4)

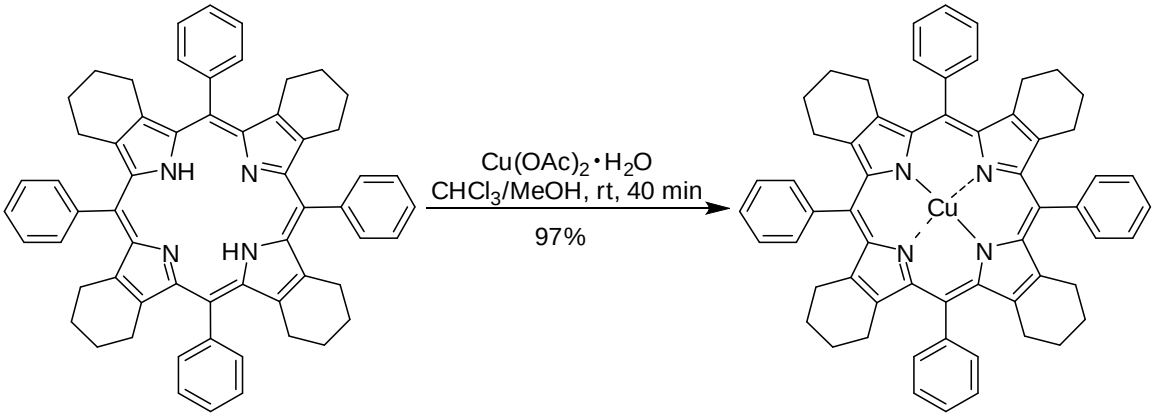

4 **Cu-4**

Following a previously published procedure [68], a solution of **4** (0.121 g, 0.146 mmol) in chloroform (110 mL) was reacted with a solution $Cu(OAc)_2 \cdot H_2O$ (0.146 g, 0.731 mmol) in methanol (12 mL) at room temperature for 40 min. The mixture was washed with 10% acetic acid and 10% and $NaHCO_3$. The organic phase was separated and dried over Na_2SO_4. Subsequently, the solvent was removed by rotary evaporator and the crude was purified by column chromatography (silica gel, CH_2Cl_2/hexanes (1:1)) to afford **Cu-4** as red solid (0.126 g, 97%). MALDI-TOF-MS m/z obsd 891.451 [M^+], calcd 892.628 [M = $C_{60}H_{54}N_4Cu$] (**Figure A-7**), $\lambda_{abs}(\varepsilon)$ 425(7.9×10^4), 558 nm (**Figure B-9**, **Figure B-10**). Other spectroscopic data were consistent with those described in the literature.

3.3.1.7 meso-Tetraphenyltetrabenzoporphyrinatocopper (Cu-1)

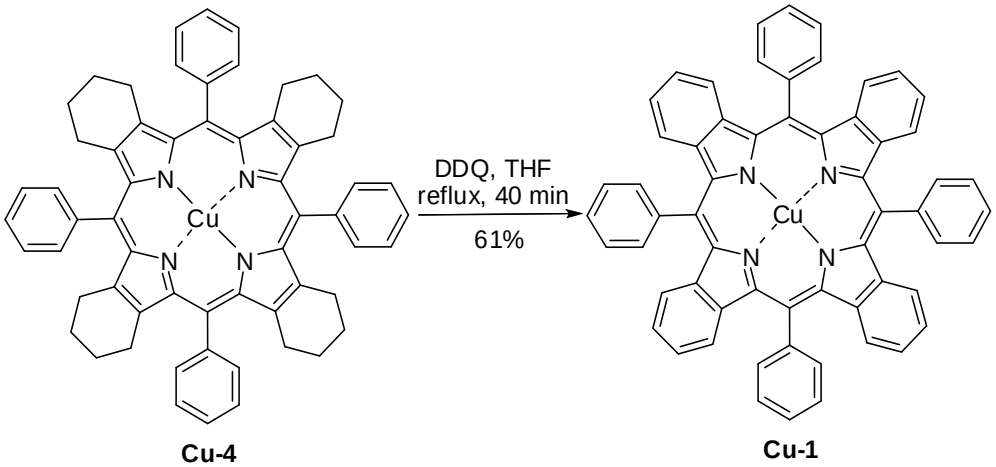

Cu-4 **Cu-1**

Following a previously published procedure [68], a solution of **Cu-4** (0.058 g, 0.059 mmol) and DDQ (0.216 g, 0.950 mmol) in THF (150 mL) was refluxed for 40 min in N_2 atmosphere. The resulting green mixture was washed with 10% Na_2SO_3, water, and brine. The organic phase was separated and dried over anhydrous Na_2SO_4. The solvent was removed by rotary evaporation and the crude was purified by column chromatography (silica gel, CH_2Cl_2/hexane (1:1)) to afford **Cu-1** as bright green solid (0.021 g, 45%). MALDI-TOF-MS m/z obsd 874.675 [M^+], calcd 876.501 [M = $C_{60}H_{36}N_4Cu$] (**Figure A-8**); $\lambda_{abs}(\varepsilon)$ 449(1.6×10^5), 463(1.9×10^5), 601(1.3×10^4), 648(7.5×10^4) nm (**Figure B-11**, **Figure B-12**, **Figure B-13**, **Figure B-14**, **Figure B-15**); Upon excitation at 463 nm, no emission peak was observed (**Figure B-16**). Other spectroscopic data were consistent with those described in the literature.

3.3.1.8 meso-Tetraphenyltetrabenzoporphyrin (1)

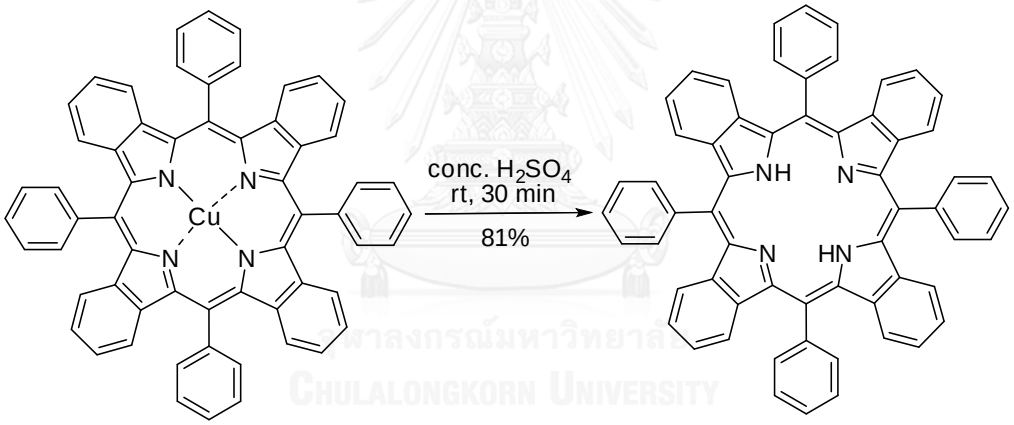

Cu-1 **1**

Following a previously published procedure [69], **Cu-1** (0.052 g, 0.060 mmol) was dissolved in concentrated sulfuric acid (10 mL) and the mixture was stirred at room temperature for 30 min. The solution was poured into a water/ice mixture and extracted with dichloromethane. The organic layer was collected and dried over anhydrous Na_2SO_4. The solvent was removed by rotary evaporation and the crude was purified by column chromatography (silica gel, CH_2Cl_2/hexanes (2:1)) to afford **1** as green solid (0.039 g, 81%). ^{1}H-NMR: δ_H –1.17 (s, 2H), 7.34–7.43 (m, 8H), 7.82–8.02 (m, 16H), 8.37 (d, J = 7.6 Hz, 4H), 8.56 (d, J = 7.2 Hz, 8H) (**Figure A-9**). ^{13}C-NMR: δ_C 114.5, 115.8, 124.3, 124.7, 125.9, 128.6, 129.0, 129.3, 129.5, 130.1, 131.5, 134.7, 136.2, 139.9, 141.5, 142.1 (**Figure A-10**). MALDI-TOF-MS m/z obsd

814.554 [M^+], calcd 814.971 (**Figure A-11**); HR-ESI-MS m/z obsd 815.3174, calcd 814.3096 [M = $C_{60}H_{38}N_4$] (**Figure A-12**); $\lambda_{abs}(\varepsilon)$ 465(5.3×10^5), 591, 626, 640, 698 nm (**Figure B-17**, **Figure B-18**); λ_{em} (λ_{ex} = 465 nm) 720, 787 nm (**Figure B-19**).

3.3.1.9 meso-Tetraphenyltetrabenzoporphyrinatozinc (Zn-1)

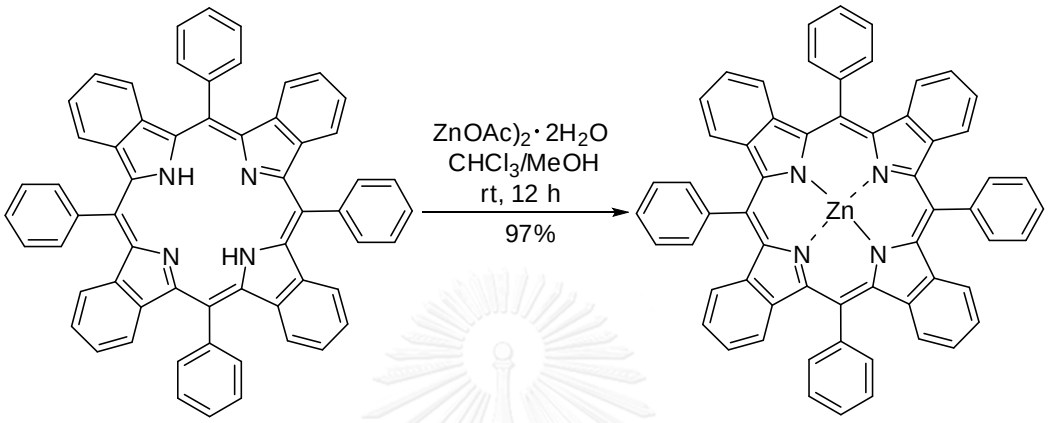

1 **Zn-1**

Following a previously published procedure [70], A solution of **1** (0.131 g, 0.161 mmol) in chloroform (117 mL) was reacted with a solution of $Zn(OAc)_2\cdot2H_2O$ (0.177 g, 0.805 mmol) in methanol (13 mL) at room temperature for 12 h. After the mixture was washed water, the organic layer was separated and dried over anhydrous Na_2SO_4. The solvent was removed by rotary evaporation and the crude was purified by column chromatography (silica gel, CH_2Cl_2/hexanes (2:1)) to afford **Zn-1** as greenish blue solid (0.136 g, 97%). ^{1}H-NMR: δ_H 7.16 (dd, *J* = 6.0, 2.8 Hz, 8H), 7.28 (dd, *J* = 6.0, 2.8 Hz, 8H) 7.86 (t, *J* = 7.2 Hz, 8H), 7.93 (t, *J* =7.2 Hz 4H), 8.30 (d, *J* = 7.2 Hz, 8H) (**Figure A-13**). ^{13}C-NMR: δ_C 117.3, 124.3, 124.4, 125.5, 128.8, 129.0, 129.1, 132.7, 134.1, 134.2, 138.6, 143.2, 143.4 (**Figure A-14**). MALDI-TOF-MS m/z observed 875.913 [M^+], calcd 875.365 [M = $C_{60}H_{36}N_4Zn$] (**Figure A-15**); HR-ESI-MS m/z obsd 876.2231, calcd 876.2231 [M = $C_{60}H_{36}N_4Zn$] (**Figure A-16**); $\lambda_{abs}(\varepsilon)$ 461(2.8×10^5), 607, 652 nm (**Figure B-20**, **Figure B-21**); λ_{em} (λ_{ex} = 461 nm) 658, 724 nm (**Figure B-22**).

3.3.1.10 meso-Tetraphenyltetrabenzoporphyrinatocobalt (Co-1)

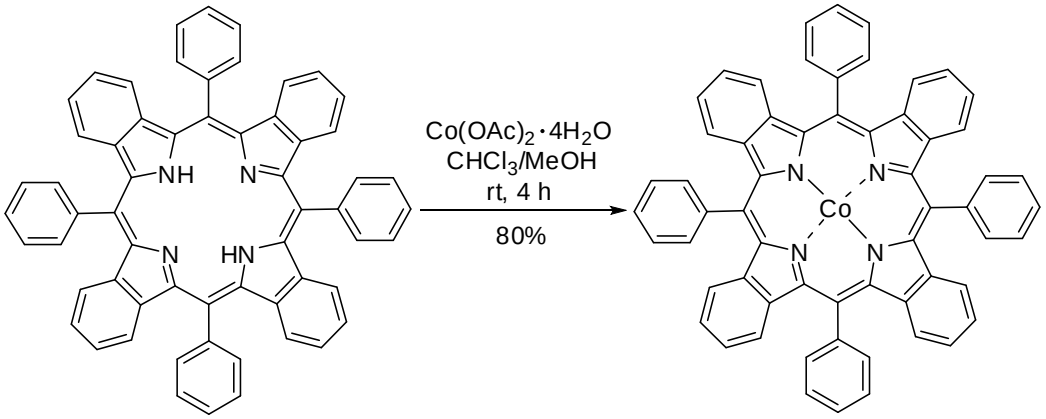

1 **Co-1**

Following a previously published procedure [71], A solution of **1** (0.048 g, 0.059 mmol) in chloroform (45 mL) was reacted with a solution of $Co(OAc)_2 \cdot 4H_2O$ (0.073g, 0.30 mmol) in methanol (5 mL) at room temperature for 4 h. After the mixture was washed water, the organic phase was separated and dried over anhydrous Na_2SO_4. The solvent was removed by rotary evaporation and the crude purified by column chromatography (silica gel, CH_2Cl_2/MeOH (99:1)) to afford **Co-1** as dark green solid (0.0472 g, 89%). MALDI-TOF-MS m/z obsd 870.594 [M^+], calcd 871.888 [M = $C_{60}H_{36}N_4Co$] (**Figure A-17**); HR-ESI-MS m/z obsd 871.2273, calcd 871.2272 [M = $C_{60}H_{36}N_4Co$] (**Figure A-18**); $\lambda_{abs}(\varepsilon)$ 446(1.7×10^5), 595, 640(8.0×10^4) nm (**Figure B-23**, **Figure B-24**, **Figure B-25**); Upon excitation at 446 nm, no emission peak was observed (**Figure B-26**).

3.3.1.11 meso-Tetraphenyltetrabenzoporphyrinatotin ($Sn(OH)_2$-1)

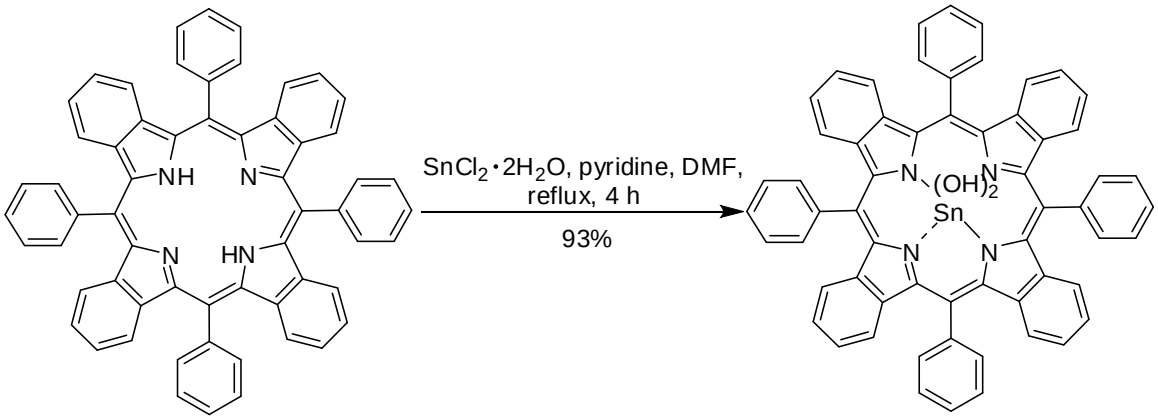

1 **$Sn(OH)_2$-1**

Following a previously published procedure [72], A solution of **1** (0.102 g, 0.125 mmol) and $SnCl_2 \cdot 2H_2O$ (0.141 g, 0.625 mmol) in DMF (5 mL) was treated with pyridine (0.05 mL) and refluxed for 4 h. The blue green precipitate was formed and collected by filtration. After that, the resulting crude product was purified by column chromatography (silica gel, CH_2Cl_2/MeOH (99:1)) to afford **Sn(OH)$_2$-1** as deep green solid (0.047 g, 90%). Due the incomplete purification of column chromatography, the achieved product was over 90% pure, based on ^{1}H-NMR spectroscopy. ^{1}H-NMR: δ_H 7.23 (dd, *J* = 6.4, 3.2 Hz, 8H), 7.43 (dd, *J* = 6.4, 3.2 Hz, 8H) 7.90 (t, *J* = 7.6 Hz, 8H), 8.00 (t, *J* =7.6 Hz 4H), 8.34 (d, *J* = 7.6 Hz, 8H) (**Figure A-19**); ^{13}C-NMR: δ_C 116.5, 125.6, 127.2, 127.6, 129.7, 129.8, 133.9, 137.4, 137.6, 137.8, 141.3, 141.6, 141.7, 141.8, 142.0 (**Figure A-20**). MALDI-TOF-MS m/z obsd 966.292 [M^+], calcd 965.679 [M = $C_{60}H_{38}N_4O_2Sn$] (**Figure A-21**); HR-ESI-MS m/z obsd 963.1883, calcd 966.2017 (**Figure A-22**); $\lambda_{abs}(\varepsilon)$ 430(3.0×10^4), 466(4.1×10^5), 612, 660(8.5×10^4) nm (**Figure B-27**, **Figure B-28**, **Figure B-29**, **Figure B-30**); λ_{em} (λ_{ex} = 466 nm) 665, 745 nm (**Figure B-31**).

3.3.2 Electrochemical Studies

3.3.2.1 Background Current

Background cyclic voltammogram was obtained in freshly distilled anhydrous DMF solution of tetrabutylammonium hexafluorophosphate ($TBAPF_6$), a supporting electrolyte at the concentration of 0.1 M. This cyclic voltammogram was recorded at the scan rate of 100 $mV \cdot s^{-1}$ in the range of –0.5 to –2.3 V. The solution was purged with nitrogen (N_2) or CO_2 for 20 min before each measurements. In the experiment under radiation, a 75-watt tungsten-halogen lamp was used and placed approximately 70 cm away from the electrochemical cell to avoid the temperature effect.

3.3.2.2 Electrochemical reduction of CO_2

Electrocatalytic activity of the porphyrins towards reduction of CO_2 was tested by means of cyclic voltammetry at the potential range of –0.5 to –1.9 V and –0.5 to –2.3 V. Cyclic voltammogram was carried out in a DMF solution containing 1.0 mM metallotetrabenzoporphyrin and 0.1 M $TBAPF_6$ in anhydrous DMF at the

scan rate of 100 $mV \cdot s^{-1}$. The solution was purged with N_2 or CO_2 for 20 min before each measurements. In the experiment under radiation, a 75-watt tungsten-halogen lamp was used and placed approximately 70 cm away from the electrochemical cell to avoid the temperature effect.

CHAPTER IV
RESULTS AND DISCUSSION

The key concept of this work is to develop the free base and metallobenzoporphyrinic derivatives for using as electrocatalysts for reduction of CO_2. The benzoporphyrin have phenyl groups at the meso positions and the fused benzene ring on the pyrrolic rings at the beta positions. The transition metals that were inserted into tetraphenyltetrabenzoporphyrin are cobalt(II), copper(II), nickel(II), tin (IV) or zinc(II). The studies for their electrocatalalytic activity for reduction of CO_2 were performed under the N_2 saturated and CO_2 saturated conditions, under ambient light and radiation. The electrochemical features and catalytic activity of these compounds were thoroughly investigated by means of cyclic voltammetry.

4.1 Synthesis and Characterization

4.1.1 Synthesis of Benzoporphyrin Derivatives

According to the published reports [67], *meso*-substituted benzoporphyrin derivatives were successfully synthesized from isoindole derivatives. As a starting material of the entire reaction sequence, 4,5,6,7-tetrahydroisoindole ester **2** was quantitatively prepared from commercially available 1-nitrocyclohexene and ethyl isocyanoacetate in a presence of DBU *via* Barton-Zard synthesis [73] (**Scheme 4–1**). Tetrahydroisoindole (**3**) was obtained as solid from refluxing compound **2** with the excess of KOH in the ethylene glycol for 2 h. Compound **3** was reacted under Lindsey's condition with benzaldehyde in the present $BF_3{\cdot}Et_2O$ at room temperature for 1 h [67]. Then, DDQ was added in the reaction mixture as an oxidizing agent, giving tetraphenylcyclohexanoporphyrin **4**. The major reason of this moderate yield is the competitive reaction in the porphyrin formation step, e.g. a polymerization of tetrahydroisoindole and the formation of other possible *N*–confused isomers. From its ^{1}H-NMR spectrum, **4** exhibited four characteristic multiplet signals indicating 32 cyclohexyl protons at δ 1.18–2.73 ppm, and multiplet signals of 8 *ortho*-phenyl protons at δ 6.69–7.51 ppm, multiplet signals of 4 *para*-phenyl protons at δ 7.51–7.88 ppm, and multiplet signals of 8 *meta*-phenyl protons at δ 7.88–8.50 ppm. Absorption spectrum of **4** showed a characteristic pattern of the porphyrins having a strong Soret band at 462 nm and Q-bands at 610 nm and 665 nm. A MALDI-TOF mass spectrum

confirmed the formation of **4** by showing the molecular ion peak $[M]^+$ at m/z 831.200, which consistent with a calculated value of m/z 831.098.

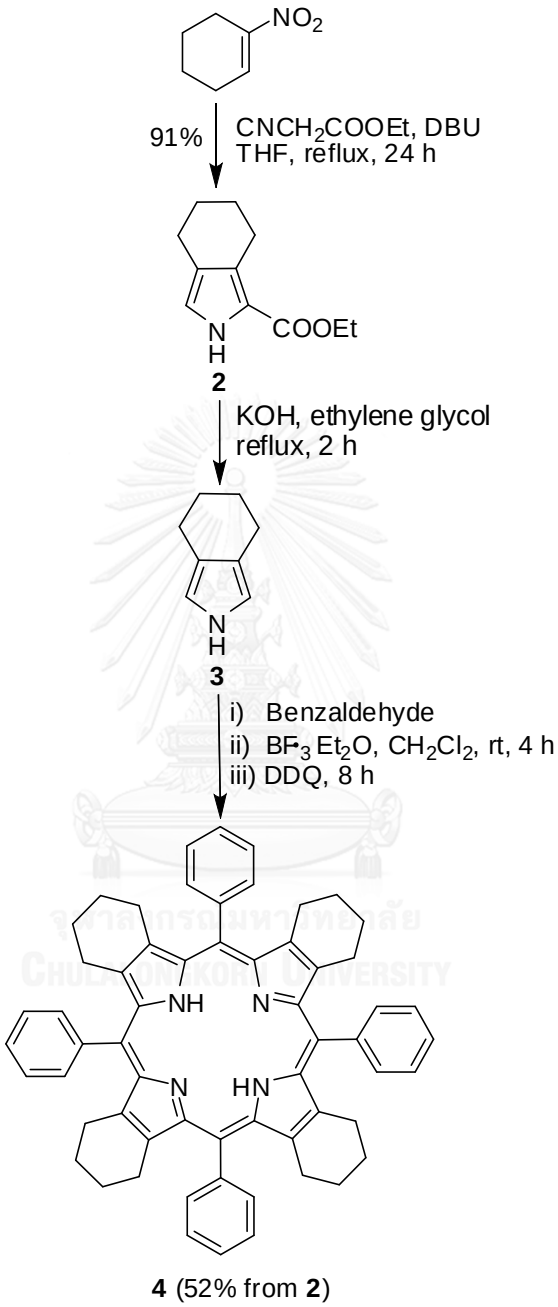

Scheme 4–1: Synthesis of compound **4**

An effort to fully aromatize **4** failed to give the desired free base benzoporphyrin **1** due to the decomposition of compound **4**. Therefore, metallation of **4** by $Cu(OAc)_2 \cdot 2H_2O$ and $Ni(OAc)_2 \cdot 2H_2O$ was performed to get **Ni-4** and **Cu-4**, respectively, first (**Scheme 4–2**). Due to templating effect caused by the metal chelation, **Ni-4** and **Cu-4** was successfully aromatized to **Ni-1** and **Cu-1**, respectively. Compound **4** was nickel-metallated in the presence of $Ni(OAc)_2 \cdot H_2O$ in chloroform/methanol at room temperature for 1 h, followed by the treatment with TEA for 40 min, to obtain compound **Ni-4** in 90% yield [68]. Then, **Ni-4** was readily aromatized by DDQ in refluxing THF for 1 h, affording compound **Ni-1** in 48% yield. Absorption spectrum of **Ni-1** showed a strong Soret band at 449 nm and Q-bands at 592 and 644 nm. However, upon excitation at 449 nm, no emission peak was observed. MALDI-TOF mass spectrum of **Ni-1** showed a molecular ion peak at m/z 869.622, which was consistent with a calculated value of m/z 871.648.

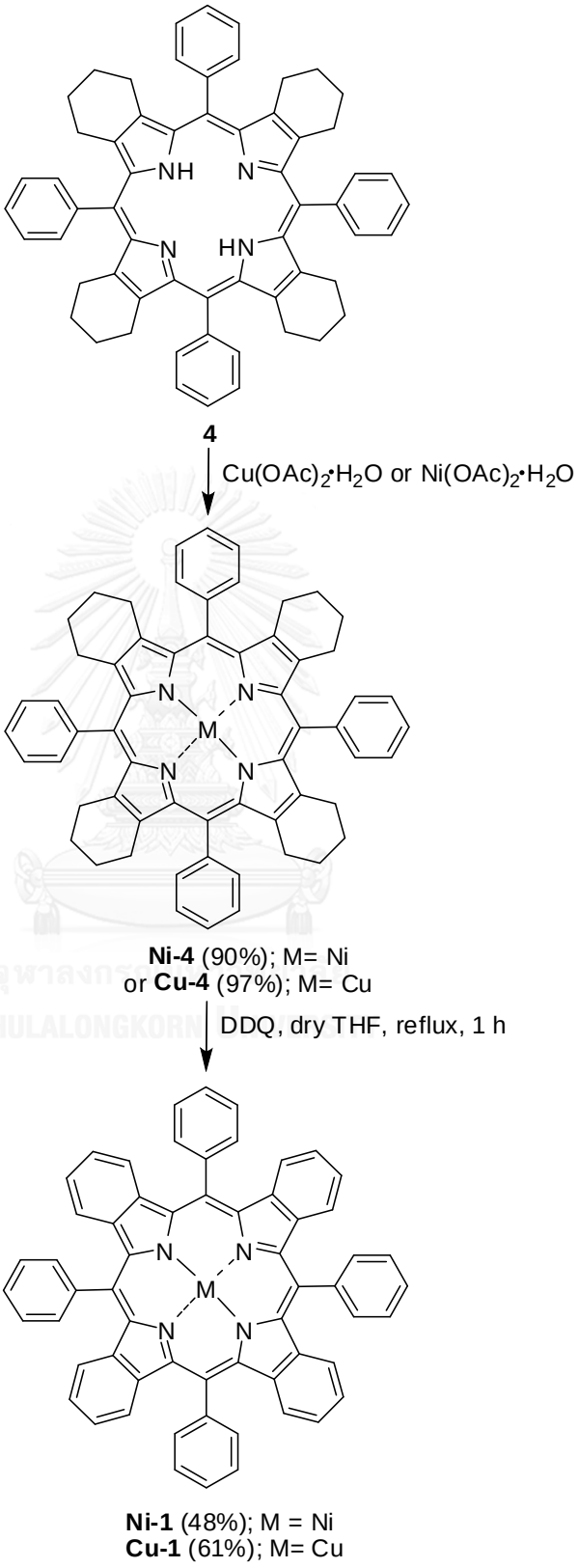

Scheme 4–2: Synthesis of **Ni-1** and **Cu-1**.

In a similar manner, compound **4** was copper-metallated in the presence of $Cu(OAc)_2 \cdot H_2O$ in chloroform/methanol at room temperature for 40 min, resulting in compound **Cu-4** in 97% yield [68]. Then, **Cu-4** was readily aromatized by DDQ in THF refluxing for 40 min, affording compound **Cu-1** in 61% yield. Absorption spectrum of **Cu-1** showed a strong band at 449 nm and 463 nm and Q-band at 595 and 643 nm. Upon excitation at 462 nm, no emission peak was observed. Based on mass spectrometry, **Cu-1** exhibited a molecular ion peak in its MALDI-TOF mass spectrum at m/z 875.675, which was consistent with a calculated value of m/z 875.501.

For the demetallation step, the experiments have to use the **Cu-1** because the **Cu-1** was stable and the copper complex can be demetallated by concentrated sulfuric acid according to the previous report [69]. Upon the treatment of **Cu-1** with the concentrated sulfuric acid at room temperature for 30 min, compound **1** was obtained in 81% yield (**Scheme 4–3**). A broad singlet signal of two inner protons at δ –1.17 ppm in its ^{1}H-NMR spectrum confirmed the formation of the free base derivative. A UV-Vis spectrum of **1** showed the characteristic pattern of the porphyrin with a Soret band at 465 nm and Q-bands at 629, 639 and 798 nm. Upon excitation at 465 nm, the emission spectrum showed emission peaks at 720 and 787 nm. MALDI-TOF mass spectrometry showed a molecular ion peak of **1** at m/z 814.554 and HR-ESI mass spectrum exhibited the $[M + H]^+$ the corresponding peaks of **1** at m/z 815.3175.

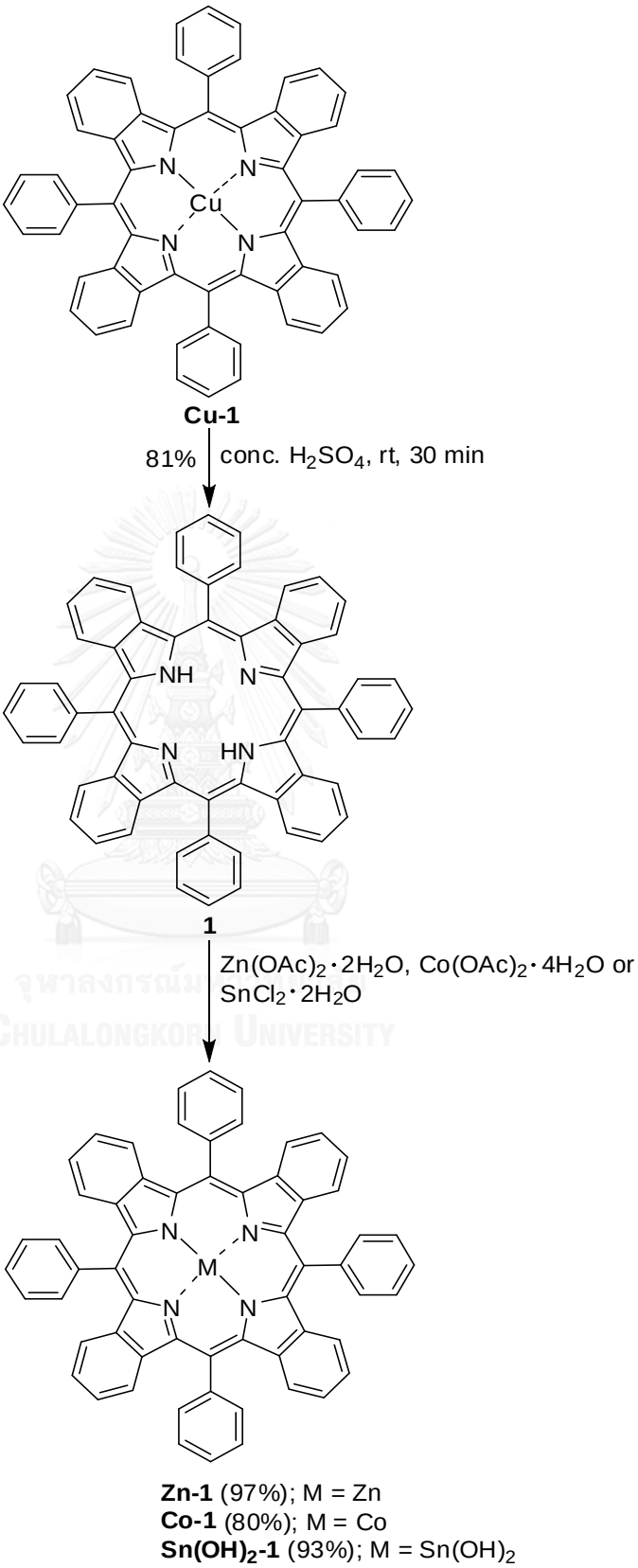

Scheme 4–3: Synthesis of Metallation of compound **1**

To obtain the desired **Zn-1**, **1** was zinc-metallated in the presence of $Zn(OAc)_2 \cdot 2H_2O$ in chloroform/methanol at room temperature overnight, as described in the previous study [70]. A UV-Vis spectrum of **Zn-1** showed the characteristic pattern of the porphyrin with a Soret band at 461 nm and Q-bands at 666 and 731 nm. Upon excitation at 461 nm, the emission spectrum showed emission peaks at 658 and 724 nm. Its ^{1}H-NMR spectrum exhibited no broad singlet signal at δ –1.17 ppm observed in the case of compound **1**, indicating the complete metallation of compound **1**. A MALDI-TOF mass spectrum and HR-ESI mass spectrum confirmed the formation of **Zn-1** by showing the molecular ion peak at m/z 875.913 and 876.2231, respectively.

In a similar manner, **Co-1** was readily synthesized by metallation of compound **1** with $Co(OAc)_2 \cdot 4H_2O$, leading to compound **Co-1** in 80% yield as described in the previous study [71]. UV-Vis spectrum of **Co-1** showed the characteristic pattern of the porphyrin with a Soret band at 447 nm and Q-bands at 595 and 643 nm. Upon excitation at 446 nm, no emission peak was observed. MALDI-TOF mass spectrometry showed a molecular ion peak of **Co-1** at m/z 870.594 and HR-ESI mass spectrum exhibited the corresponding peak of **Co-1** at m/z 871.2273.

$Sn(OH)_2$-1 was prepared by metallation of **1** with $SnCl_2 \cdot 2H_2O$ in refluxing anhydrous DMF for 4 h, resulting in **$Sn(OH)_2$-1** in 89% yield, as described in the previous study [72]. UV-Vis spectrum showed a Soret band at 466 nm and Q-bands at 612 and 660 nm. Upon excitation at 466 nm, the emission spectrum showed emission peaks at 665 and 745 nm. No broad singlet signal at δ –1.17 ppm was observed in its ^{1}H-NMR spectrum, indicating the complete metallation of compound **1**. MALDI-TOF and HR-ESI mass spectrometry confirmed the formation of **$Sn(OH)_2$-1** by showing a molecular ion peak at m/z 966.292 and 963.1883, respectively.

4.1.2 Investigation of Photophysical Properties

The photophysical properties of **1**, **Ni-1**, **Cu-1**, **Zn-1**, **Co-1** and **$Sn(OH)_2$-1** were investigated in toluene by using UV-Vis spectrophotometry and fluorescent spectrophotometry. The results of all compounds are summarized in **Table 4–1**.

Table 4–1 Photophysical properties of **1** and its metallated derivatives

Compound	λ_{abs}/nm (ε)		λ_{em}/nm (λ_{ex}/nm)
	Soret band	Q-bands	
1	465 (5.3×10^5)	626[a], 640 [a] 698[a]	720, 787 (465)
Ni-1	449 (2.2×10^5)	592[a] 644 (9.3×10^4)	–[b] (449)
Cu-1	449 (1.6×10^5) 463 (1.9×10^5)	601 (1.3×10^4) 648 (7.5×10^4)	–[b] (463)
Zn-1	461 (2.8×10^5)	607[a] 652[a]	658, 724 (461)
Co-1	446 (1.7×10^5)	595[a] 640 (8.0×10^4)	–[b] (446)
Sn(OH)$_2$-1	430 (3.0×10^4) 466 (4.1×10^5)	612[a] 660 (8.5×10^4)	665, 745 (466)

[a] Due to low absorption, the ε value could not be determined.

[b] No emission peak was observed.

Normalized absorption spectra of all compounds were recorded in toluene and are shown in **Figure 4–1**. All compounds exhibited chacteristic absorption patterns of the metal chelated benzoporphyrin with intense Soret band in the range of 446–466 nm with the absorption coefficient of 1.6×10^5–5.3×10^5 $M^{-1}\cdot cm^{-1}$, and the Q-band in the range of 592–698 nm. Upon excitation at the absorption maxima, **1**, **Zn-1** and **Sn(OH)$_2$-1** showed emission peaks in the range of 658–787 nm as shown in **Figure 4–2**, while **Ni-1, Cu-1** and **Co-1** showed no significant emission.

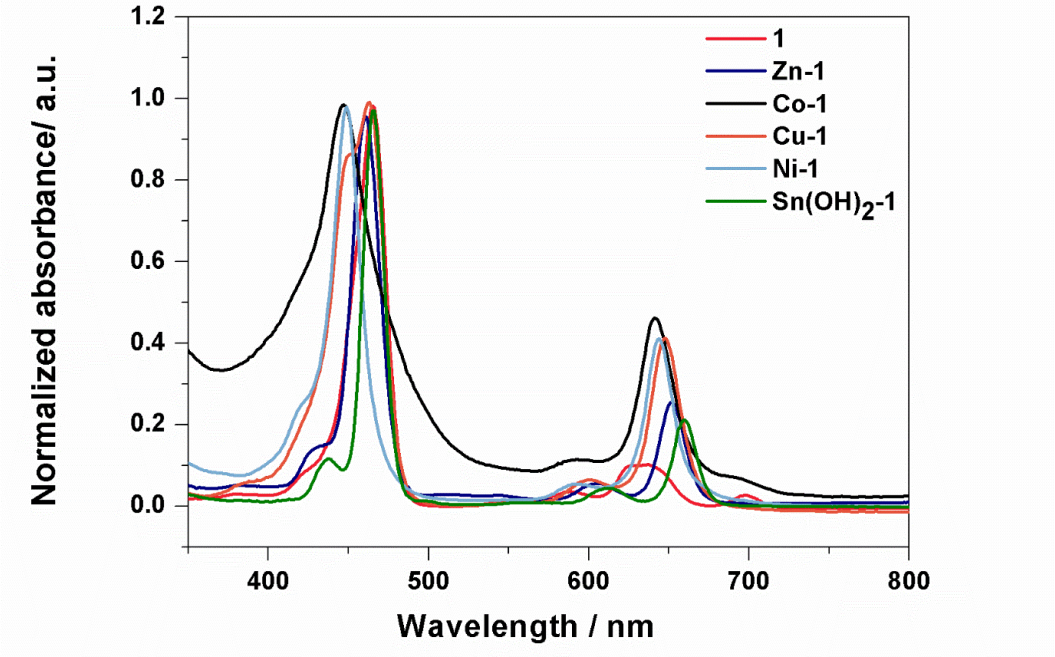

Figure 4–1: Normalized UV-Vis absorption spectra of **1** and its derivatives

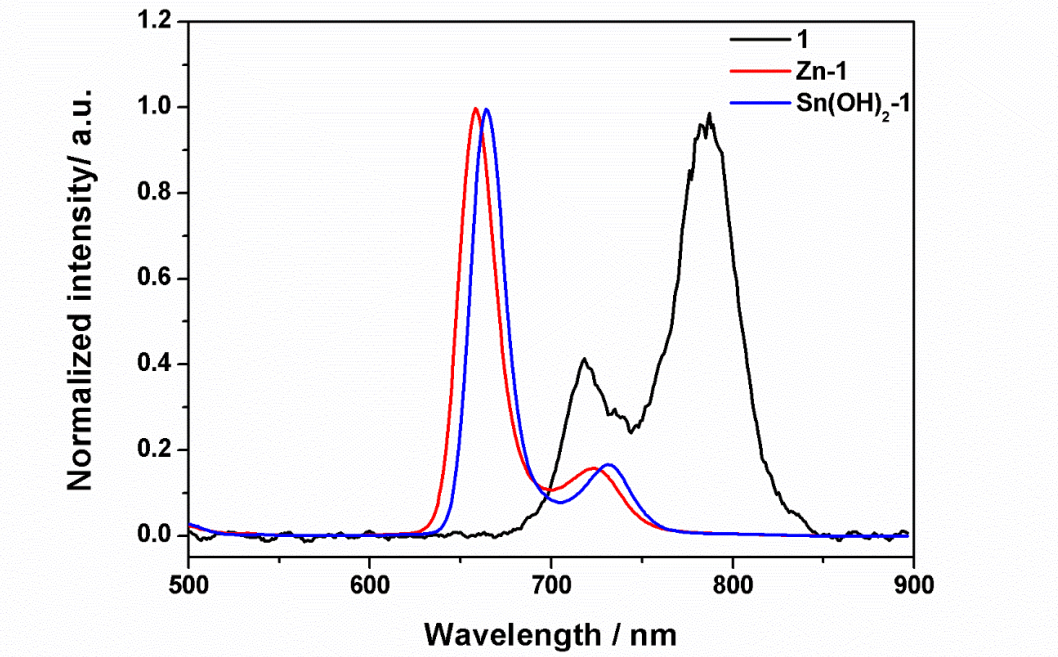

Figure 4–2: Normalized intensity emission spectra of **1**, **Zn-1** and **Sn(OH)$_2$-1**

4.2 Investigation of Elctrochemical Properties

All compounds were studied by means of cyclic voltammetry to evaluate their catalytic activity for the reduction of CO_2 as described below.

4.2.1 Electrolyte Solution

Figure 4–3 shows typical cyclic voltammograms of 0.1 M $TBAPF_6$ in anhydrous DMF solution at the scan rate of 100 $mV \cdot s^{-1}$ in the potential range of –0.5 and –2.3 V. No peak was observed under N_2 saturated condition with the ambient light, indicating no reduction or oxidation of any species in the system. Under CO_2 saturated condition with the ambient light, the current enhancement showed in the potential range of –2.0 to –2.3 V. Upon radiation by the halogen lamp, cyclic voltammograms recorded under both N_2 and CO_2 saturated conditions were found to be almost identical to those recorded with the ambient light, indicating that light did not significantly affect the electrochemical behavior of the background solution. According to previous research [74] and this work, since a 0.1 M $TBAPF_6$ solution did not give any peak in the range of –0.5 to –2.3 V, it can be used as a background for the cyclic voltammetric studies.

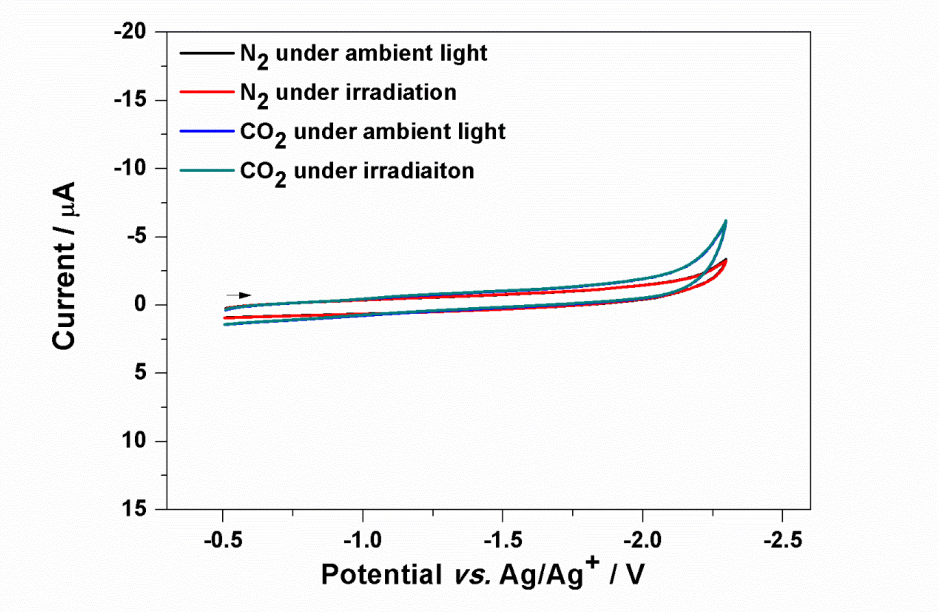

Figure 4–3: Cyclic voltammograms for a DMF solution containing 0.1 M $TBAPF_6$ in the presence of N_2 under the ambient light (black line), N_2 under halogen-lamp radiation (red line), CO_2 under the ambient light (blue line) and CO_2 under halogen-lamp radiation (green line) recorded at the scan rate of 100 $mV \cdot s^{-1}$ in the range of –0.5 to –2.3 V

4.2.2 Compound 1

Cyclic voltammograms of compound **1** were recorded in the potential ranges of –0.5 to –1.65 V for observing the first reduction peak in particular and –0.5 to –2.3 V for obtaining the the overall reduction pattern at 100 $mV \cdot s^{-1}$ as shown in **Figure 4–4** and **Figure 4–5**, respectively. Under the N_2 saturated condition with the ambient light (black lines), the first reduction of compound **1** showed reversible reduction peak at –1.49 V. As seen in **Figure 4–4**, when the DMF solution of compound **1** was saturated with CO_2 and its cyclic voltammogram under ambient light showed reduction peak at –1.46 V and the cyclic voltammogram undergoes one irrevesible reduction step. Compared with the result obtained under N_2 saturated condition, the reduction peak positively shifts by 30 mV with approximately 2 folds of peak current from 10.6 μA to 26.8 μA. The reduction peak was also observed with new oxidation signal at –0.90 V, implying that compound **1** might bind with CO_2 to form unknown species. As display in **Figure 4–5**, another reversible reduction peak appears under N_2 saturated condition at –1.78 V. When the DMF solution of compound **1** was saturated with CO_2, its cyclic voltammogram under ambient light shows irreversible reduction peaks at –2.06 V with the disappearance of the anodic peak at –1.78 V, and the peak shifts negatively by –0.28 V with the peak current enhancement from 14.4 μA to 31.5 μA. The new oxidation signals were observed at –0.75 and –0.80 V, implying that the unknown species is likely to be obtained from the second irrevesible reduction. The results revealed that the second reduction was more negatively shifted under CO_2 saturated condition because compound **1** might bind with CO_2 to yield unknown species changing the electrochemical behavior. Cyclic voltammograms upon radiation by the halogen lamp under N_2 and CO_2 saturated conditions were very similar to those observed under the ambient light, indicating that the reduction of CO_2 by compound **1** is not affected by halogen-lamp irradiation.

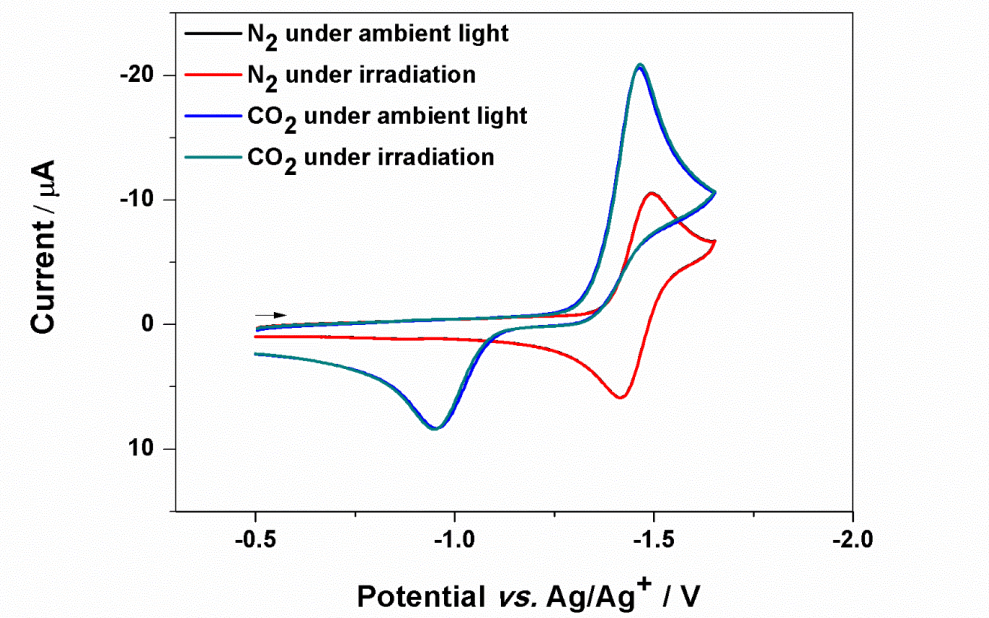

Figure 4–4: Cyclic voltammograms for a DMF solution containing 1.0 mM compound **1** and 0.1 M $TBAPF_6$ in the presence of N_2 under the ambient light (black line), N_2 under halogen-lamp radiation (red line), CO_2 under the ambient light (blue line) and CO_2 under halogen-lamp radiation (green line) recorded at the scan rate of 100 $mV \cdot s^{-1}$ in the range of –0.5 to –1.65 V

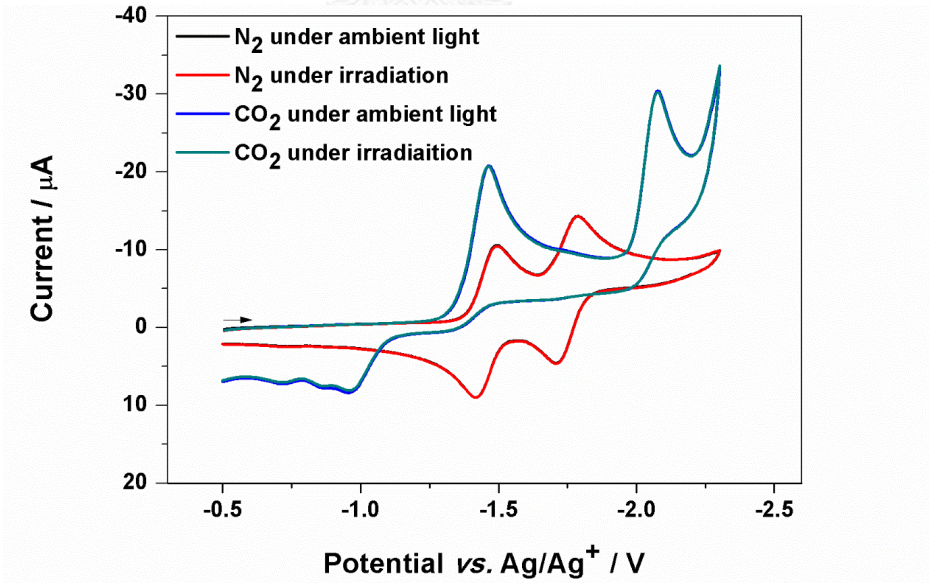

Figure 4–5: Cyclic voltammograms for a DMF solution containing 1.0 mM compound **1** and 0.1 M $TBAPF_6$ in the presence of N_2 under the ambient light (black line), N_2 under halogen-lamp radiation (red line), CO_2 under the ambient light (blue line) and CO_2 under halogen-lamp radiation (green line) recorded at the scan rate of 100 $mV \cdot s^{-1}$ in the range of –0.5 to –2.3 V

4.2.3 Compound Ni-1

To observe the first and second reduction of compound **Ni-1**, its cyclic voltammograms were performed in the ranges of –0.5 to –1.85 V and –0.5 to –2.3 V as shown in **Figure 4–6** and **4–7**, respectively. Cyclic voltammograms of compound **Ni-1** in the presence of N_2 under both the ambient light and the halogen-lamp light showed the first reversible reduction peak at –1.46 V and the second irrevesible one at –2.27 V. Since the oxidation peak at –0.60 V of **Figure 4–7** was not observed in **Figure 4–6**, this new species is likely to be obtained from the second irrevesible reduction. When the solution of compound **Ni-1** was saturated with CO_2 and its cyclic voltammograms were recorded under the ambient light (black line), the cathodic peak for the first reduction was observed at similar potenital but with a decrease in current. Compared to those observed under N_2-saturated condition, the second reduction peak (**Figure 4–7**) shifts positively by 70 mV with the current increase from 10.5 μA to 20.2 μA. The current enhancement and the positive shift at the second reduction peak indicate that compound **Ni-1** is capable of electrochemically catalyzing the reduction of CO_2. Under hallogen-lamp radiation in the presence of N_2 and CO_2, the cyclic voltammograms showed similar pattern, illustrating that light has no effect on the electrocatalytic activity of compound **Ni-1** for the reduction of CO_2.

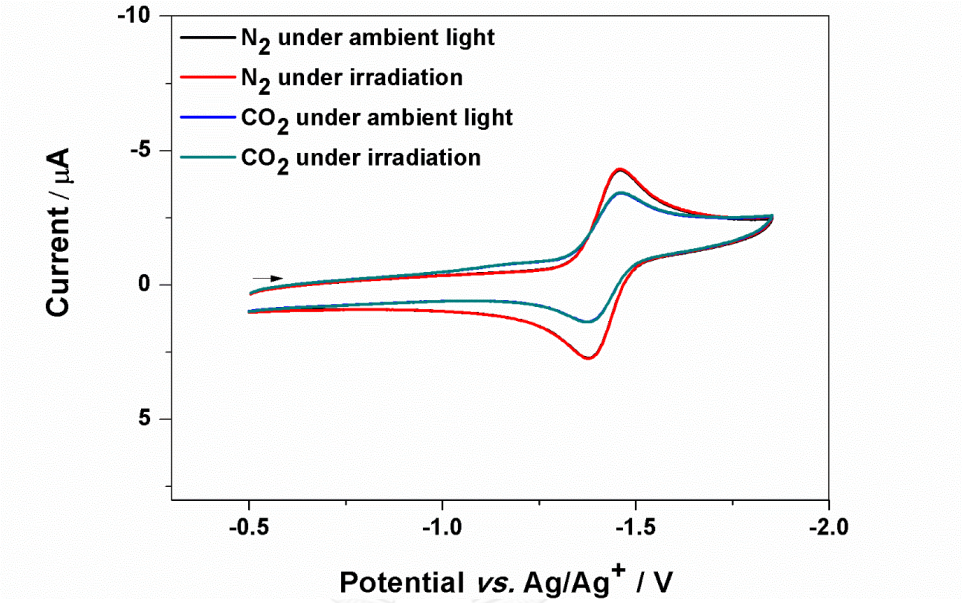

Figure 4–6: Cyclic voltammograms for a DMF solution containing 1.0 mM compound **Ni-1** and 0.1 M $TBAPF_6$ in the presence of N_2 under the ambient light (black line), N_2 under halogen-lamp radiation (red line), CO_2 under the ambient light (blue line) and CO_2 under halogen-lamp radiation (green line) recorded at the scan rate of 100 $mV \cdot s^{-1}$ in the range of –0.5 to –1.85 V

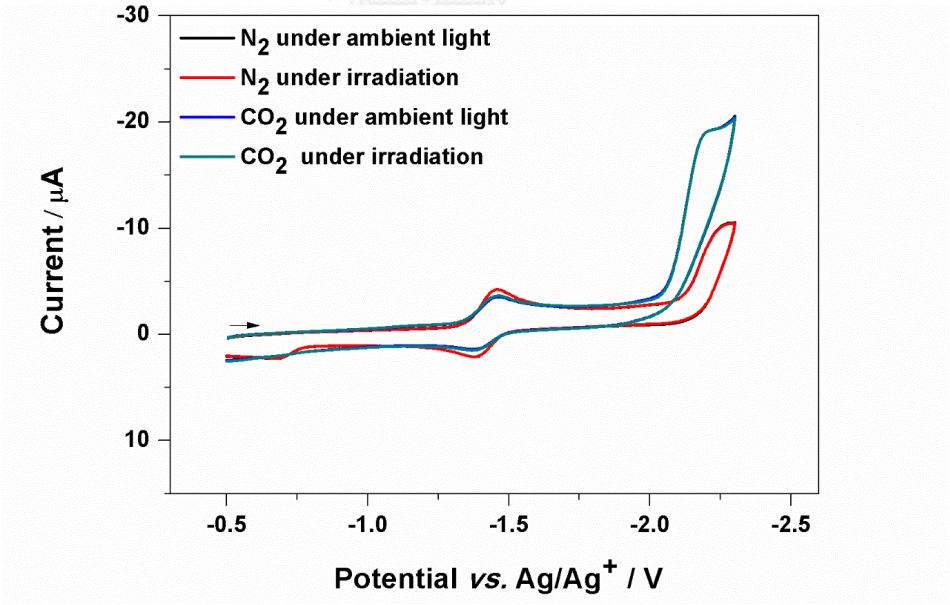

Figure 4–7: Cyclic voltammograms for a DMF solution containing 1.0 mM compound **Ni-1** and 0.1 M $TBAPF_6$ in the presence of N_2 under the ambient light (black line), N_2 under halogen-lamp radiation (red line), CO_2 under the ambient light (blue line) and CO_2 under halogen-lamp radiation (green line) recorded at the scan rate of 100 $mV \cdot s^{-1}$ in the range of –0.5 to –2.3 V

4.2.4 Compound Cu-1

To observe the first and the second reduction of compound **Cu-1**, cyclic voltammograms were recorded in the range of –0.5 to –1.9 V (**Figure 4–8**) and –0.5 to –2.3 V (**Figure 4–9**) at the scan rate of 100 $mV \cdot s^{-1}$. As seen in **Figure 4–8**, cyclic voltammograms of an N_2-saturated solution of **Cu-1** under the ambient light (black line) and halogen-lamp radiation (red line) exhibited the first reversible reduction peak at –1.52 V. Under the CO_2 saturated condition with the exposure to the ambient light (blue line) and the halogen-lamp radiation (green line), the reduction process occurred at similar potential with slight current increase from 11.3 μA to 12.2 μA. This result indicates that the first reduction was not affected by CO_2. As displayed in **Figure 4–9**, cyclic voltammograms of N_2-saturated solution of **Cu-1** under the ambient light and the radiation showed the second quasi-revesible peak at –2.16 V. Additional oxidation signal was observed at –0.75 V, indicating the formation of the unknown species from the second reduction. When the solution of compound **Cu-1** was saturated with CO_2 under the ambient light and the radiation, the cyclic voltammogram was observed with the positive shift by 30 mV and the dramatic increase in current from 18.5 μA to 47.1 μA. The cyclic voltammogram exhibited the enhancement of the second reduction peak and the hysteresis at –1.90 V. On the reverse scan, the anodic peak appeared at similar potential with higher current. The oxidation signal at –1.45 V of **Figure 4–9** showed the current decrease compared with those in **Figure 4–8**. This new species is likely to be obtained from the second irrevesible reduction. The slight positive shift of the second reduction peak and the great current enhancement observed in this experiment suggested that compound **Cu-1** could be a good candidate for using as an electrocatalyst for the reduction of CO_2. Upon radiation with the halogen lamp, the cyclic voltammograms under N_2 and CO_2 saturated conditions were very similar to those observed under the ambient light, indicating that the reduction of CO_2 by compound **Cu-1** is hardly affected by halogen-lamp irradiation.

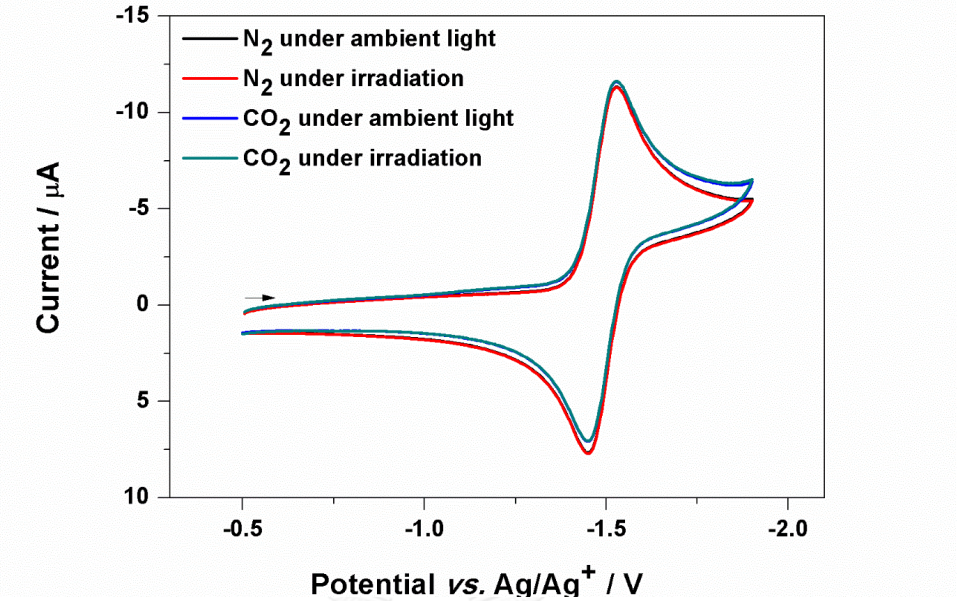

Figure 4–8: Cyclic voltammograms for a DMF solution containing 1.0 mM compound **Cu-1** and 0.1 M $TBAPF_6$ in the presence of N_2 under the ambient light (black line), N_2 under halogen-lamp radiation (red line), CO_2 under the ambient light (blue line) and CO_2 under halogen-lamp radiation (green line) recorded at the scan rate of 100 $mV \cdot s^{-1}$ in the range of –0.5 to –1.9 V

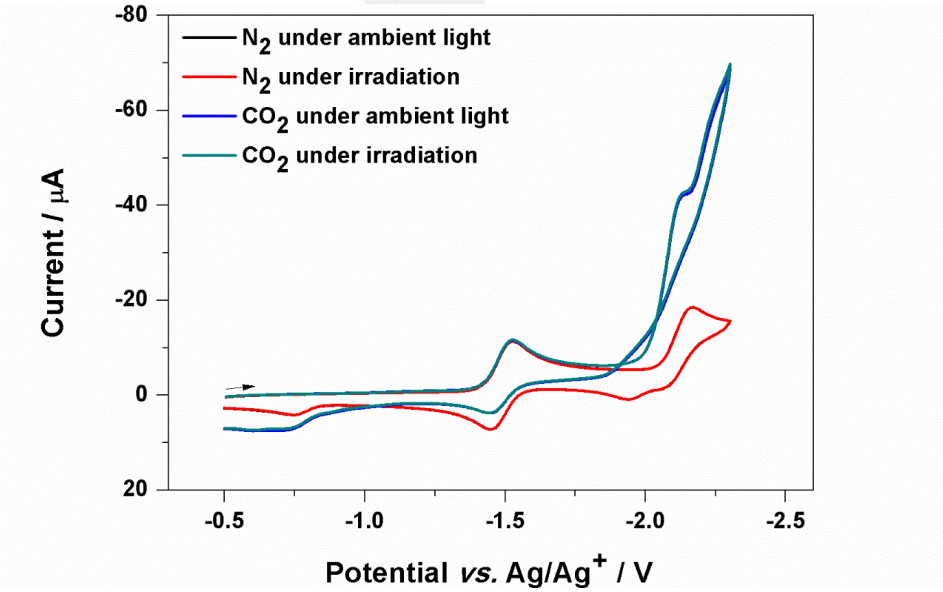

Figure 4–9: Cyclic voltammograms for a DMF solution containing 1.0 mM compound **Cu-1** and 0.1 M $TBAPF_6$ in the presence of N_2 under the ambient light (black line), N_2 under halogen-lamp radiation (red line), CO_2 under the ambient light (blue line) and CO_2 under halogen-lamp radiation (green line) recorded at the scan rate of 100 $mV \cdot s^{-1}$ in the range of –0.5 to –2.3 V

4.2.5 Compound Zn-1

Cyclic voltammograms of compound **Zn-1** were recorded in the potential ranges of –0.5 to –1.9 V (**Figure 4–10**) for observing the first reduction peak and –0.5 to –2.3 V (**Figure 4–11**) for obtaining the overall reduction pattern of compound **Zn-1** at 100 $mV \cdot s^{-1}$. As seen in **Figure 4–10**, cyclic voltammograms of an N_2-saturated solution of **Zn-1** under the ambient light and halogen-lamp radiation exhibited reversible reduction peak at –1.79 V. Under the CO_2 saturated condition with the exposure to the ambient light and the halogen-lamp radiation, the reduction process occurred at similar potential with slight current increase current from 9.8 μA to 10.6 μA. This result indicates that the first reduction was not affected by CO_2. As displayed in **Figure 4–11**, cyclic voltammograms of N_2-saturated solution of **Zn-1** under the ambient light and the radiation exhibited another quasi-reversible reduction peak at –2.06 V. Additional oxidation signals were observed in the potential range of –0.75 V to –0.90 V when the potential scan went beyond –1.9 V, indicating the formation of the unknown species from the second reduction. Under the CO_2 saturated condition with the exposure to the ambient light and the radiation, reduction process occurred with slight current increase from 14.4 μA to 16.9 μA for the second peak. Unknown oxidation signals were found in the potential range of –0.60 V to –0.90 V, indicating the occurrence of the different reductive process(es), compared to that observed from the N_2 saturated system. Since the results showed the increase in current in the presence of CO_2, it can be suggested that **Zn-1** might be used as an electrocatalyst for the reduction of CO_2. Under radiation in presence of N_2 and CO_2, cyclic voltammograms showed similar pattern with the ambient light, illustrating that light has no effect on the electrocatalytic activity of compound **Zn-1** on the reduction of CO_2.

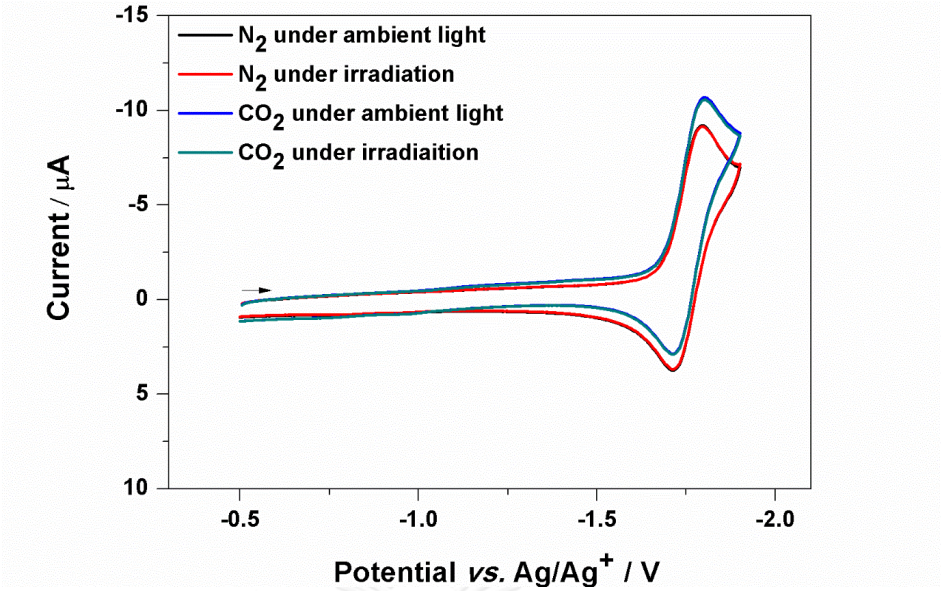

Figure 4–10: Cyclic voltammograms for a DMF solution containing 1.0 mM compound **Zn-1** and 0.1 M $TBAPF_6$ in the presence of N_2 under the ambient light (black line), N_2 under halogen-lamp radiation (red line), CO_2 under the ambient light (blue line) and CO_2 under halogen-lamp radiation (green line) recorded at the scan rate of 100 $mV \cdot s^{-1}$ in the range of –0.5 to –1.9 V

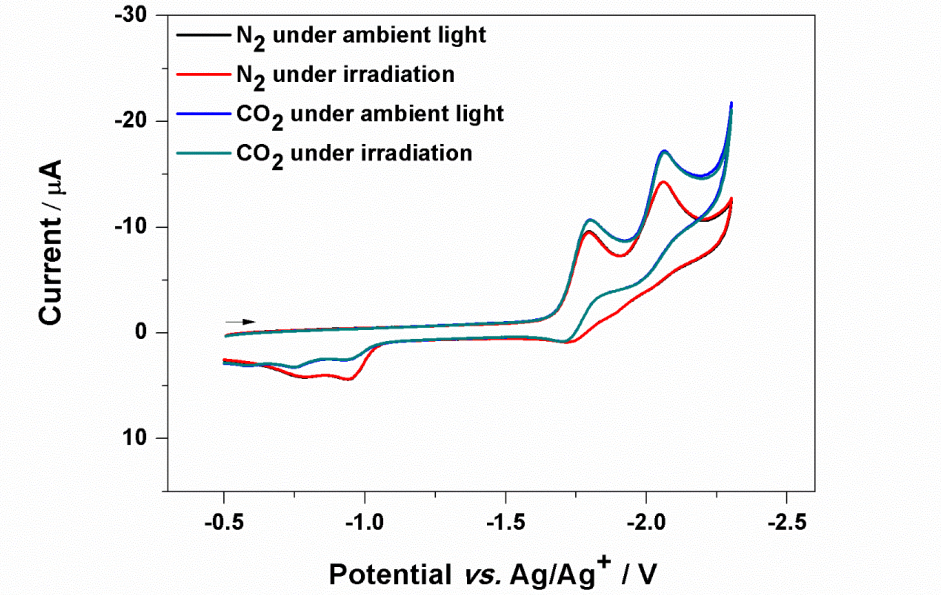

Figure 4–11: Cyclic voltammograms for a DMF solution containing 1.0 mM compound **Zn-1** and 0.1 M $TBAPF_6$ in the presence of N_2 under the ambient light (black line), N_2 under halogen-lamp radiation (red line), CO_2 under the ambient light (blue line) and CO_2 under halogen-lamp radiation (green line) recorded at the scan rate of 100 $mV \cdot s^{-1}$ in the range of –0.5 to –2.3 V

4.2.6 Compound Co-1

In a similar manner to the electrochemical measurement of compound **1**, cyclic voltammograms of compound **Co-1** were recorded in the potential ranges of –0.5 to –1.65 V (**Figure 4–12**) and –0.5 to –2.3 V (**Figure 4–13**) at 100 $mV \cdot s^{-1}$. Under N_2 saturated condition, a solution of compound **Co-1** in the ambient light and halogen-lamp light gave similar voltammograms and showed one reversible reduction peak with the cathodic peak potential of –1.04 V. The second reduction peak was not observed in this potential range. According to the previously published results [selected publications: [61, 75, 76]], Co(II)-porphyrins normally gave two reduction peaks. However, only one reduction peak was observed in this experiment. It is possible that more negative potential was required. In the presence of CO_2 under the ambient light and the radiation, the first reduction peak appears almost the same potential with slight decrease in the current in comparison with the peak observed under N_2-saturated condition. At –2.3 V, the current increasingly changed from 11.9 μA as observed in N_2 saturated condition to 23.5 μA. These results indicated that the first reduction of **Co-1** was not affected by the halogen lamp in the presence of CO_2 and the second reduction, which seemed to occur beyond –2.3 V, changed in current size with CO_2, implying that **Co-1** has somewhat tendency to accelerate reduction of CO_2.

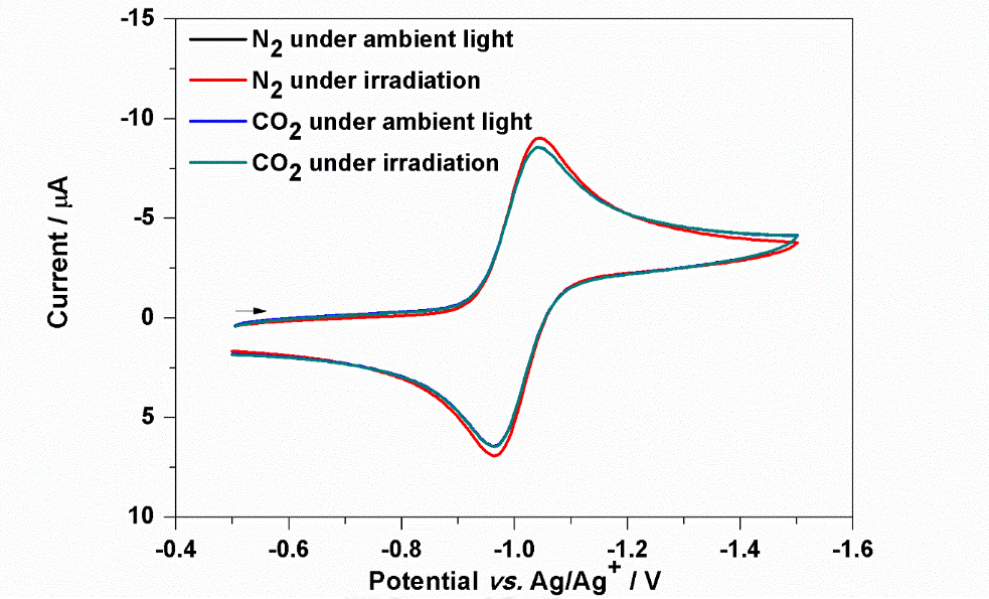

Figure 4–12: Cyclic voltammograms for a DMF solution containing 1.0 mM compound **Co-1** 0.1 M $TBAPF_6$ in the presence of N_2 under the ambient light (black line), N_2 under halogen-lamp radiation (red line), CO_2 under the ambient light (blue line) and CO_2 under halogen-lamp radiation (green line) recorded at the scan rate of 100 $mV \cdot s^{-1}$ in the range of –0.5 to –1.5 V

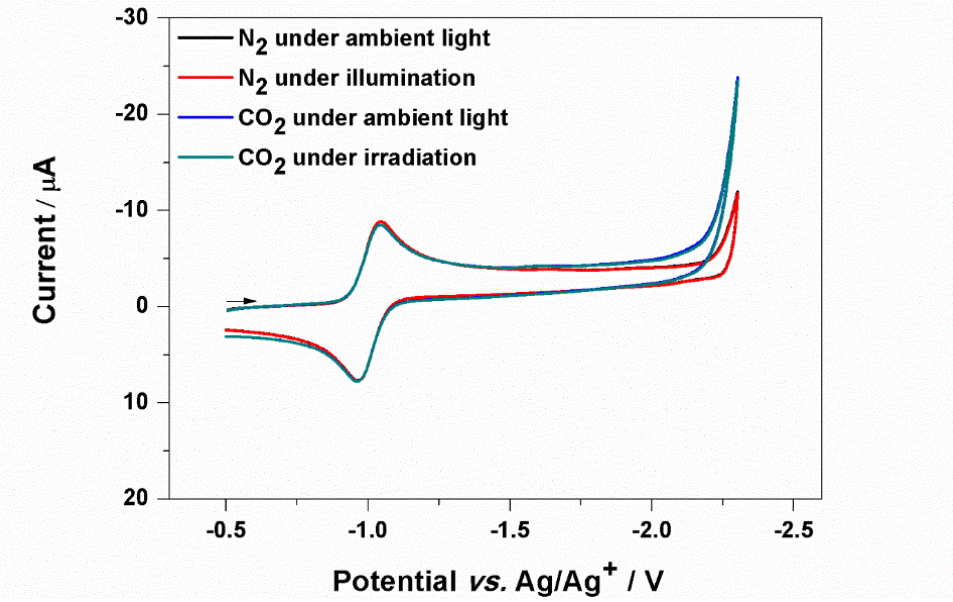

Figure 4–13: Cyclic voltammograms for a DMF solution containing 1.0 mM compound **Co-1** and 0.1 M $TBAPF_6$ in the presence of N_2 under the ambient light (black line), N_2 under halogen-lamp radiation (red line), CO_2 under the ambient light (blue line) and CO_2 under halogen-lamp radiation (green line) recorded at the scan rate of 100 $mV \cdot s^{-1}$ in the range of –0.5 to –2.3 V

4.2.7 Compound $Sn(OH)_2$-1

Cyclic voltammograms of **$Sn(OH)_2$-1** were recorded in the range of –0.5 to –1.4 V (**Figure 4–14**) and –0.5 to –2.3 V (**Figure 4–15**) at the scan rate of 100 $mV \cdot s^{-1}$. As shown in **Figure 4–14**, cyclic voltammograms of N_2 saturated solution of **$Sn(OH)_2$-1** under the ambient light (black line) and under radiation (red line) showed the first reversible reduction peak at –1.21 V. When the compound **$Sn(OH)_2$-1** solution was saturated with CO_2 under the ambient light (blue line) and the radiation (green line), its cyclic voltammograms showed reversible reduction peak with small increase in cathodic current. This result indicates that the first reduction was not affected by CO_2.

In **Figure 4–15**, the second reduction showed quasi-reversible peak at –1.64 V in N_2 atmosphere. Under CO_2 saturated condition, a solution of compound **$Sn(OH)_2$-1** showed irreversible potential peaks at –1.21 and –1.62 V. The second reduction peak was found with the positive shift by 20 mV and the increase in current from 7.4 μA to 7.7 μA. Moreover, three new irrevesible anodic peaks were found in the range of –0.60 and –1.30 V, indicating the different reductive procees(es) compared to that happened in the N_2 saturated system. Since the results showed small current enhancement and small positive shift of potential in the presence of **$Sn(OH)_2$-1** and CO_2, it can suggest that **$Sn(OH)_2$-1** showed low tendency for catalyzing the reduction of CO_2. Upon radiation by the halogen lamp, the cyclic voltammograms under N_2 and CO_2 saturated conditions were very similar to those observed under the ambient light, indicating that **$Sn(OH)_2$-1** catalyzed reduction of CO_2 was hardly affected by halogen-lamp irradiation.

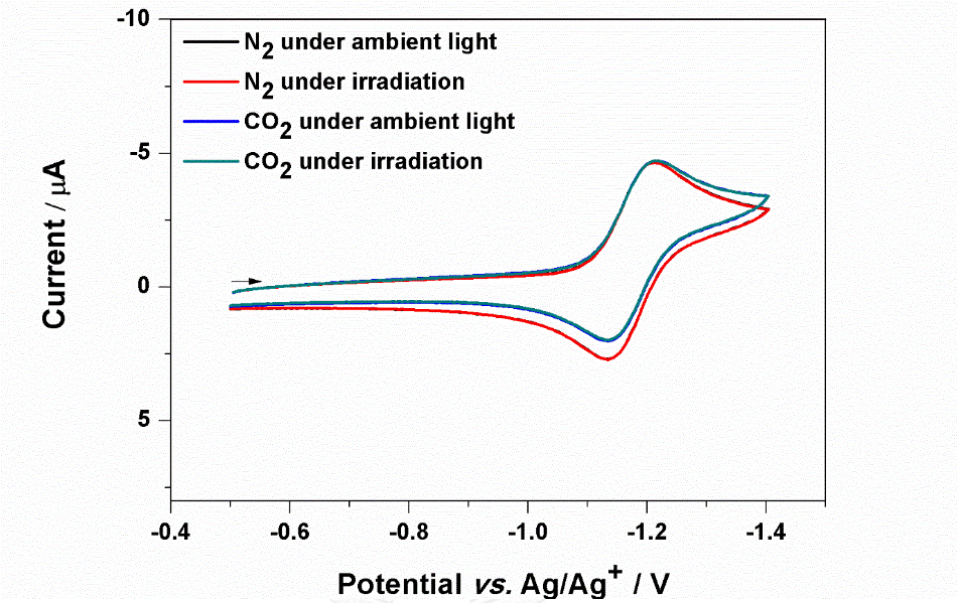

Figure 4–14: Cyclic voltammograms for a DMF solution containing 1.0 mM compound **Sn(OH)$_2$-1** and 0.1 M TBAPF$_6$ in the presence of N_2 under the ambient light (black line), N_2 under halogen-lamp radiation (red line), CO_2 under the ambient light (blue line) and CO_2 under halogen-lamp radiation (green line) recorded at the scan rate of 100 mV·s^{-1} in the range of –0.5 to –1.4 V

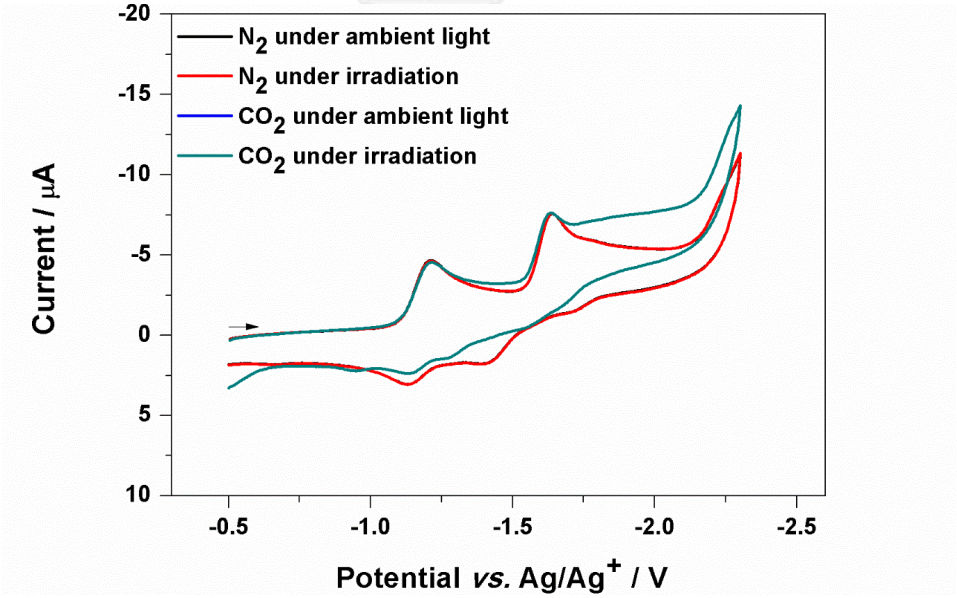

Figure 4–15: Cyclic voltammograms for a DMF solution containing 1.0 mM compound **Sn(OH)$_2$-1** and 0.1 M TBAPF$_6$ in the presence of N_2 under the ambient ligh t (black line), N_2 under halogen-lamp iradiation (red line), CO_2 under the ambient light (blue line) and CO_2 under halogen-lamp radiation (green line) recorded at the scan rate of 100 mV·s^{-1} in the range of –0.5 to –2.3 V

According to the cyclic voltammetric result, the electrochemical data of **1** and its metallobenzoporphyrin derivatives were summarized in **Tables 4–2**. It should be noted that the reduction peaks and potentials observed under the ambient light and radiation were almost identical, revealing that light from the halogen lamp did not affect the electrochemical behavior of all compounds significantly. Under the N_2 saturated and CO_2 conditions, the second reduction of compound **1** showed great negative shift of the reduction potential, suggesting that the compound **1** may bind with CO_2 to generate the new species that has different electrochemical behavior, as mentioned above. The first reduction under the N_2 saturated and CO_2 saturated conditions of **Co-1**, **Sn(OH)$_2$-1**, **Ni-1**, **Cu-1** and **Zn-1** presented similar potential reduction in the range of –1.04 V to –1.79 V. As for the second reduction, cyclic voltammograms of these compounds recorded under both N_2 and CO_2 saturated conditions were found to be varied. **Zn-1** and **Sn(OH)$_2$-1** showed similar electrochemical behaviors with small positive shift at –2.06 V and –1.64 V, respectively. **Ni-1** and **Cu-1** gave irreversible reduction peaks at –2.27 and –2.16 V, respectively, that positively shifted by 70 and 30 mV, respectively. The second reduction peak of **Co-1** was not observed in this potential range and more negative potential may be required as mentioned in section **4.2.6**. From these results, it indicates that the metallobenzoporphyrin derivatives gave small shift of the redox potentials on the reduction of CO_2.

Table 4–2 Electrochemical data of compound **1** and metallobenzoporphyrin derivatives from their cyclic voltammograms in a DMF solution containing 0.1 M $TBAPF_6$ saturated with N_2 and CO_2 under the ambient light and the halogen-lamp radiation at 100 $mV \cdot s^{-1}$ in the potential range of –0.5 to –2.3 V.

Compound	Condition	Cathodic peak potential (V)	
		First peak	Second peak
1	N_2	–1.49	–1.78
	CO_2	–1.46	–2.06
Ni-1	N_2	–1.46	–2.27
	CO_2	–1.46	–2.20
Cu-1	N_2	–1.52	–2.16
	CO_2	–1.52	–2.13
Zn-1	N_2	–1.79	–2.06
	CO_2	–1.79	–2.06
Co-1	N_2	–1.04	–[a]
	CO_2	–1.04	–[a]
Sn(OH)$_2$-1	N_2	–1.21	–1.64
	CO_2	–1.21	–1.62

[a] The peak potential cannot be measured.

The current and the current enhancement caused by the presence of compound **1** and its metallobenzoporphyrin derivatives under the N_2 and CO_2 saturated conditions are shown in **Table 4–3**. Compared between the cyclic voltammograms of compound **1** obtained under the N_2 and CO_2 saturated conditions, the first reduction peaks was slightly increased, while the second one showed high current enhancement. However, as mentioned above, the mechanistic investigation of the process has to be studied in detail. The first reduction of **Ni-1**, **Cu-1**, **Zn-1**, **Co-1** and **Sn(OH)$_2$-1** under the N_2 and CO_2 saturated conditions showed the current change in the range of −0.3 µA and 0.9 µA, which is equivalent to a −7.3% and a 9.5% current enhancement, suggesting that the metallobenzoporphyrin derivatives showed no significant current enhancement in their first reduction. As for their second reduction peaks under the N_2 and CO_2 saturated conditions, **Zn-1** and **Sn(OH)$_2$-1** gave current enhancement of 2.5 µA and 0.3 µA, or 17.3% and 4.1%, respectively, while **Ni-1** and **Cu-1** exhibited the current enhancement of 20.2 µA and 47.1 µA, which is equivalent to 92.4% and 154.0%, respectively. The second peak of compound **Co-1** was not observed in these potential ranges. Therefore, the current enhancement was evaluated at −2.3 V, and found to be 97.5%.

The above-mentioned observation suggested that the reduction of CO_2 can be electrochemically catalyzed by these metallobenzoporphyrins. Based on the previous study [77], the reactions are possibly metal centered and simplified mechanism is presented in the below reaction. It is possible that the electrons are transferred to the electrocatalyst and then $M(I)L^{\bullet -}$ may further react with CO_2.

$$M(II)L + e^{-} \longrightarrow M(I)L^{\bullet -}$$

Since good electrocatalyst should exhibit proper reduction potential reduction and gave the high current enhancement, we can hereby conclude that the good electrocatalyst for the electrochemical reduction of CO_2 is **Cu-1**, the moderate catalysts are **Ni-1** and **Co-1**, and **Zn-1** and **Sn(OH)$_2$-1** are poor catalysts. As for compound **1**, it is hard to conclude from the results in this study and therefore detailed studies are required.

Table 4–3 Current and increase in current of the reduction of CO_2 catalyzed by **1** and its metallobenzoporphyrin derivatives.

Compound	Cathodic Peak	Current under ambient light (μA)		$I_{CO_2}–I_{N_2}$ (μA)	% increase in current[a]
		N_2 saturated condition (I_{N_2})	CO_2 saturated condition (I_{CO_2})		
1	1	10.6	21.8	11.2	105.0
	2	14.4	31.5	17.1	119.0
Ni-1	1	4.1	3.9	–0.3	–7.3
	2	10.5	20.2	9.7	92.4
Cu-1	1	11.3	12.2	0.9	8.0
	2	18.5	47.1	28.5	154.0
Zn-1	1	9.8	10.6	0.8	8.2
	2	16.9	16.9	2.5	17.3
Co-1	1	8.5	8.8	0.8	8.2
	2	11.9[b]	23.5[b]	11.6[b]	97.5[b]
$Sn(OH)_2$-1	1	4.2	4.6	0.4	9.5
	2	7.4	7.7	0.3	4.1

[a] % increase in current was calculated from: % increase = $((I_{CO_2}–I_{N_2})/I_{N_2})\times100$

[b] The values from the signal at –2.3 V

CHAPTER V
CONCLUSION

The metallobenzoporphyrin derivatives and compound **1** were successfully synthesized from the condensation between isoindole **3** and benzaldehyde under Lindsey's condition. The overall yields for all compounds are 48 to 97%. The formation of the benzoporphyrin derivatives were confirmed by spectroscopic techniques. Their electrocatalytic activity on the homogeneous system for the reduction of CO_2 was performed by means of cyclic voltammetry. Cyclic voltammetric results exhibited that **Cu-1** is found to be the most potential catalyst for the reduction of CO_2. **Ni-1** and **Co-1** showed moderate catalytic activity, and **Zn-1** and **Sn(OH)$_2$-1** are poor catalysts. As for compound **1**, further studies have yet to be done. The results also indicated that light had no significant effect on the electrochemical behavior of all compounds. To further develop these compounds as good electrocatalysts for the reduction of CO_2, the product analysis of the reduction should be investigated.

REFERENCES

1. Aresta, M., *Carbon dioxide recovery and utilization*. 2003: Springer.
2. Taniguchi, I., *Electrochemical and photoelectrochemical reduction of carbon dioxide*, in *Modern Aspects of Electrochemistry No. 20*. 1989, Springer. p. 327-400.
3. Aresta, M., *Carbon dioxide as chemical feedstock*. 2010: John Wiley & Sons.
4. O'Connor, A.E., W.M. Gallagher, and A.T. Byrne, *Porphyrin and nonporphyrin photosensitizers in oncology: preclinical and clinical advances in photodynamic therapy.* Photochemistry and photobiology, 2009. **85**(5): p. 1053-1074.
5. Anderson, H.L., *Building molecular wires from the colours of life: conjugated porphyrin oligomers.* Chemical Communications, 1999(23): p. 2323-2330.
6. Krebs, F.C. and H. Spanggaard, *Antibatic photovoltaic response in zinc-porphyrin-linked oligothiophenes.* Solar energy materials and solar cells, 2005. **88**(4): p. 363-375.
7. Kadish, K.M., K.M. Smith, and R. Guilard, *The porphyrin handbook*. 1999: Elsevier.
8. Van Patten, P.G., et al., *Energy-transfer modeling for the rational design of multiporphyrin light-harvesting arrays.* The Journal of Physical Chemistry B, 1998. **102**(21): p. 4209-4216.
9. Metz, B., et al., *Carbon dioxide capture and storage*. 2005: IPCC Geneva, Switzerland.
10. Furukawa, H. and O.M. Yaghi, *Storage of hydrogen, methane, and carbon dioxide in highly porous covalent organic frameworks for clean energy applications.* Journal of the American Chemical Society, 2009. **131**(25): p. 8875-8883.
11. Grodkowski, J., et al., *Iron porphyrin-catalyzed reduction of CO2. Photochemical and radiation chemical studies.* The Journal of Physical Chemistry A, 1997. **101**(3): p. 248-254.
12. Hammouche, M., et al., *Chemical catalysis of electrochemical reactions. Homogeneous catalysis of the electrochemical reduction of carbon dioxide by iron (" 0") porphyrins. Role of the addition of magnesium cations.* Journal of the American Chemical Society, 1991. **113**(22): p. 8455-8466.
13. Battersby, A.R., et al., *Biosynthesis of the pigments of life: formation of the macrocycle.* Nature, 1980. **285**(5759): p. 17-21.
14. Miller, J.W., et al., *Photodynamic therapy of experimental choroidal neovascularization using lipoprotein-delivered benzoporphyrin.* Archives of ophthalmology, 1995. **113**(6): p. 810-818.
15. Matsuo, Y., et al., *Columnar structure in bulk heterojunction in solution-processable three-layered pin organic photovoltaic devices using tetrabenzoporphyrin precursor and silylmethyl [60] fullerene.* Journal of the American Chemical Society, 2009. **131**(44): p. 16048-16050.
16. Scheer, H. and J.J. Katz, *Nuclear magnetic resonance spectroscopy of porphyrins and metalloporphyrins.* 1975.

17. Saito, S. and A. Osuka, *Expanded porphyrins: intriguing structures, electronic properties, and reactivities.* Angewandte Chemie International Edition, 2011. **50**(19): p. 4342-4373.
18. Yoon, Z.S., A. Osuka, and D. Kim, *Möbius aromaticity and antiaromaticity in expanded porphyrins.* Nature chemistry, 2009. **1**(2): p. 113-122.
19. Vicente, M.G.H., L. Jaquinod, and K.M. Smith, *Oligomeric porphyrin arrays.* Chemical Communications, 1999(18): p. 1771-1782.
20. Thunell, S., *Porphyrins, porphyrin metabolism and porphyrias. I. Update.* Scandinavian journal of clinical & laboratory investigation, 2000. **60**(7): p. 509-540.
21. Smith, K.M. and J.E. Falk, *Porphyrins and metalloporphyrins*. 1975: Elsevier Amsterdam.
22. Paolesse, R., et al., *Photophysical behaviour of corrole and its symmetrical and unsymmetrical dyads.* Journal of Porphyrins and Phthalocyanines, 1999. **3**(05): p. 364-370.
23. Stępień, M., et al., *Expanded Porphyrin with a Split Personality: A Hückel–Möbius Aromaticity Switch.* Angewandte Chemie, 2007. **119**(41): p. 8015-8019.
24. Granström, M., et al., *Laminated fabrication of polymeric photovoltaic diodes.* Nature, 1998. **395**(6699): p. 257-260.
25. Kay, A. and M. Graetzel, *Artificial photosynthesis. 1. Photosensitization of titania solar cells with chlorophyll derivatives and related natural porphyrins.* The Journal of Physical Chemistry, 1993. **97**(23): p. 6272-6277.
26. Campbell, W.M., et al., *Highly efficient porphyrin sensitizers for dye-sensitized solar cells.* The Journal of Physical Chemistry C, 2007. **111**(32): p. 11760-11762.
27. Friend, R., et al., *Electroluminescence in conjugated polymers.* Nature, 1999. **397**(6715): p. 121-128.
28. Li, B., et al., *Porphyrins with four monodisperse oligofluorene arms as efficient red light-emitting materials.* Journal of the American Chemical Society, 2004. **126**(11): p. 3430-3431.
29. Kathiravan, A., et al., *Photoinduced electron transfer reactions between meso-tetrakis (4-sulfonatophenyl) porphyrin and colloidal metal-semiconductor nanoparticles.* Colloids and Surfaces A: Physicochemical and Engineering Aspects, 2009. **333**(1): p. 175-181.
30. Berezin, B., et al., *Chlorophyll and its derivatives, chlorins and porphyrins, as a promising class of environmentally friendly dyes.* Russian journal of applied chemistry, 2003. **76**(12): p. 1958-1961.
31. Lee, C.Y. and J.T. Hupp, *Dye sensitized solar cells: TiO2 sensitization with a bodipy-porphyrin antenna system.* Langmuir, 2009. **26**(5): p. 3760-3765.
32. Breton, M.P., A.R. Davidson, and F.M. Winnik, *Colorless fast-drying ink compositions for printing concealed images detectable by fluorescence*. 1994, Google Patents.
33. Rahiman, A.K., et al., *Catalytic oxidation of alkenes by manganese (III) porphyrin-encapsulated Al, V, Si-mesoporous molecular sieves.* Inorganica Chimica Acta, 2009. **362**(5): p. 1491-1500.

34. Ogawa, T., et al., *Completely Regioselective Synthesis of Directly Linked meso, meso and meso, β Porphyrin Dimers by One-Pot Electrochemical Oxidation of Metalloporphyrins.* Angewandte Chemie International Edition, 1999. **38**(1-2): p. 176-179.
35. Wang, Z., C.J. Medforth, and J.A. Shelnutt, *Self-metallization of photocatalytic porphyrin nanotubes.* Journal of the American Chemical Society, 2004. **126**(51): p. 16720-16721.
36. Fang, Z. and B. Liu, *A cationic porphyrin-based self-assembled film for mercury ion detection.* Tetrahedron Letters, 2008. **49**(14): p. 2311-2315.
37. Mizutani, T., K. Wada, and S. Kitagawa, *Porphyrin receptors for amines, amino acids, and oligopeptides in water.* Journal of the American Chemical Society, 1999. **121**(49): p. 11425-11431.
38. Papkovsky, D.B., et al., *Phosphorescent complexes of porphyrin ketones: optical properties and application to oxygen sensing.* Analytical Chemistry, 1995. **67**(22): p. 4112-4117.
39. Fukushima, K., K. Tabata, and I. Okura, *Photochemical properties of water-soluble fluorinated zinc phthalocyanines and their photocytotoxicity against HeLa cells.* Journal of Porphyrins and Phthalocyanines, 1998. **2**(3): p. 219-222.
40. Bonnett, R., *Photosensitizers of the porphyrin and phthalocyanine series for photodynamic therapy.* Chem. Soc. Rev., 1995. **24**(1): p. 19-33.
41. Wolf, P., E. Rieger, and H. Kerl, *Topical photodynamic therapy with endogenous porphyrins after application of 5-aminolevulinic acid: an alternative treatment modality for solar keratoses, superficial squamous cell carcinomas, and basal cell carcinomas?* Journal of the American Academy of Dermatology, 1993. **28**(1): p. 17-21.
42. Baker, E.W., *Mass Spectrometric Characterization of Petroporphyrins1*. Journal of the American Chemical Society, 1966. **88**(10): p. 2311-2315.
43. Ménard, F., et al., *Synthesis of tetraglucosyl-and tetrapolyamine–tetrabenzoporphyrin conjugates for an application in PDT.* Bioorganic & medicinal chemistry, 2009. **17**(22): p. 7647-7657.
44. Husain, D., et al., *Intravenous infusion of liposomal benzoporphyrin derivative for photodynamic therapy of experimental choroidal neovascularization.* Archives of ophthalmology, 1996. **114**(8): p. 978-985.
45. Ciofini, I., et al., *Solvent effects on molecular reactivity descriptors: some test cases.* Theoretical Chemistry Accounts, 2004. **111**(2-6): p. 188-195.
46. Oulianov, D.A., et al. *Investigation of benzoporphyrin and azulenic compounds by two-dimensional z-scan technique*. in *SPIE Proceedings*. 1998.
47. Vinogradov, S.A. and D.F. Wilson, *Metallotetrabenzoporphyrins. New phosphorescent probes for oxygen measurements.* J. Chem. Soc., Perkin Trans. 2, 1995(1): p. 103-111.
48. Ku, S.Y., et al., *Solution-Processed Nanostructured Benzoporphyrin with Polycarbonate Binder for Photovoltaics.* Advanced Materials, 2011. **23**(20): p. 2289-2293.
49. Sato, Y., et al. *Organic photovoltaic cell based on benzoporphyrin with pin junction*. in *Proc. SPIE*. 2008.
50. Wang, J., *Analytical electrochemistry*. 2006: John Wiley & Sons.

51. *http://www.gamry.com/products/electrochemical-cells/eurocell-corrosion-cell/.* (Barton-Zard).
52. Nicholson, R.S., *Theory and Application of Cyclic Voltammetry for Measurement of Electrode Reaction Kinetics.* Analytical Chemistry, 1965. **37**(11): p. 1351-1355.
53. Catalyst, o.A.f.h.g.i.o.C.h., Dec 3]. *catalyst*. 2013, http://goldbook.iupac.org/C00876.html
54. Type of catalyst, o.A.f.h.c.c.u.p.c.i.h., *Type of catalyst*. http://chemguide.co.uk/physical/.
55. https://en.wikipedia.org/wiki/Heterogeneous_catalysis, *heterogeous catalyst.*
56. Andrieux, C., et al., *Homogeneous redox catalysis of electrochemical reactions: Part V. Cyclic voltammetry.* Journal of Electroanalytical Chemistry and Interfacial Electrochemistry, 1980. **113**(1): p. 19-40.
57. Plass, G.N., *The carbon dioxide theory of climatic change.* Tellus, 1956. **8**(2): p. 140-154.
58. Idso, S.B., et al., *Effects of atmospheric CO2 enrichment and foliar methanol application on net photosynthesis of sour orange tree (Citrus aurantium; Rutaceae) leaves.* American Journal of Botany, 1995: p. 26-30.
59. Rajeshwar, K., J. Ibanez, and G. Swain, *Electrochemistry and the environment.* Journal of Applied Electrochemistry, 1994. **24**(11): p. 1077-1091.
60. Wang, W., et al., *Recent advances in catalytic hydrogenation of carbon dioxide.* Chem. Soc. Rev., 2011. **40**(7): p. 3703-3727.
61. Behar, D., et al., *Cobalt porphyrin catalyzed reduction of CO2. Radiation chemical, photochemical, and electrochemical studies.* The Journal of Physical Chemistry A, 1998. **102**(17): p. 2870-2877.
62. Sonoyama, N., M. Kirii, and T. Sakata, *Electrochemical reduction of CO< sub> 2</sub> at metal-porphyrin supported gas diffusion electrodes under high pressure CO< sub> 2</sub>*. Electrochemistry communications, 1999. **1**(6): p. 213-216.
63. Hammouche, A., E. Siebert, and A. Hammou, *Crystallographic, thermal and electrochemical properties of the system La< sub> 1− x</sub> Sr< sub> x</sub> MnO< sub> 3</sub> for high temperature solid electrolyte fuel cells.* Materials Research Bulletin, 1989. **24**(3): p. 367-380.
64. Ramirez, G., et al., *Enhanced photoelectrochemical catalysis of CO< sub> 2</sub> reduction mediated by a supramolecular electrode of packed Co< sup> II</sup>(tetrabenzoporphyrin).* Inorganica Chimica Acta, 2009. **362**(1): p. 5-10.
65. Pavlishchuk, V.V. and A.W. Addison, *Conversion constants for redox potentials measured versus different reference electrodes in acetonitrile solutions at 25 C.* Inorganica Chimica Acta, 2000. **298**(1): p. 97-102.
66. Fercher, A., et al., *A thermal light source technique for optical coherence tomography.* Optics communications, 2000. **185**(1): p. 57-64.
67. Borek, C., et al., *Highly Efficient, Near-Infrared Electrophosphorescence from a Pt–Metalloporphyrin Complex.* Angewandte Chemie, 2007. **119**(7): p. 1127-1130.

68. Finikova, O.S., et al., *Novel versatile synthesis of substituted tetrabenzoporphyrins.* The Journal of organic chemistry, 2004. **69**(2): p. 522-535.
69. Vogler, A., H. Kunkely, and B. Rethwisch, *Tetrabenzporphyrin complexes of iron, palladium and platinum.* Inorganica Chimica Acta, 1980. **46**: p. 101-105.
70. Strohmeier, M., et al., *Solid state 15N and 13C NMR study of several metal 5, 10, 15, 20-tetraphenylporphyrin complexes.* Journal of the American Chemical Society, 1997. **119**(30): p. 7114-7120.
71. Lysenko, A.B., et al., *Diverse porphyrin dimers as candidates for high-density charge-storage molecules.* Journal of Porphyrins and Phthalocyanines, 2006. **10**(01): p. 22-32.
72. Wang, S., et al., *Hydrogen evolution sensitized by tin-porphyrin in microheterogeneous systems.* Dyes and pigments, 2002. **55**(1): p. 27-33.
73. *Barton-Zard*. reaction: http://en.wikipedia.org/wiki/Barton%E2%80%93Zard_reaction.
74. Portenkirchner, E., et al., *Electrocatalytic and photocatalytic reduction of carbon dioxide to carbon monoxide using the alkynyl-substituted rhenium (I) complex (5, 5'-bisphenylethynyl-2, 2'-bipyridyl) Re (CO) 3 Cl.* Journal of Organometallic Chemistry, 2012. **716**: p. 19-25.
75. D'Souza, F., et al., *Electrochemical and spectroelectrochemical behavior of cobalt (III), cobalt (II), and cobalt (I) complexes of meso-tetraphenylporphyrinate bearing bromides on the. beta.-pyrrole positions.* Inorganic Chemistry, 1993. **32**(19): p. 4042-4048.
76. Aga, H., A. Aramata, and Y. Hisaeda, *The electroreduction of carbon dioxide by macrocyclic cobalt complexes chemically modified on a glassy carbon electrode.* Journal of Electroanalytical Chemistry, 1997. **437**(1): p. 111-118.
77. Isaacs, M., et al., *Electrochemical reduction of CO< sub> 2</sub> mediated by poly-M-aminophthalocyanines (M= Co, Ni, Fe): poly-Co-tetraaminophthalocyanine, a selective catalyst.* Journal of Molecular Catalysis A: Chemical, 2005. **229**(1): p. 249-257.

APPENDIX A

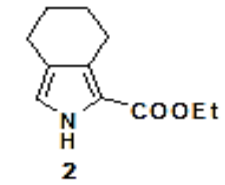

2

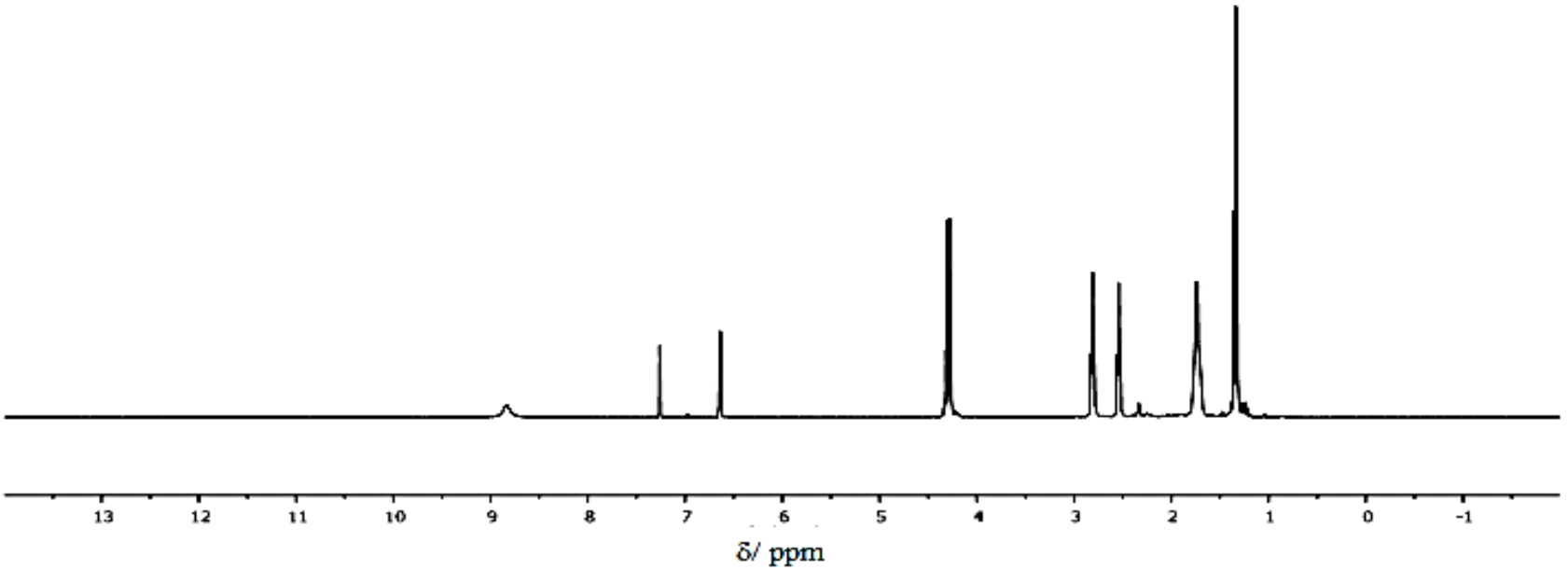

Figure A-1: ^{1}H-NMR spectrum of compound **2**

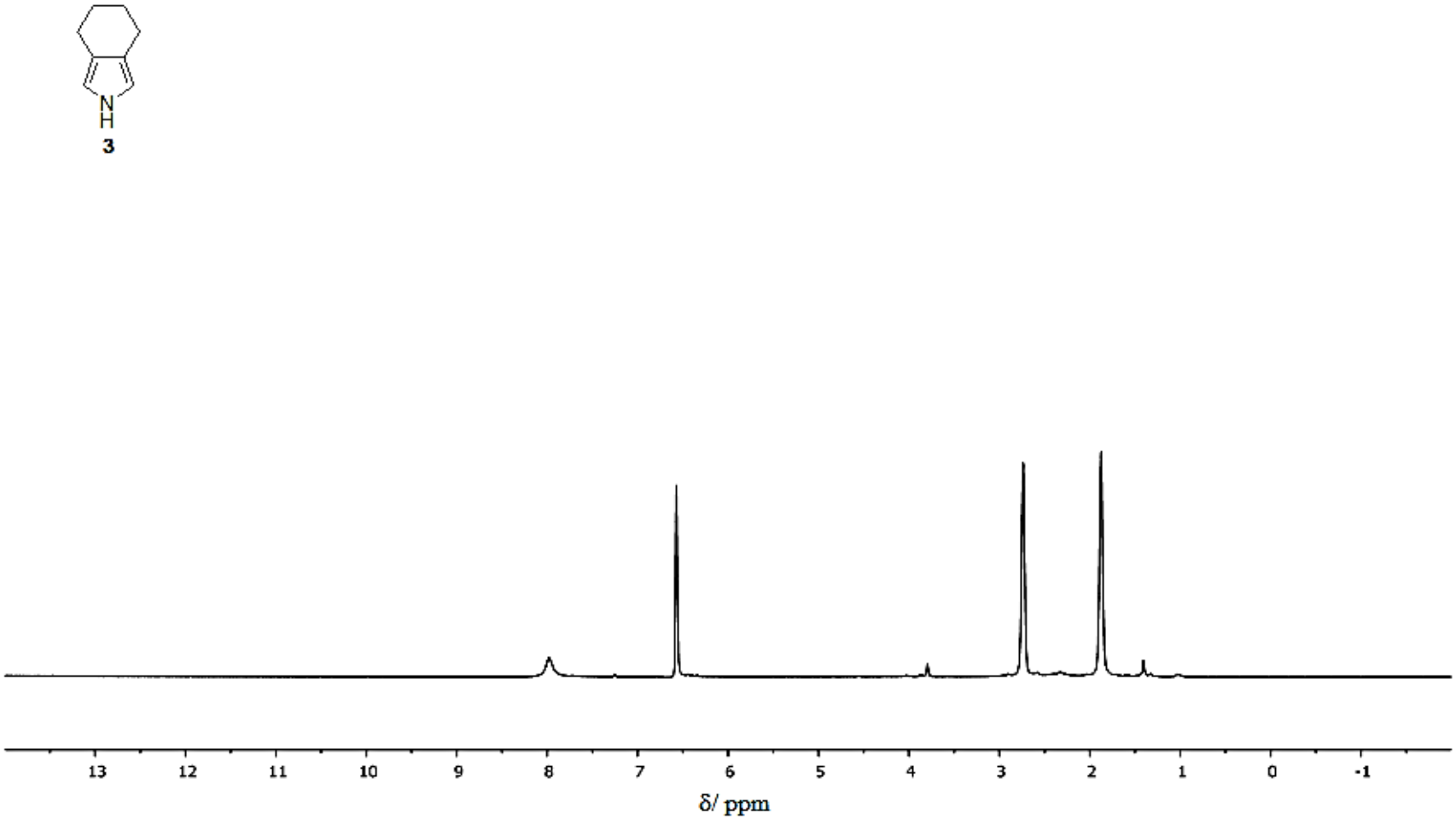

Figure A-2: ^{1}H-NMR spectrum of compound **3**

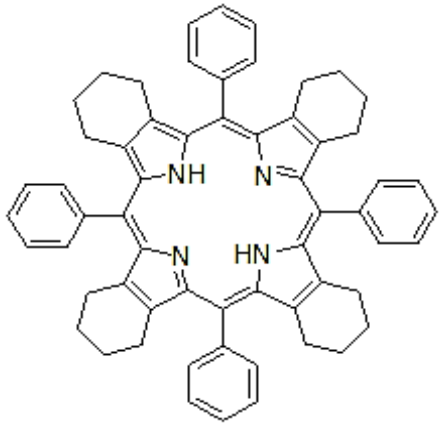

4

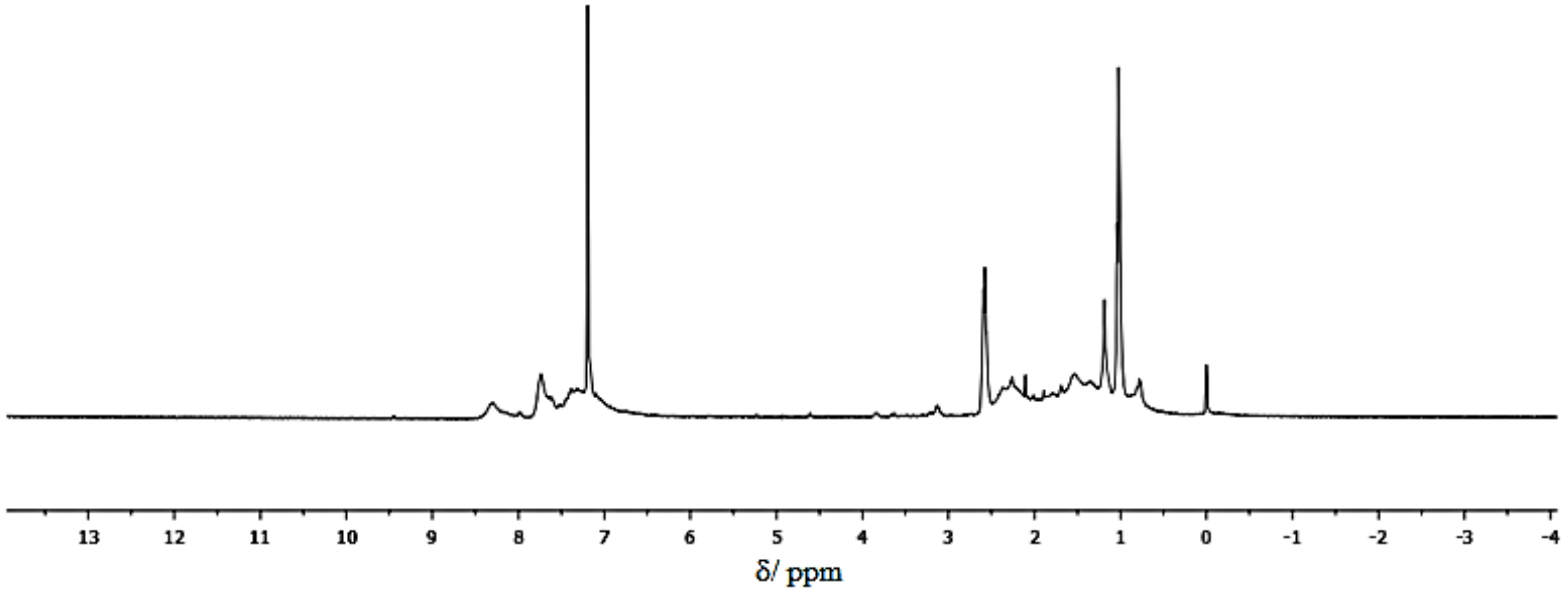

Figure A-3: ^{1}H-NMR spectrum of compound **4**

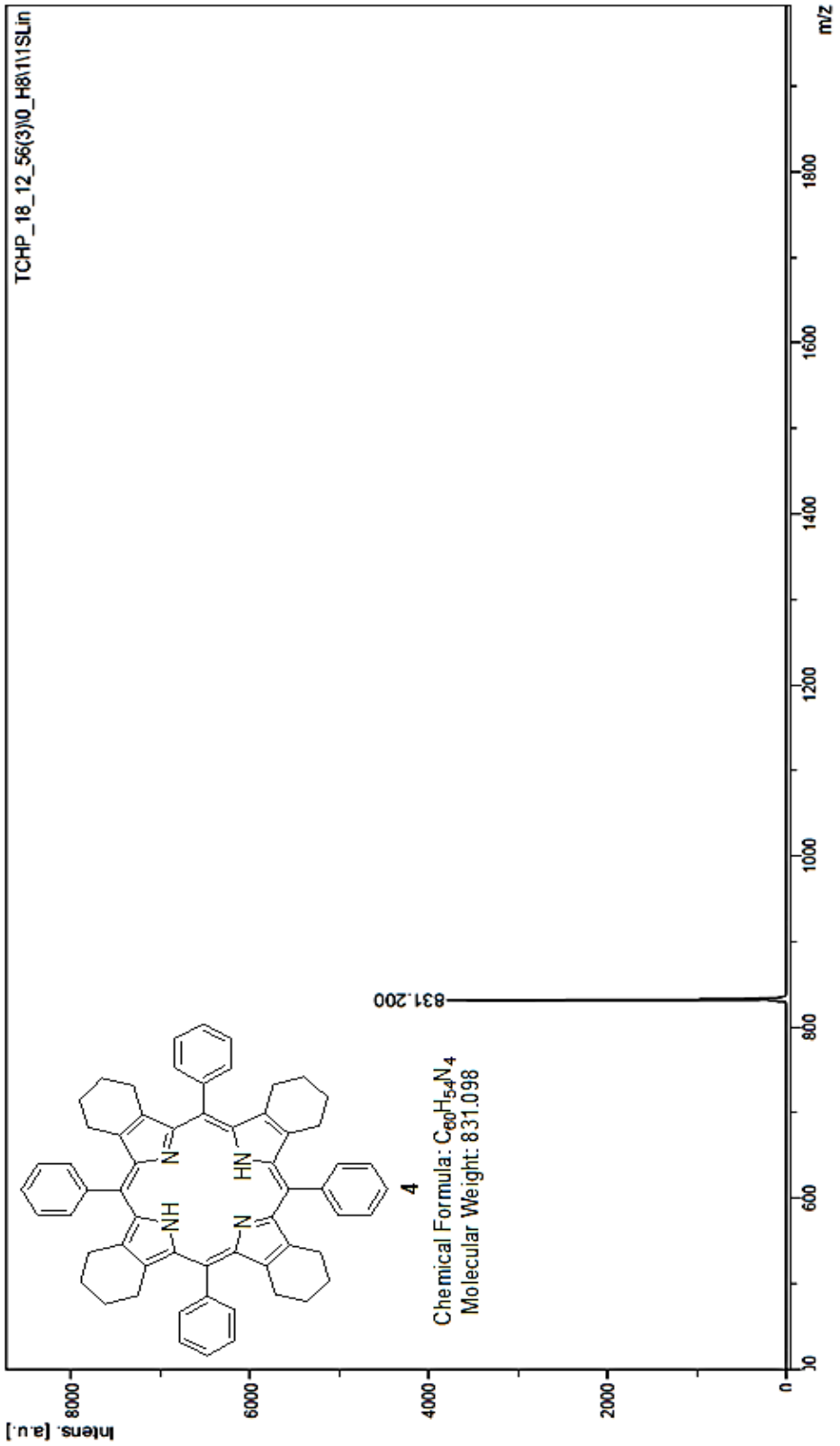

Figure A-4: MALDI-TOF mass spectrum of **4**

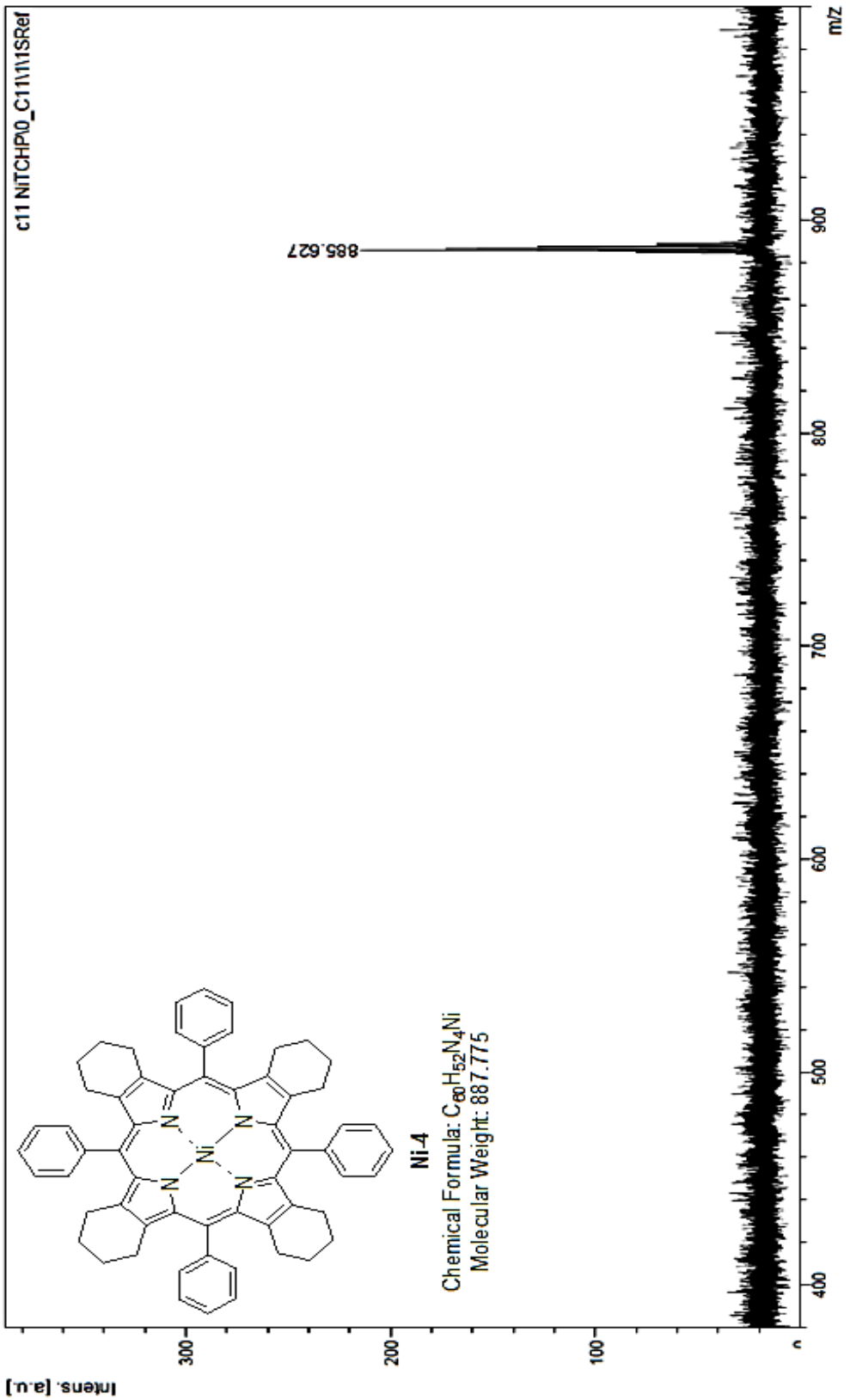

Figure A-5: MALDI-TOF mass spectrum of **Ni-4**

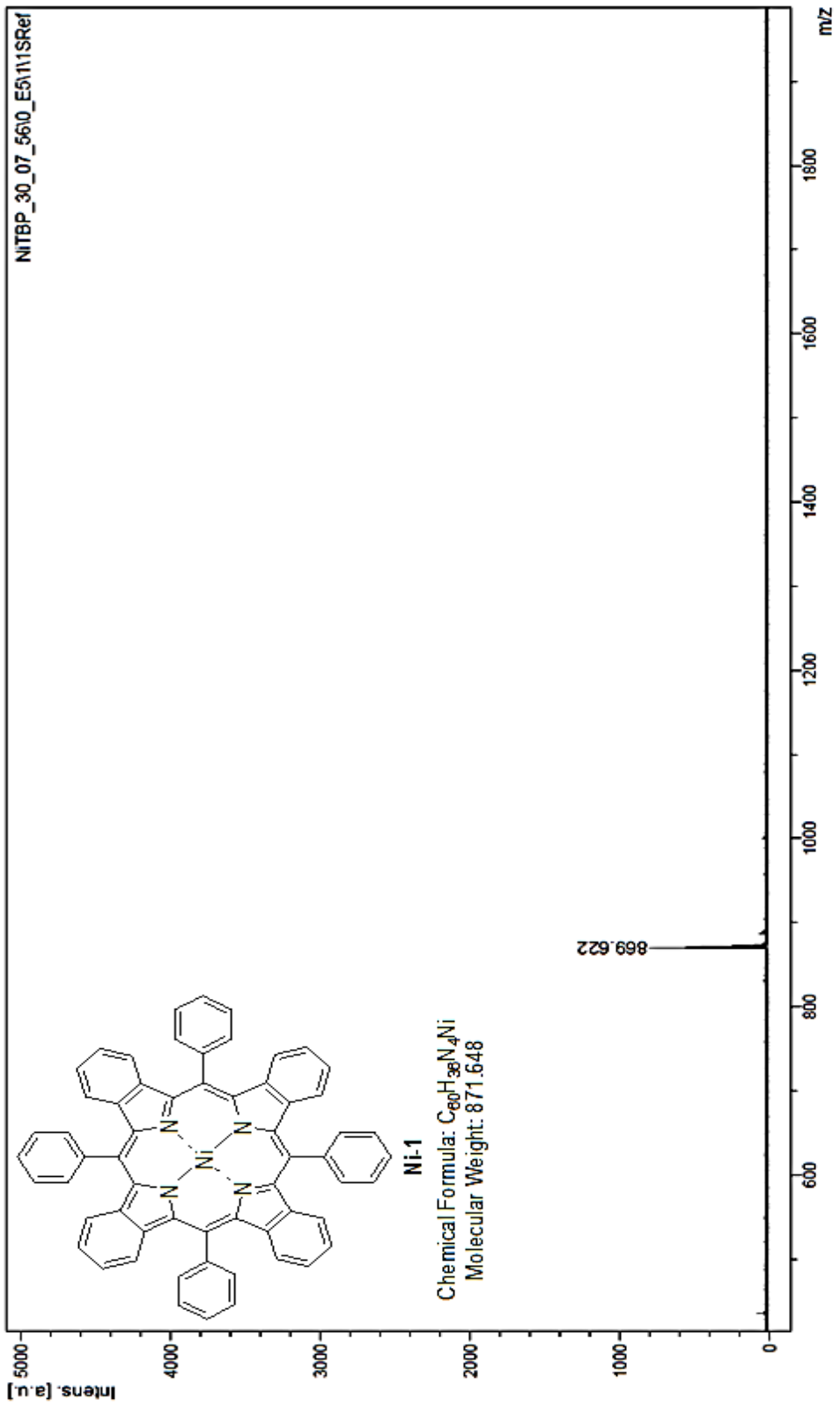

Figure A-6: MALDI-TOF mass spectrum of **Ni-1**

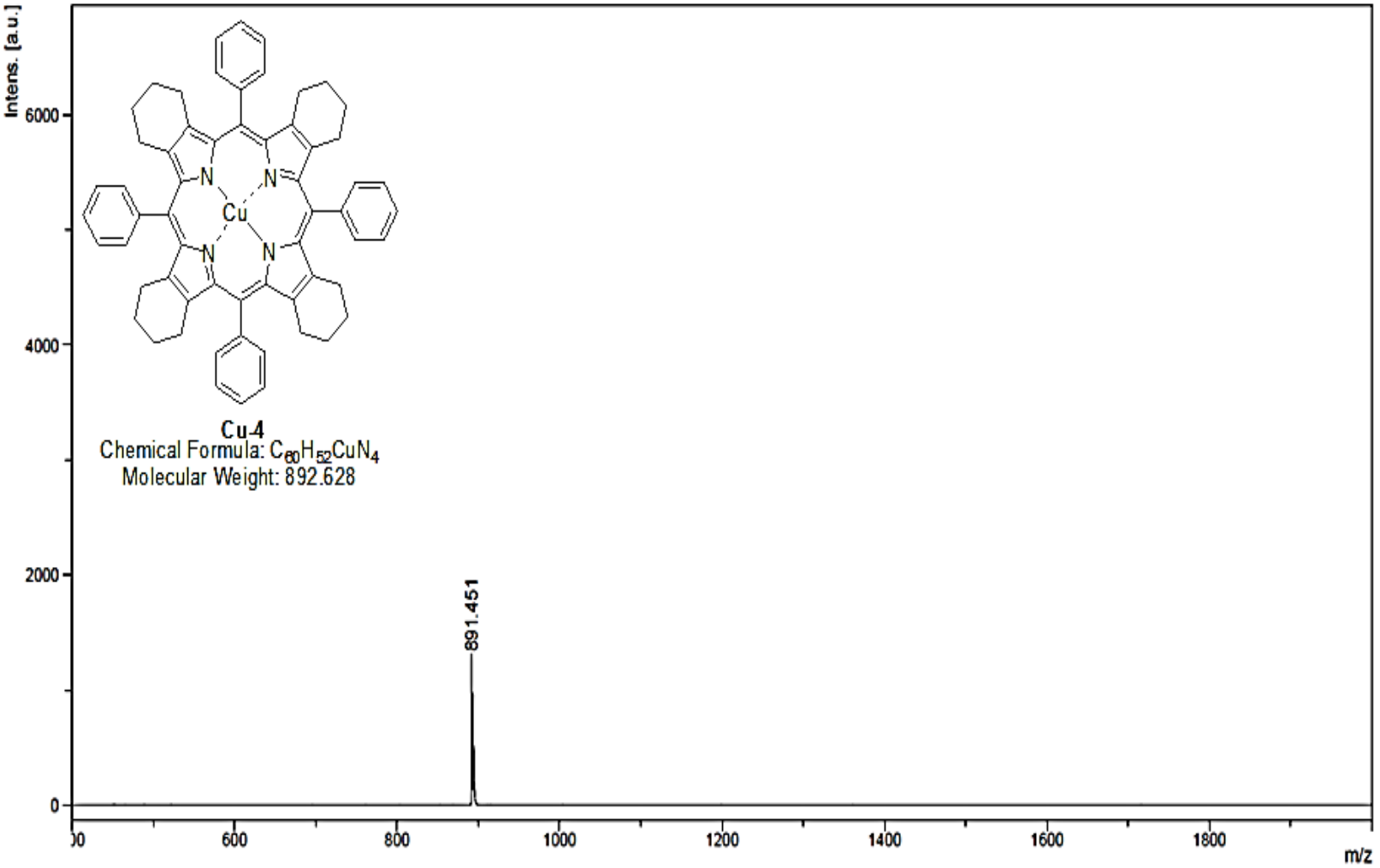

Figure A-7: MALDI-TOF mass spectrum of **Cu-4**

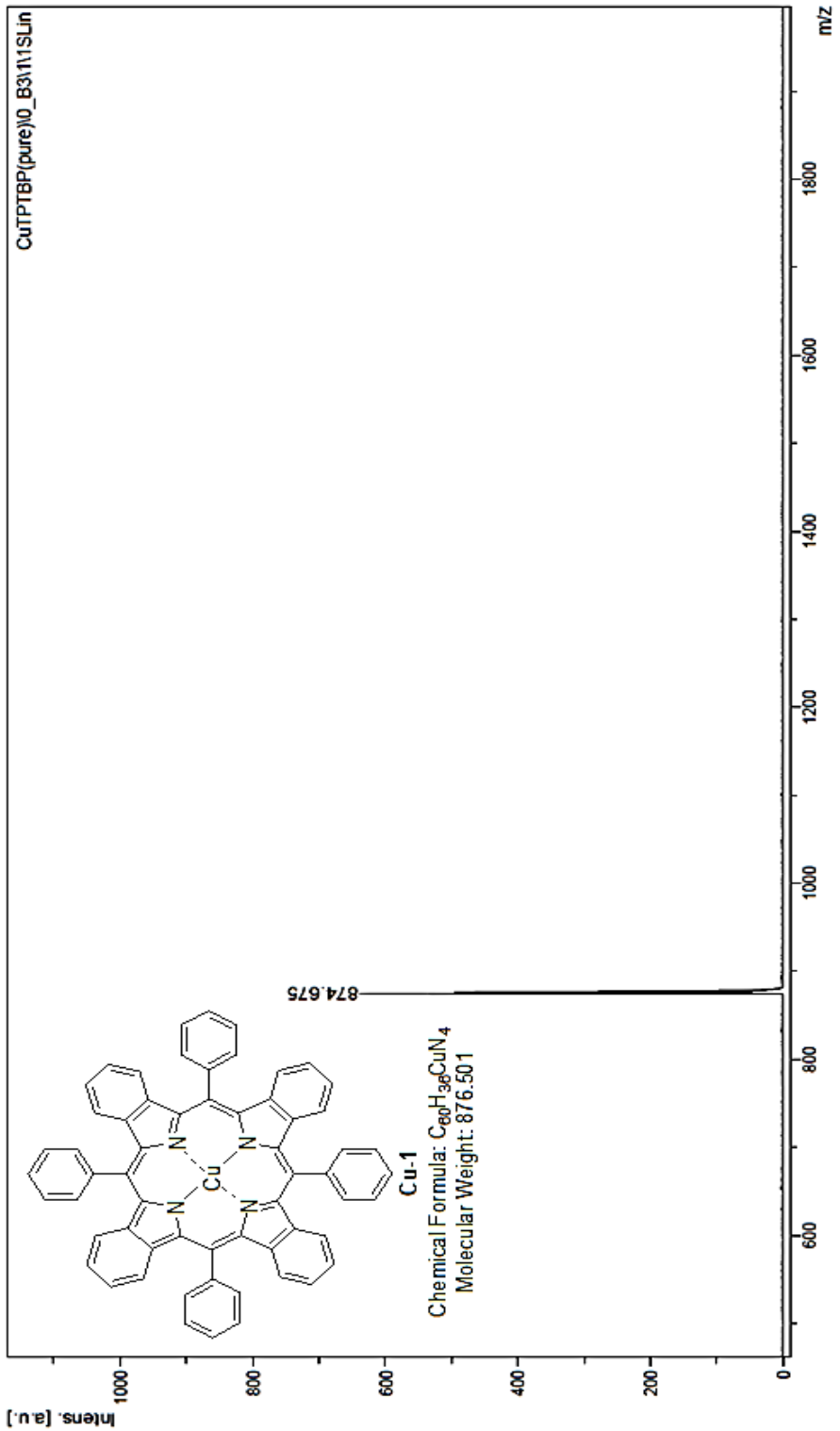

Figure A-8: MALDI-TOF mass spectrum of **Cu-1**

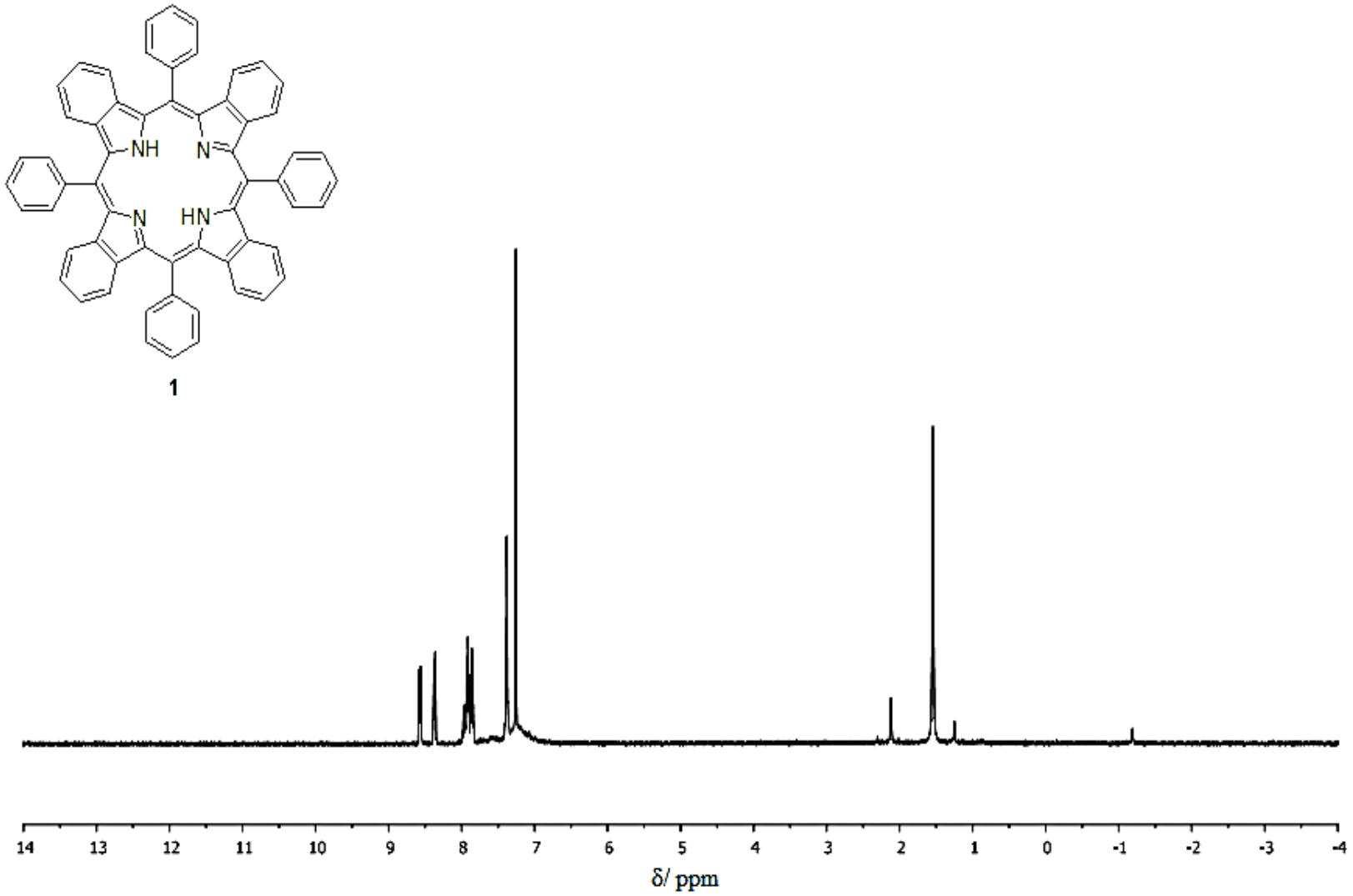

Figure A-9: ^{1}H-NMR spectrum of compound **1**

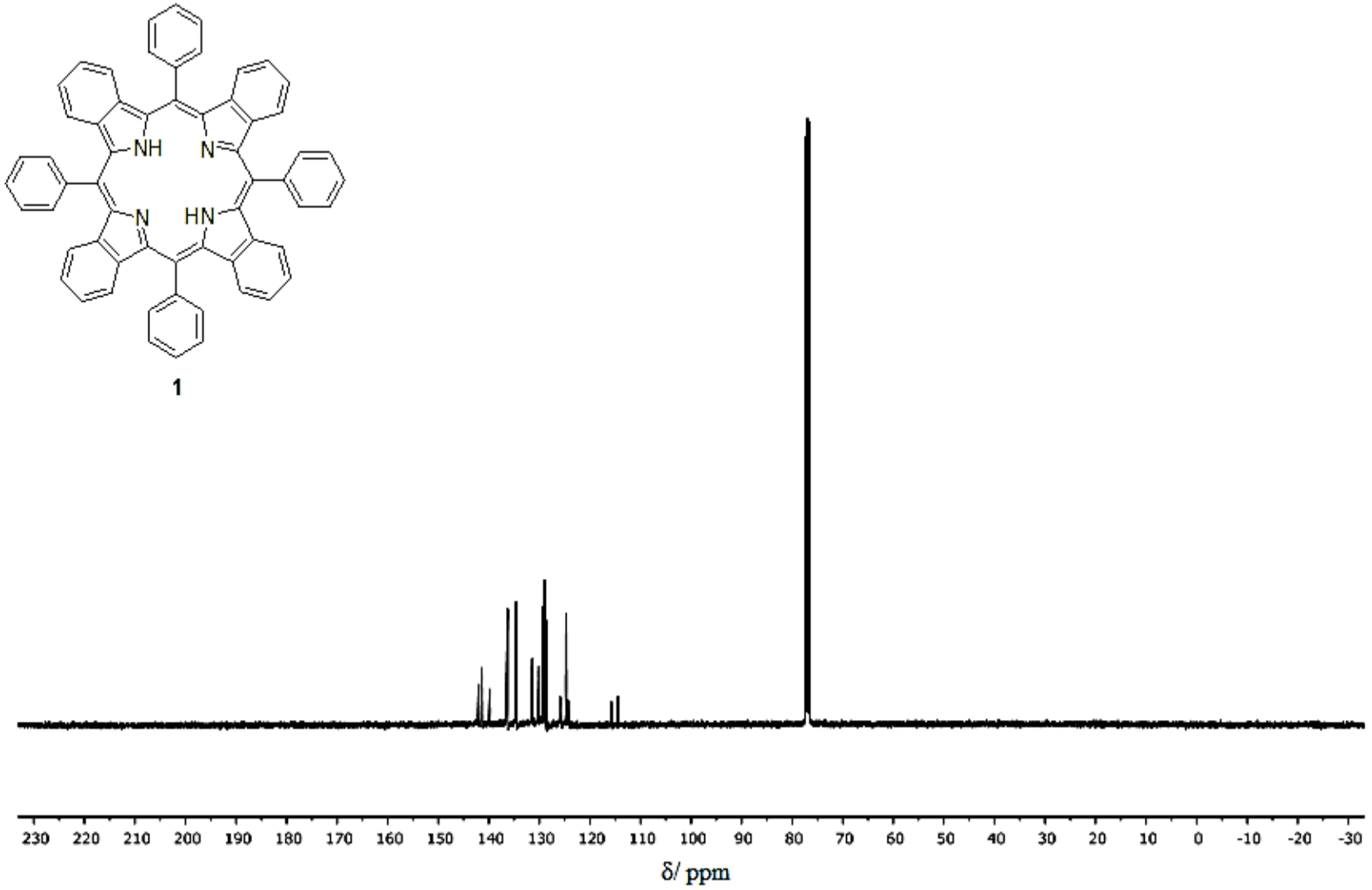

Figure A-10: ^{13}C-NMR spectrum of compound **1**

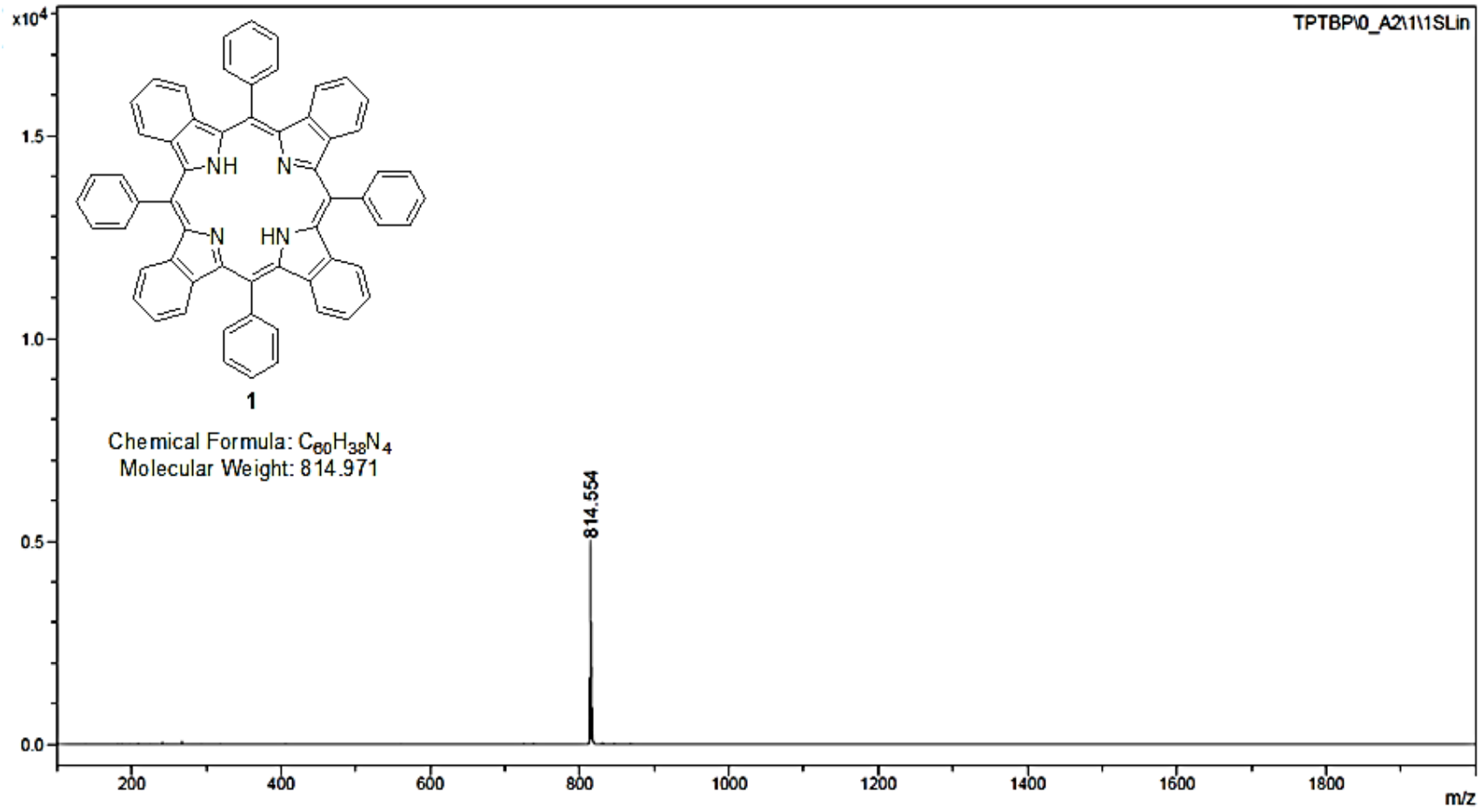

Figure A-11: MALDI-TOF mass spectrum of **1**

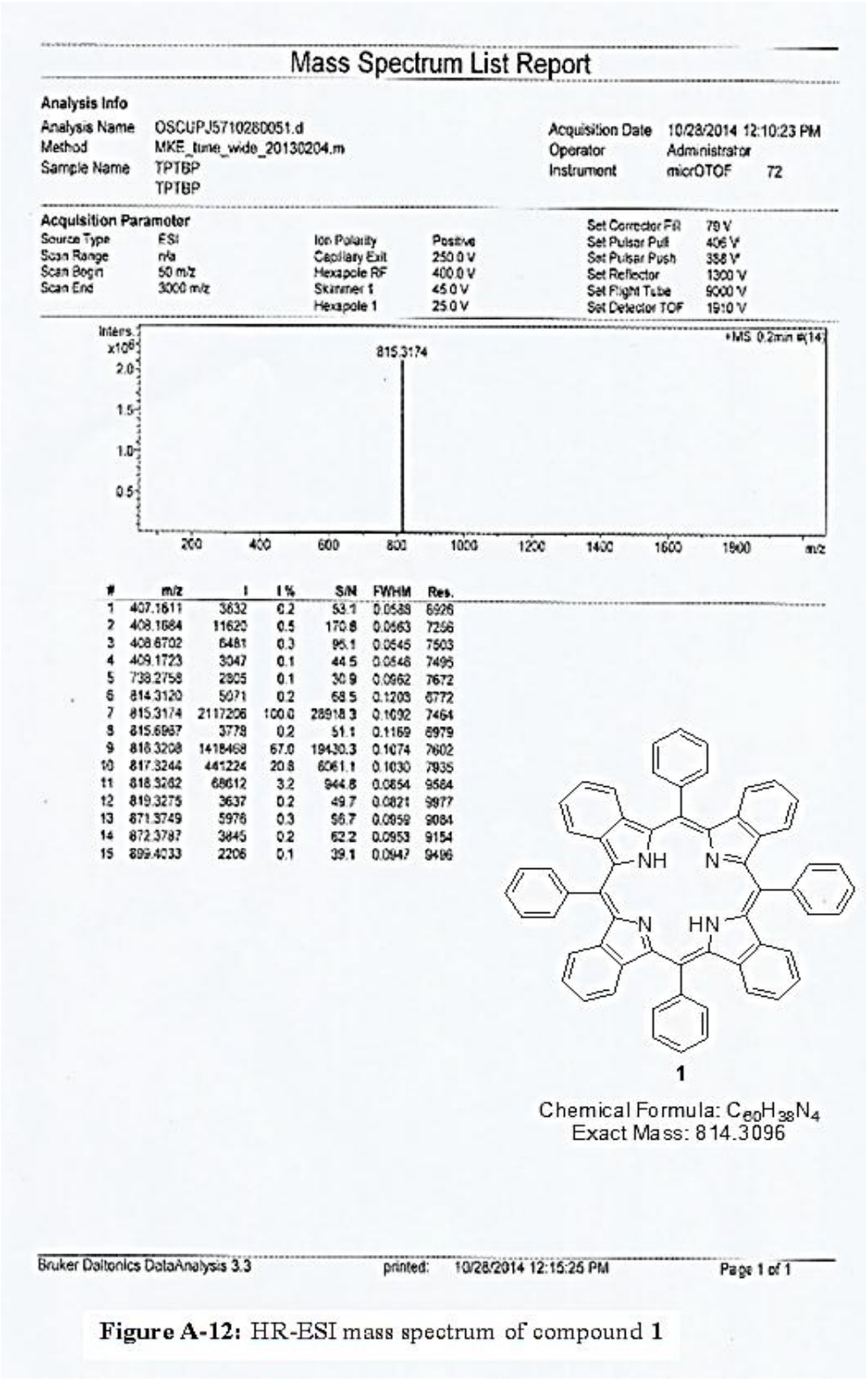

Mass Spectrum List Report

Analysis Info

Analysis Name	OSCUPJ5710280051.d	Acquisition Date	10/28/2014 12:10:23 PM
Method	MKE_time_wide_20130204.m	Operator	Administrator
Sample Name	TPTBP	Instrument	micrOTOF 72
	TPTBP		

Acquisition Parameter

Source Type	ESI	Ion Polarity	Positive	Set Corrector Fill	79 V
Scan Range	n/a	Capillary Exit	250.0 V	Set Pulsar Pull	406 V
Scan Begin	50 m/z	Hexapole RF	400.0 V	Set Pulsar Push	358 V
Scan End	3000 m/z	Skimmer 1	45.0 V	Set Reflector	1300 V
		Hexapole 1	25.0 V	Set Flight Tube	9000 V
				Set Detector TOF	1910 V

#	m/z	I	I %	S/N	FWHM	Res.
1	407.1611	3632	0.2	53.1	0.0588	6926
2	408.1684	11620	0.5	170.8	0.0563	7256
3	408.6702	6481	0.3	95.1	0.0545	7503
4	409.1723	3047	0.1	44.5	0.0548	7495
5	738.2758	2805	0.1	30.9	0.0962	7672
6	814.3120	5071	0.2	68.5	0.1203	6772
7	815.3174	2117206	100.0	28918.3	0.1092	7464
8	815.6987	3778	0.2	51.1	0.1169	6979
9	816.3208	1418468	67.0	19430.3	0.1074	7602
10	817.3244	441224	20.8	6061.1	0.1030	7935
11	818.3262	68612	3.2	944.8	0.0854	9584
12	819.3275	3637	0.2	49.7	0.0821	9977
13	871.3749	5976	0.3	86.7	0.0959	9084
14	872.3787	3845	0.2	62.2	0.0953	9154
15	899.4033	2206	0.1	39.1	0.0947	9496

1

Chemical Formula: $C_{60}H_{38}N_4$
Exact Mass: 814.3096

Bruker Daltonics DataAnalysis 3.3 printed: 10/28/2014 12:15:25 PM Page 1 of 1

Figure A-12: HR-ESI mass spectrum of compound **1**

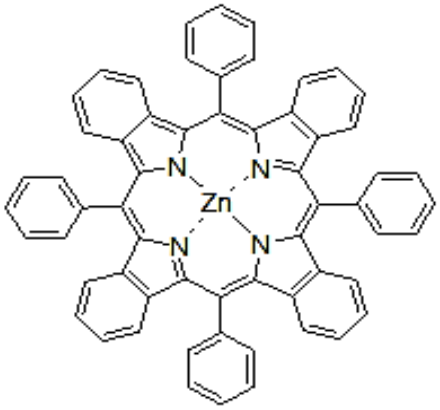

Zn-1

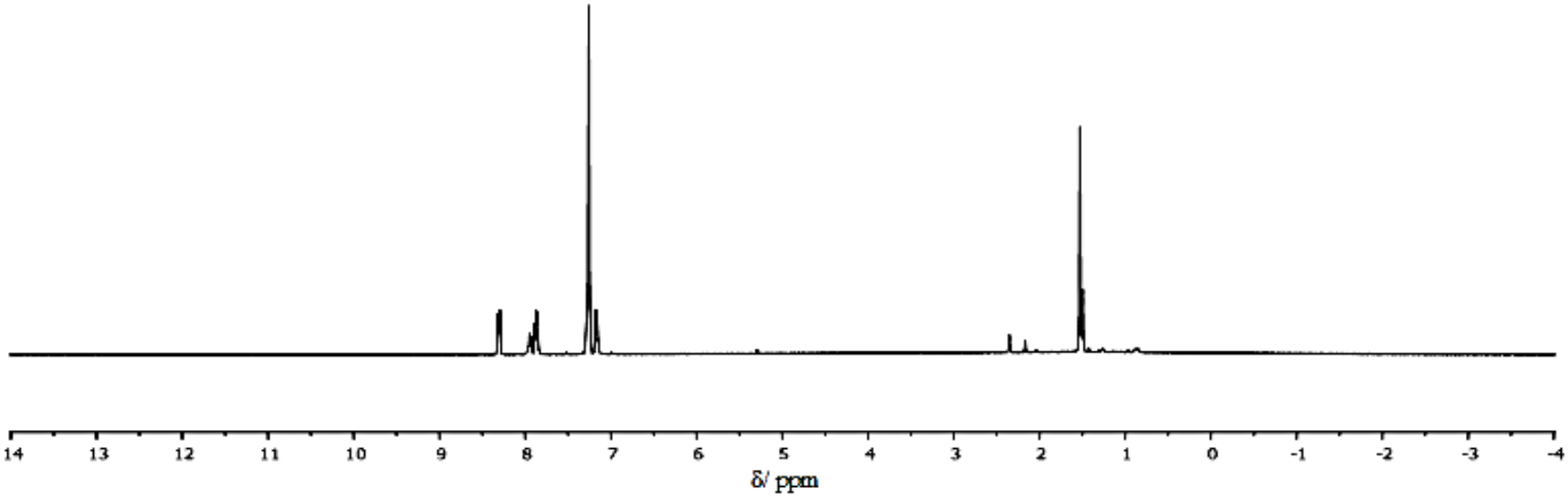

Figure A-13: ^{1}H-NMR spectrum of compound **Zn-1**

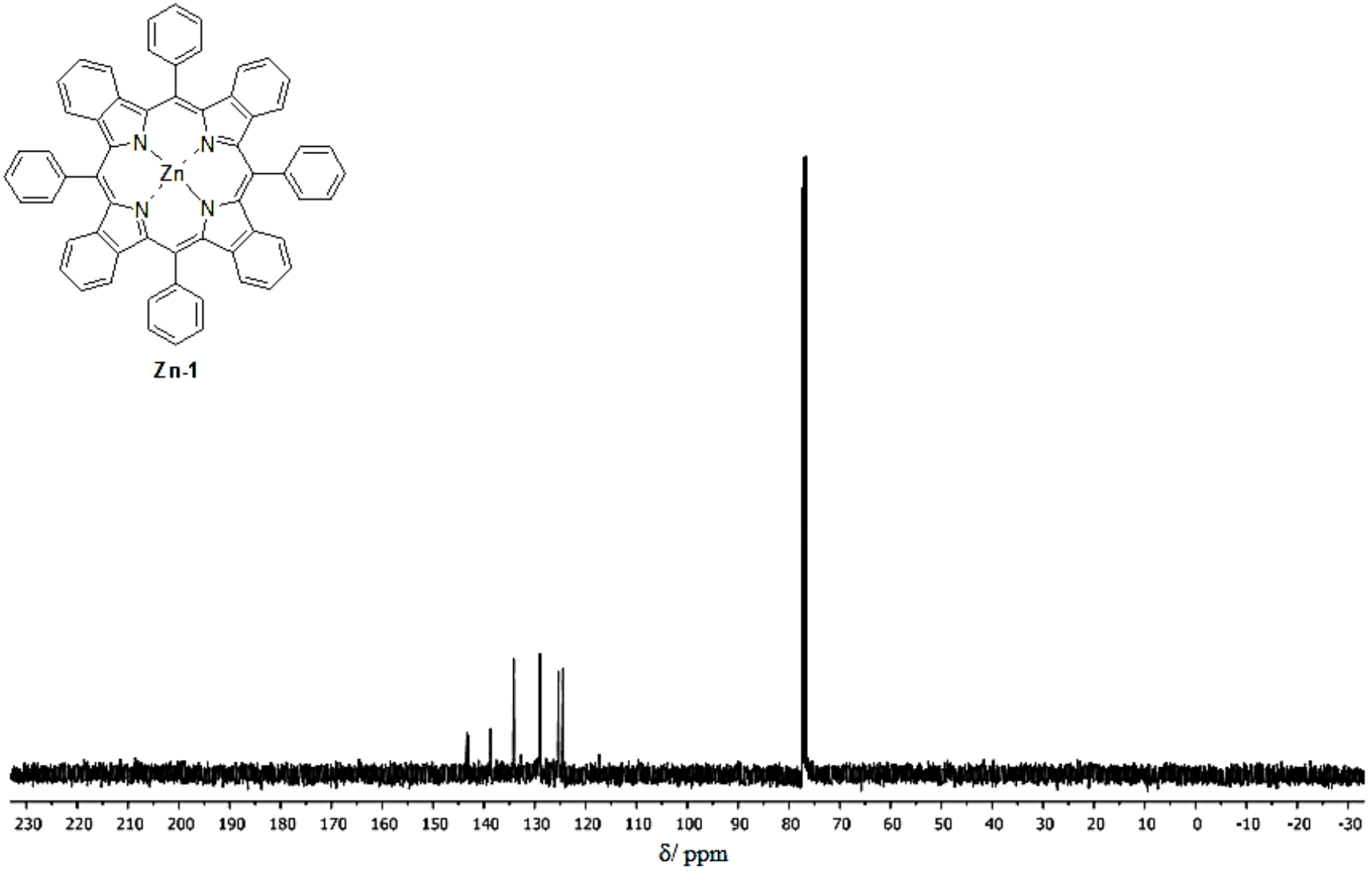

Figure A-14: ^{13}C-NMR spectrum of compound **Zn-1**

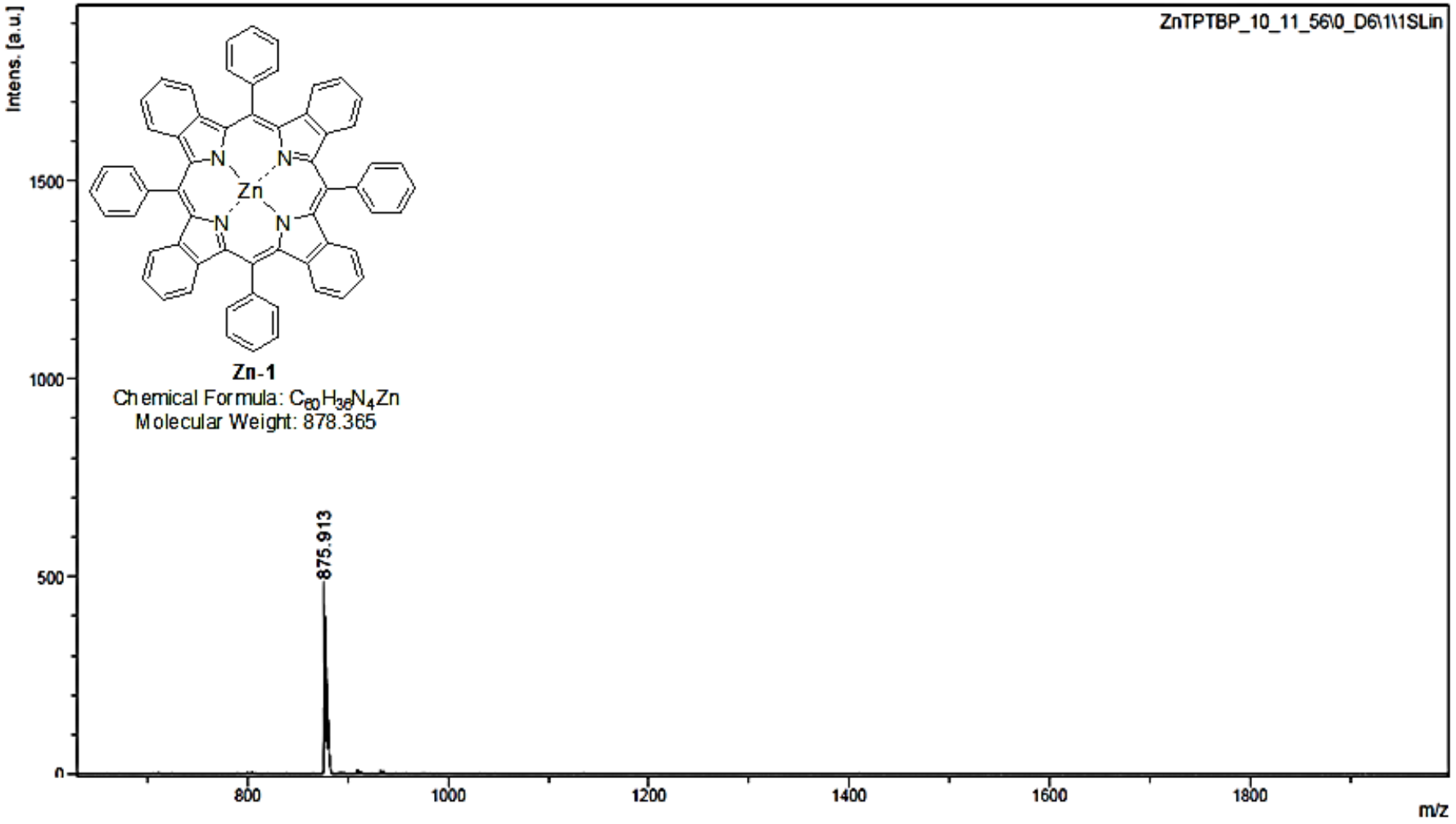

Figure A-15: MALDI-TOF mass spectrum of **Zn-1**

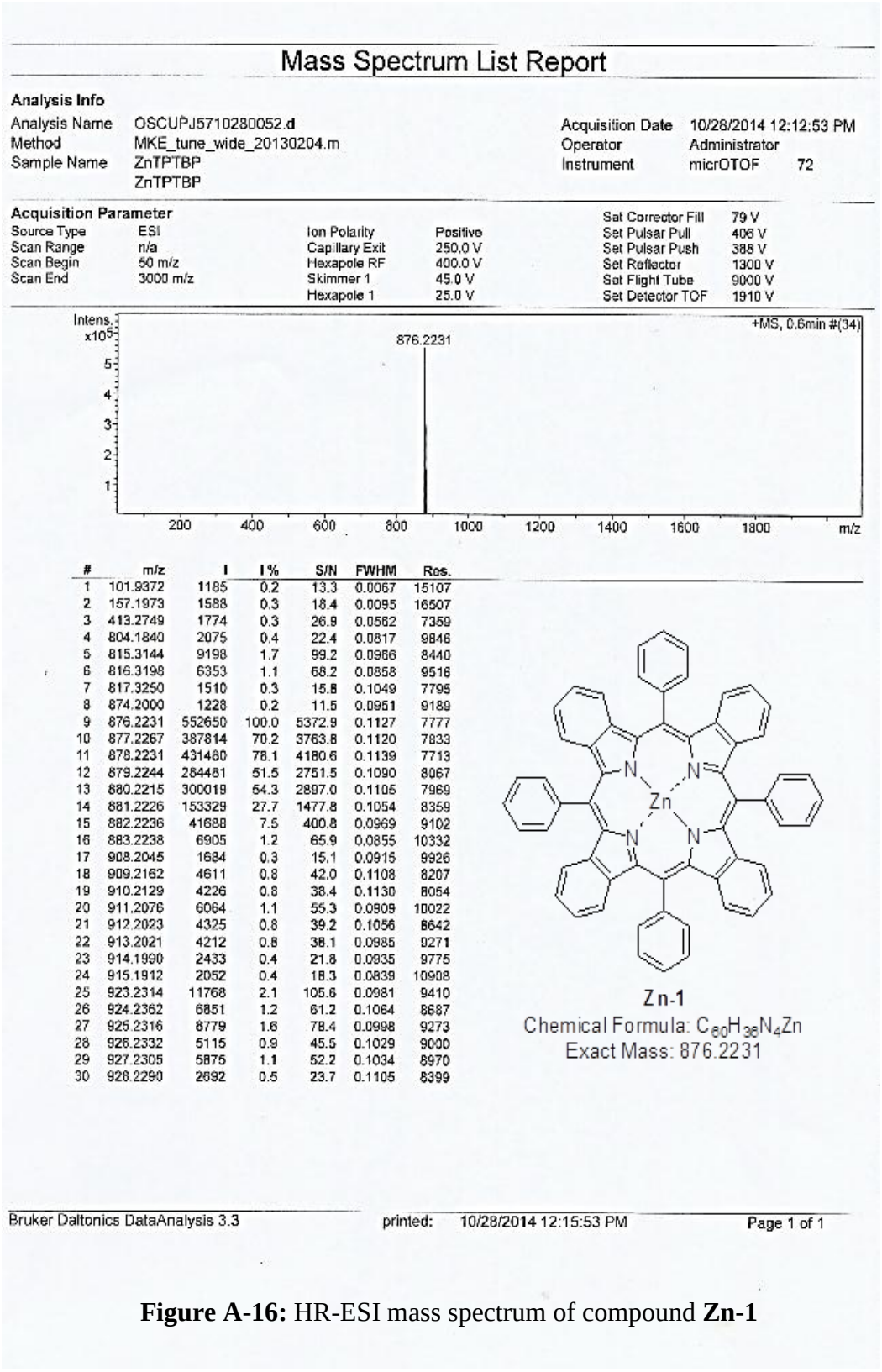

Mass Spectrum List Report

Analysis Info

Analysis Name	OSCUPJ5710280052.d	Acquisition Date	10/28/2014 12:12:53 PM
Method	MKE_tune_wide_20130204.m	Operator	Administrator
Sample Name	ZnTPTBP	Instrument	micrOTOF 72
	ZnTPTBP		

Acquisition Parameter

Source Type	ESI	Ion Polarity	Positive	Set Corrector Fill	79 V
Scan Range	n/a	Capillary Exit	250.0 V	Set Pulsar Pull	406 V
Scan Begin	50 m/z	Hexapole RF	400.0 V	Set Pulsar Push	388 V
Scan End	3000 m/z	Skimmer 1	45.0 V	Set Reflector	1300 V
		Hexapole 1	25.0 V	Set Flight Tube	9000 V
				Set Detector TOF	1910 V

#	m/z	I	I %	S/N	FWHM	Res.
1	101.9372	1185	0.2	13.3	0.0067	15107
2	157.1973	1588	0.3	18.4	0.0095	16507
3	413.2749	1774	0.3	26.9	0.0562	7359
4	804.1840	2075	0.4	22.4	0.0817	9846
5	815.3144	9198	1.7	99.2	0.0966	8440
6	816.3198	6353	1.1	68.2	0.0858	9516
7	817.3250	1510	0.3	15.8	0.1049	7795
8	874.2000	1228	0.2	11.5	0.0951	9189
9	876.2231	552650	100.0	5372.9	0.1127	7777
10	877.2267	387814	70.2	3763.8	0.1120	7833
11	878.2231	431480	78.1	4180.6	0.1139	7713
12	879.2244	284481	51.5	2751.5	0.1090	8067
13	880.2215	300019	54.3	2897.0	0.1105	7969
14	881.2226	153329	27.7	1477.8	0.1054	8359
15	882.2236	41688	7.5	400.8	0.0969	9102
16	883.2238	6905	1.2	65.9	0.0855	10332
17	908.2045	1684	0.3	15.1	0.0915	9926
18	909.2162	4611	0.8	42.0	0.1108	8207
19	910.2129	4226	0.8	38.4	0.1130	8054
20	911.2076	6064	1.1	55.3	0.0909	10022
21	912.2023	4325	0.8	39.2	0.1056	8642
22	913.2021	4212	0.8	38.1	0.0985	9271
23	914.1990	2433	0.4	21.8	0.0935	9775
24	915.1912	2052	0.4	18.3	0.0839	10908
25	923.2314	11768	2.1	105.6	0.0981	9410
26	924.2362	6851	1.2	61.2	0.1064	8687
27	925.2316	8779	1.6	78.4	0.0998	9273
28	926.2332	5115	0.9	45.5	0.1029	9000
29	927.2305	5875	1.1	52.2	0.1034	8970
30	928.2290	2692	0.5	23.7	0.1105	8399

Zn-1

Chemical Formula: $C_{60}H_{36}N_4Zn$

Exact Mass: 876.2231

Bruker Daltonics DataAnalysis 3.3 printed: 10/28/2014 12:15:53 PM Page 1 of 1

Figure A-16: HR-ESI mass spectrum of compound **Zn-1**

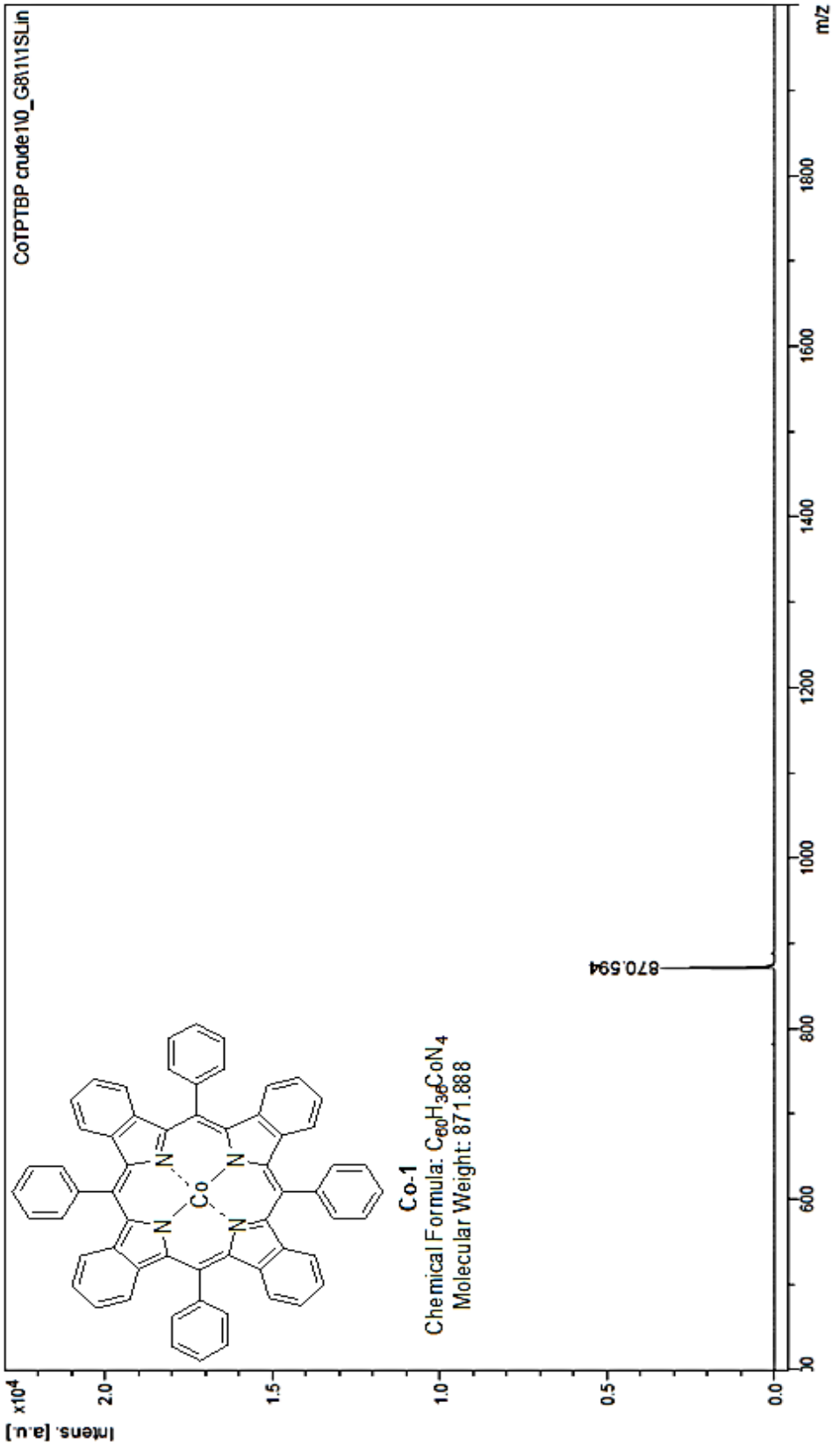

Figure A-17: MALDI-TOF mass spectrum of **Co-1**

Mass Spectrum List Report

Analysis Info

Analysis Name	OSBEE570331003.d	Acquisition Date	3/31/2014 12:18:05 PM
Method	MKE_tune_wide_20130204.m	Operator	Administrator
Sample Name	CoTPTBP	Instrument	micrOTOF 72
	CoTPTBP		

Acquisition Parameter

Source Type	ESI	Ion Polarity	Positive	Set Corrector Fill	79 V
Scan Range	n/a	Capillary Exit	180.0 V	Set Pulsar Pull	406 V
Scan Begin	50 m/z	Hexapole RF	400.0 V	Set Pulsar Push	388 V
Scan End	3000 m/z	Skimmer 1	45.0 V	Set Reflector	1300 V
		Hexapole 1	25.0 V	Set Flight Tube	9000 V
				Set Detector TOF	1910 V

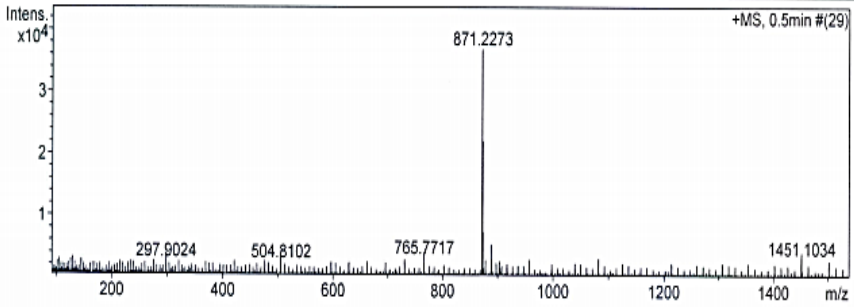

#	m/z	I	I %	S/N	FWHM	Res.
1	53.7136	3021	8.2	7.6	0.0071	7553
2	56.1583	4184	11.4	10.6	0.0093	6050
3	58.6231	2956	8.0	7.4	0.0093	6330
4	61.1417	2471	6.7	6.1	0.0096	6390
5	63.6829	2557	7.0	6.4	0.0073	8764
6	89.1662	2662	7.2	6.6	0.0080	11168
7	129.9718	2471	6.7	6.1	0.0531	2449
8	145.1311	2834	7.7	7.1	0.0103	14082
9	145.2039	2760	7.5	6.9	0.0213	6812
10	297.9024	2559	7.0	7.3	0.1046	2847
11	765.7717	3141	8.5	9.4	0.0199	38506
12	871.2273	36750	100.0	111.1	0.1122	7766
13	872.2322	21981	59.8	66.3	0.1262	6913
14	873.2325	7318	19.9	21.9	0.1118	7813
15	877.9350	2734	7.4	8.0	0.0309	28394
16	888.2305	4886	13.3	14.5	0.1168	7603
17	889.2336	2910	7.9	8.6	0.1334	6664
18	903.2148	2617	7.1	7.7	0.1044	8652
19	956.8043	2753	7.5	8.1	0.0286	33505
20	1451.1034	3182	8.7	9.4	0.1528	9498
21	1451.1544	2602	7.1	7.6	0.1916	7574
22	1501.1722	2875	7.8	8.5	0.0410	36635
23	1763.7040	2758	7.5	8.0	0.0298	59246
24	2048.0937	2771	7.5	7.9	0.0795	25758
25	2290.6062	2646	7.2	7.7	0.0845	27122
26	2352.9588	3718	10.1	11.0	0.0354	66484
27	2353.3494	4056	11.0	12.0	0.0403	58332
28	2612.3883	2601	7.1	7.6	0.0420	62137
29	2885.7497	2953	8.0	8.6	0.0602	47951
30	2956.2100	2800	7.6	8.2	0.0785	37669

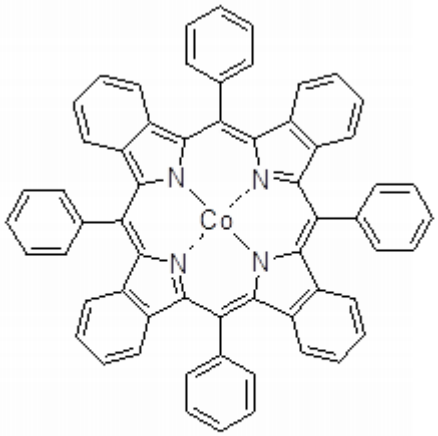

Co-1

Chemical Formula: $C_{60}H_{36}CoN_4$

Exact Mass: 871.2272

Figure A-18: HR-ESI mass spectrum of compound **Co-1**

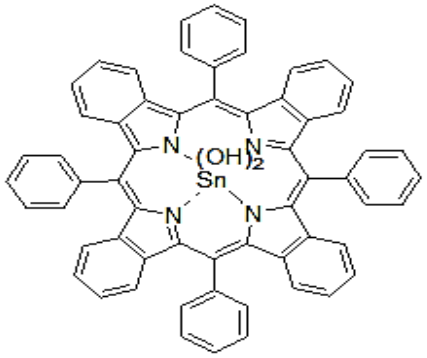

$Sn(OH)_2$-1

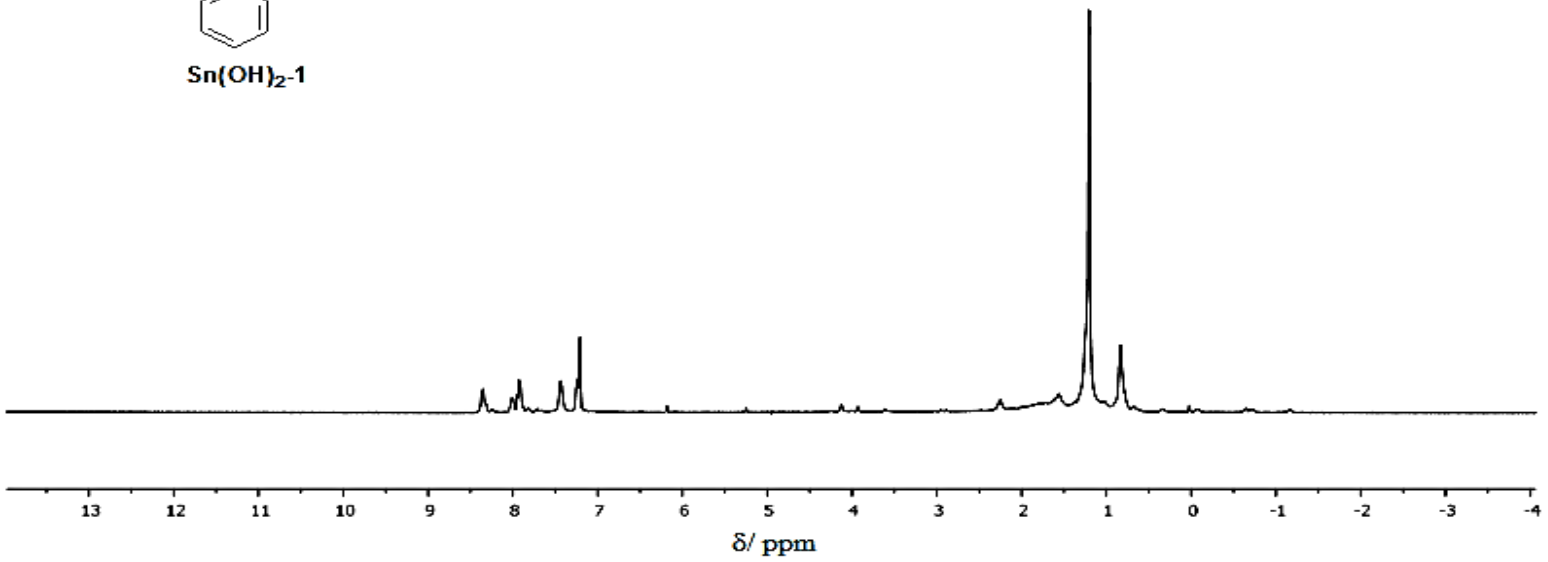

Figure A-19: ^{1}H-NMR spectrum of compound **$Sn(OH)_2$-1**

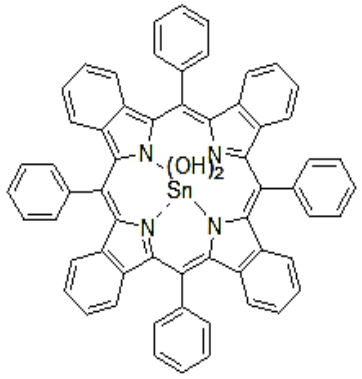

$Sn(OH)_2$-1

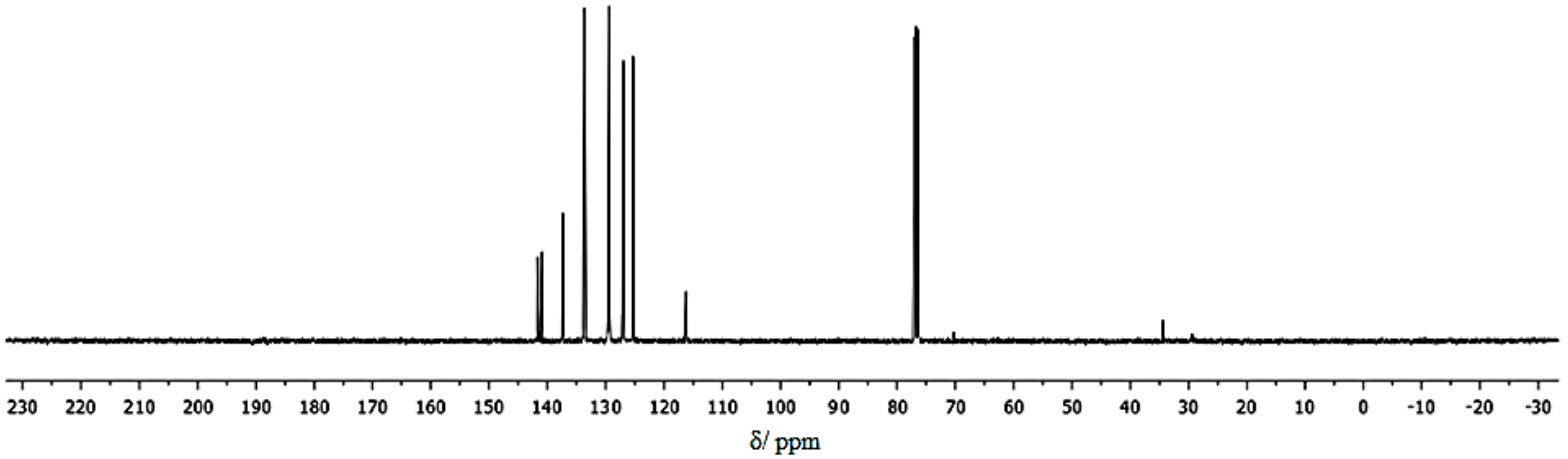

Figure A-20: ^{13}C-NMR spectrum of compound **$Sn(OH)_2$-1**

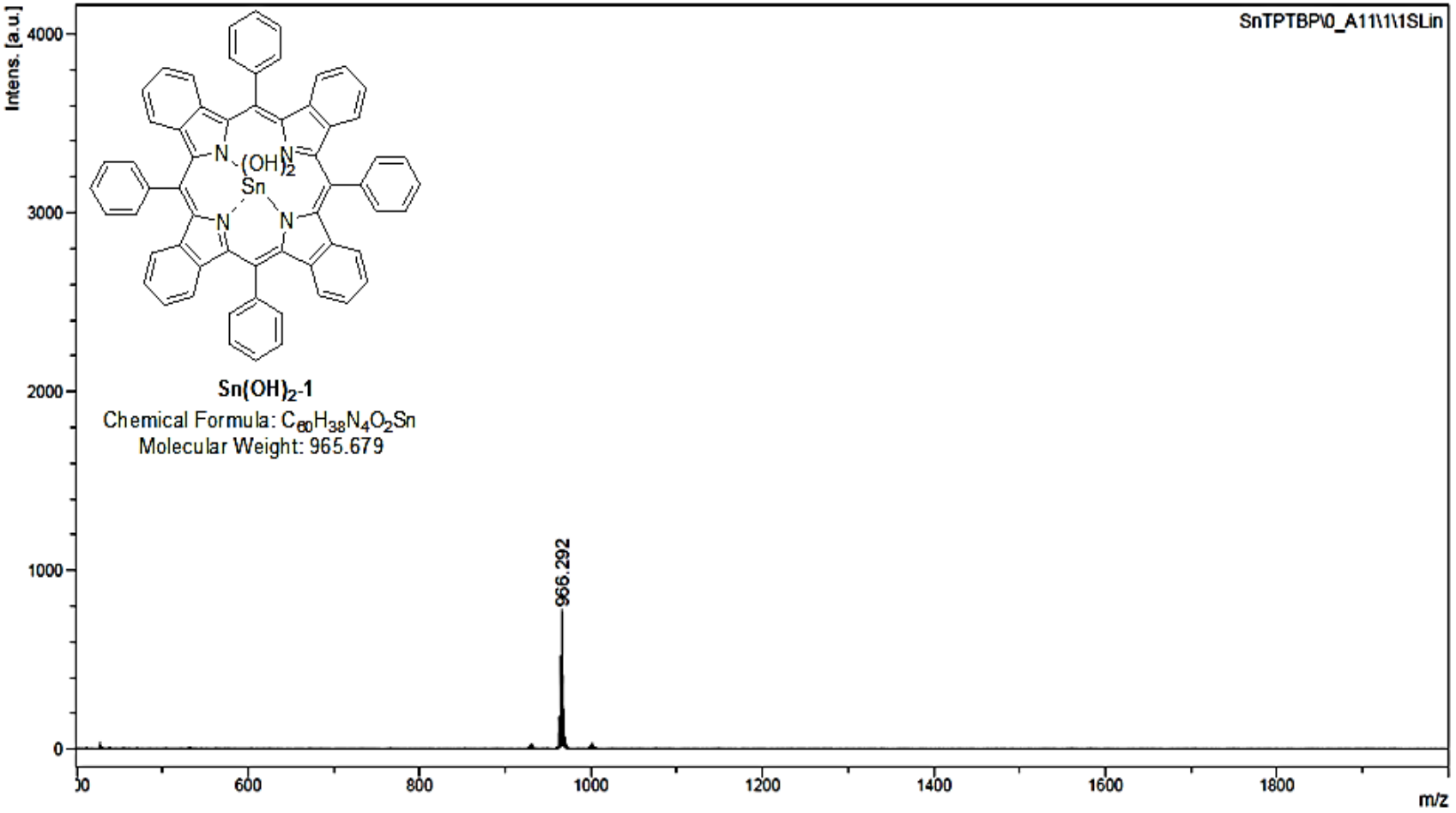

Figure A-21: HR-ESI mass spectrum of **Sn(OH)$_2$-1**

Mass Spectrum List Report

Analysis Info

Analysis Name	OSCUJS560924001.d	Acquisition Date	9/24/2013 3:58:45 PM
Method	Natee20130403.m	Operator	Administrator
Sample Name	Sn(OH)2-TPTBP Sn(OH)2-TPTBP	Instrument	micrOTOF 72

Acquisition Parameter

Source Type	ESI	Ion Polarity	Positive	Set Corrector Fill	75 V
Scan Range	n/a	Capillary Exit	300.0 V	Set Pulsar Pull	398 V
Scan Begin	50 m/z	Hexapole RF	400.0 V	Set Pulsar Push	380 V
Scan End	3000 m/z	Skimmer 1	54.4 V	Set Reflector	1300 V
		Hexapole 1	21.4 V	Set Flight Tube	9000 V
				Set Detector TOF	1910 V

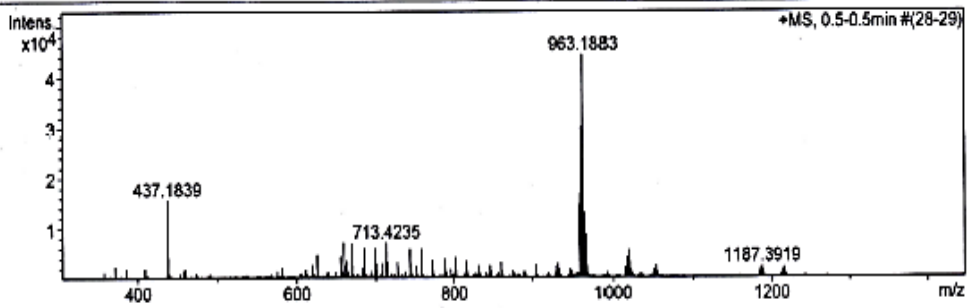

#	m/z	I	I %	S/N	FWHM	Res.
1	437.1839	15721	35.5	759.6	0.0547	7995
2	438.1874	4270	9.6	204.9	0.0554	7903
3	625.3722	4727	10.7	106.2	0.0721	8668
4	655.3187	4400	9.9	89.3	0.0820	7992
5	659.2706	7184	16.2	144.8	0.0752	8768
6	663.4428	3601	8.1	70.9	0.0788	8416
7	669.3981	6845	15.4	133.7	0.0734	9120
8	685.4142	5973	13.5	111.0	0.0770	8900
9	699.3450	5954	13.4	106.3	0.0849	8236
10	713.4235	7190	16.2	123.8	0.0797	8950
11	743.3685	5882	13.3	94.5	0.0839	8865
12	757.4473	5859	13.2	92.6	0.0845	8969
13	771.4609	3658	8.3	56.3	0.0830	9294
14	787.3958	3892	8.8	58.9	0.0985	7998
15	801.4733	4235	9.6	63.3	0.0845	9480
16	815.4901	3502	7.9	51.3	0.0902	9040
17	959.1878	14600	32.9	208.5	0.0986	9733
18	960.1889	16866	38.1	241.8	0.1011	9496
19	961.1891	30108	67.9	434.2	0.1066	9018
20	962.1899	26292	59.3	379.9	0.1014	9489
21	963.1883	44314	100.0	643.1	0.1018	9457
22	964.1897	23571	53.2	342.0	0.1066	9042
23	965.1849	13222	29.8	191.5	0.1084	8905
24	966.1772	5804	13.1	83.1	0.1167	8276
25	967.1753	8735	19.7	126.4	0.1226	7891
26	968.1767	5391	12.2	77.5	0.1188	8151
27	1017.2424	4179	9.4	67.9	0.1187	8567
28	1018.2465	3684	8.3	59.8	0.1125	9049
29	1019.2460	5549	12.5	91.4	0.1061	9610
30	1020.2504	3284	7.4	53.4	0.1090	9360

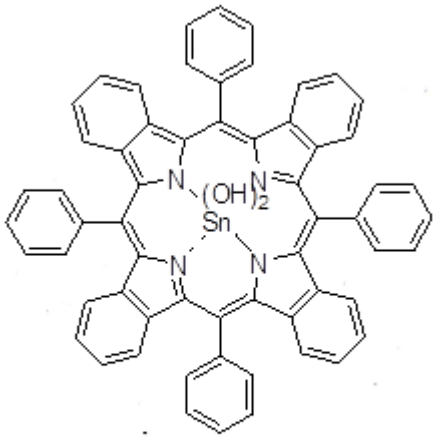

$Sn(OH)_2$-1

Chemical Formula: $C_{60}H_{38}N_4O_2Sn$

Exact Mass: 966.2017

Bruker Daltonics DataAnalysis 3.3 printed: 9/24/2013 4:16:29 PM Page 1 of 1

Figure A-22: HR-ESI mass spectrum of compound **$Sn(OH)_2$-1**

APPENDIX B

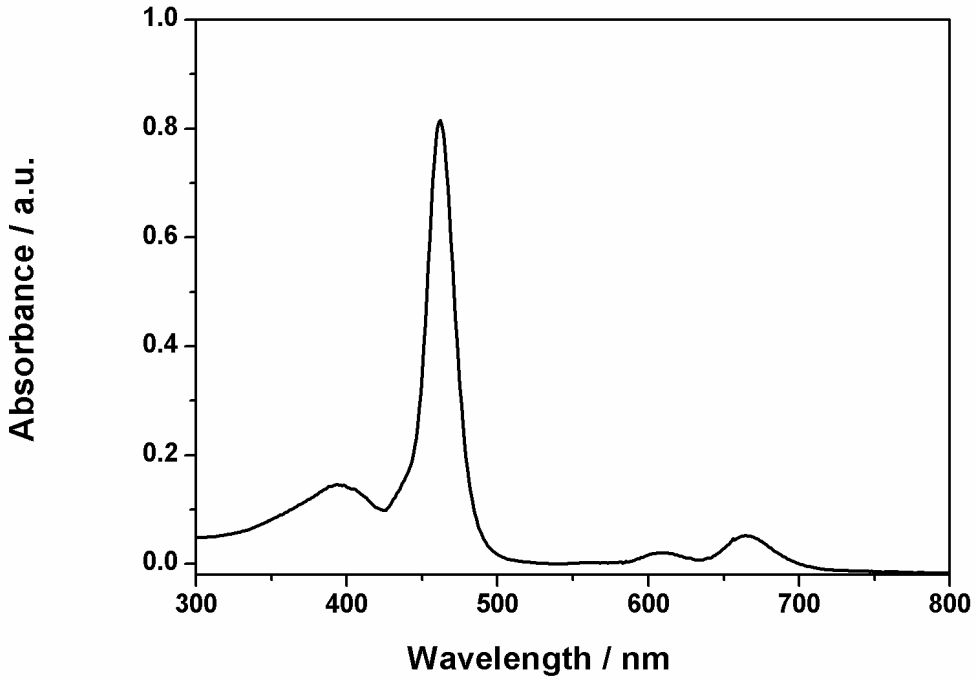

Figure B-1: Absorption spectrum of compound **4** in toluene

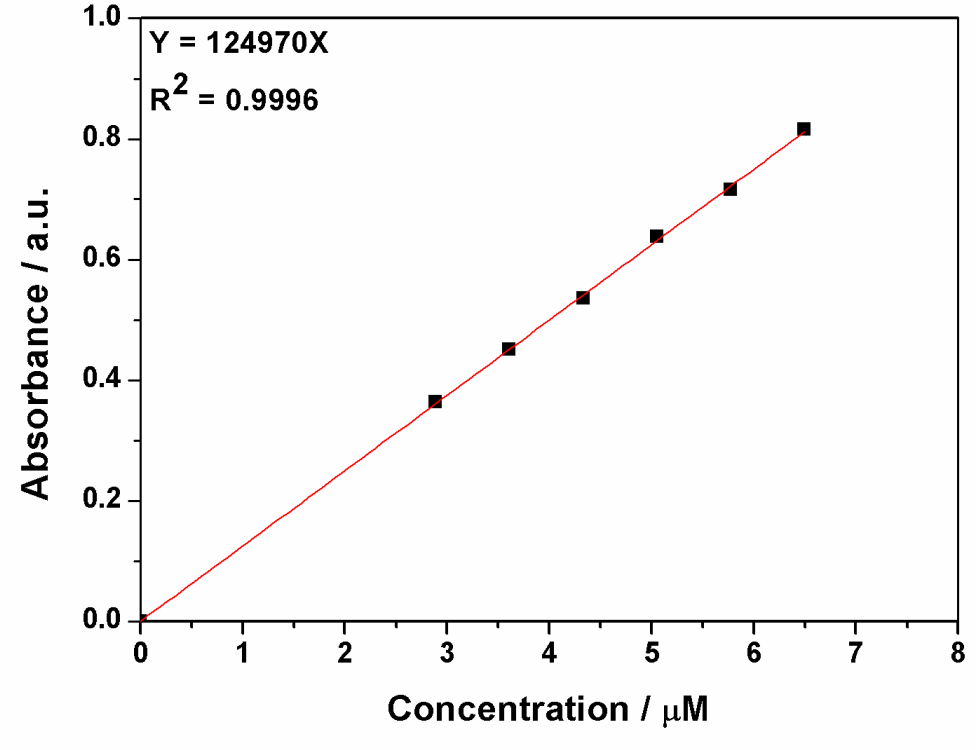

Figure B-2: Calibration curve of the 462 nm absorption for quantitative determination of compound **4** in toluene

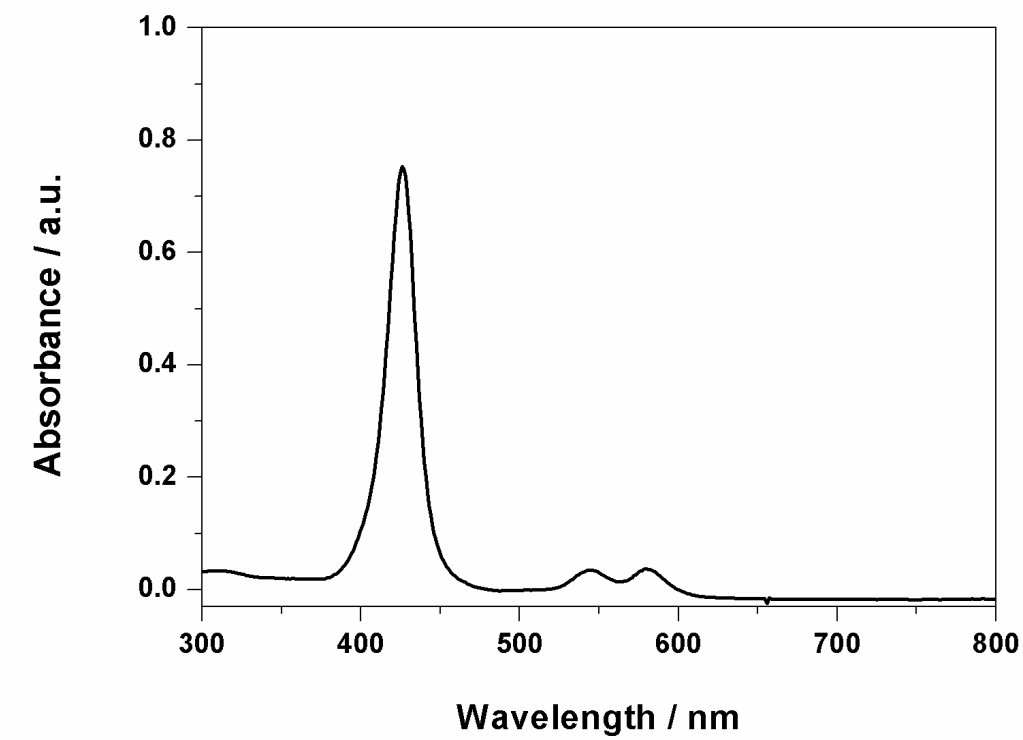

Figure B-3: Absorption spectrum of compound **Ni-4** in toluene

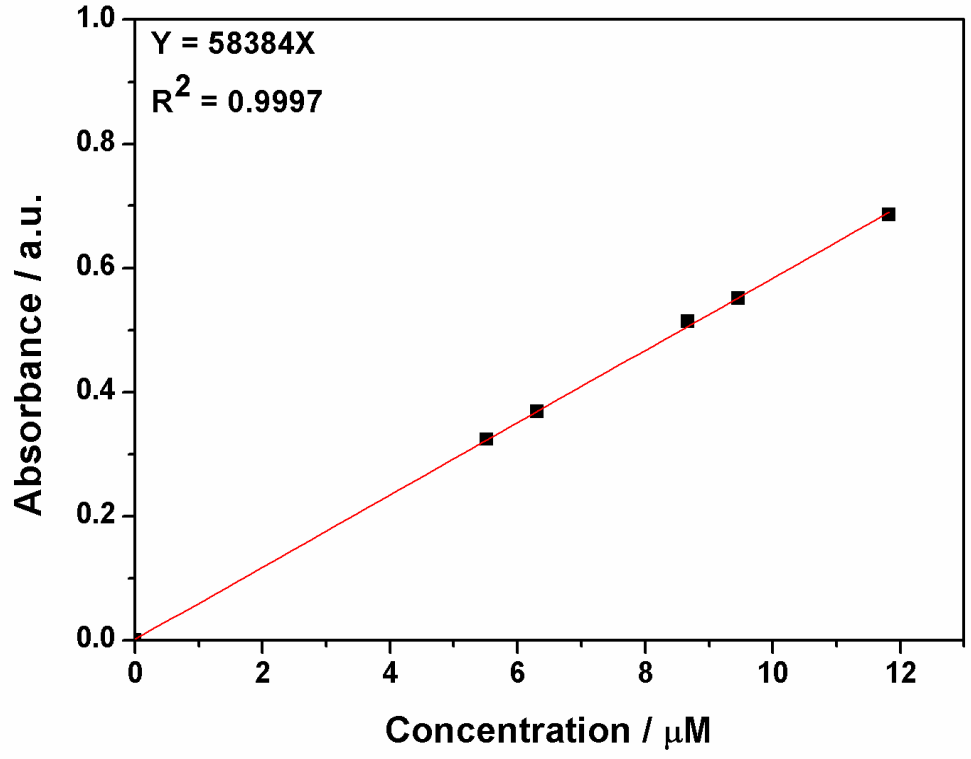

Figure B-4: Calibration curve of the 425 nm absorption for quantitative determination of compound **Ni-4** in toluene

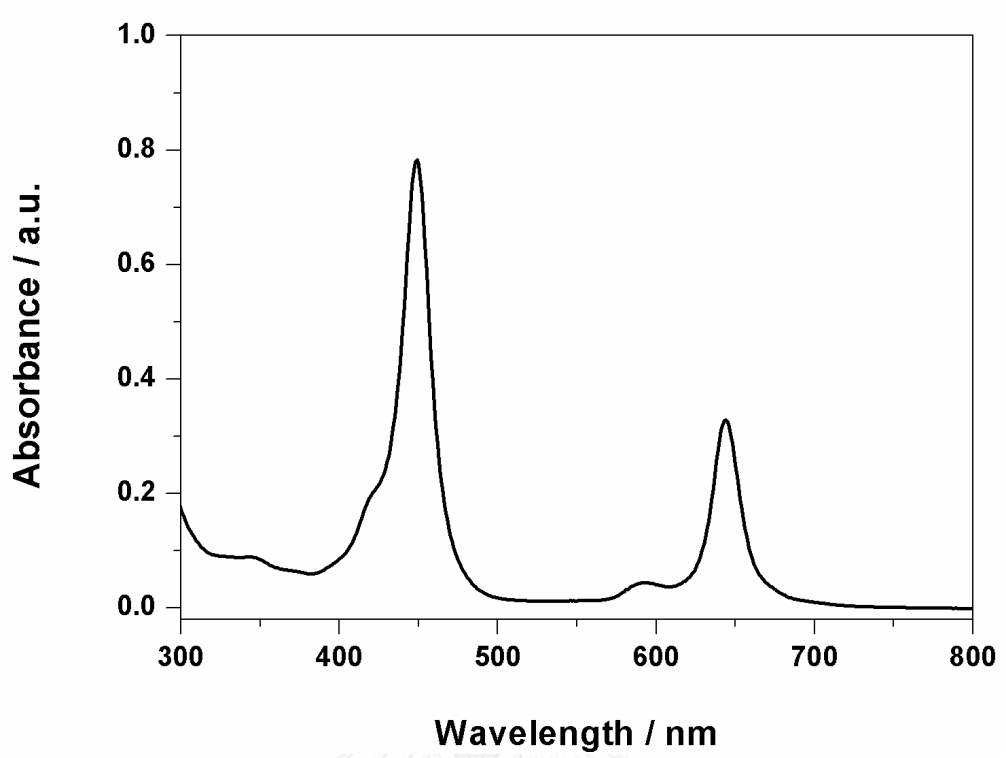

Figure B-5: Absorption spectrum of compound **Ni-1** in toluene

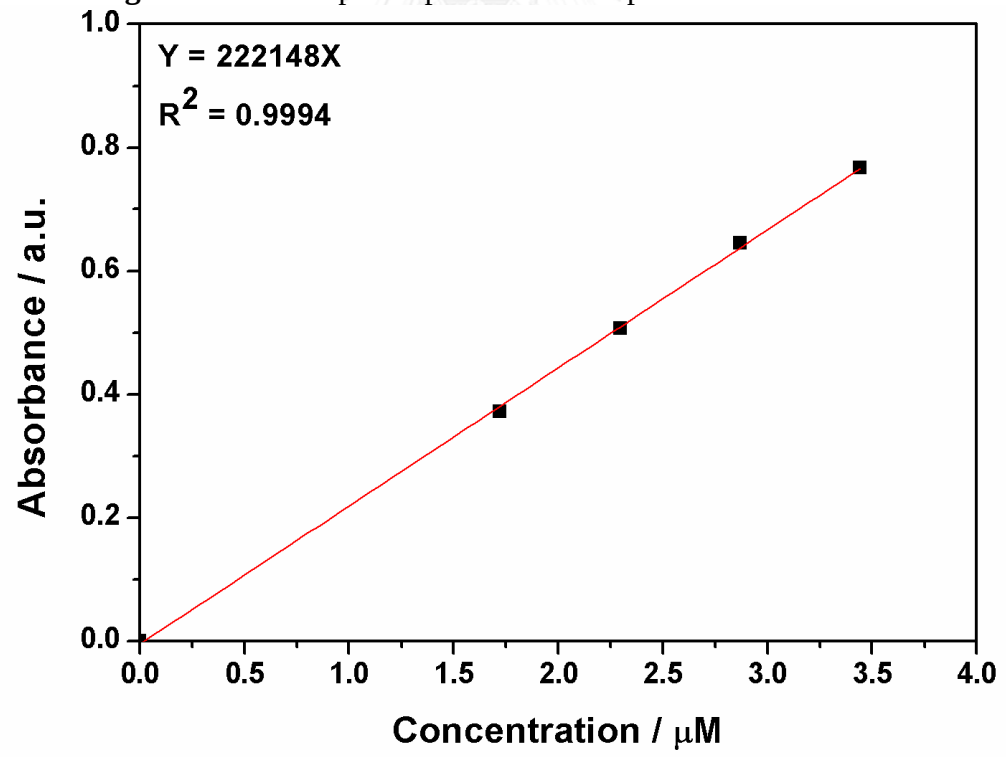

Figure B-6: Calibration curve of the 449 nm absorption for quantitative determination of compound **Ni-1** in toluene

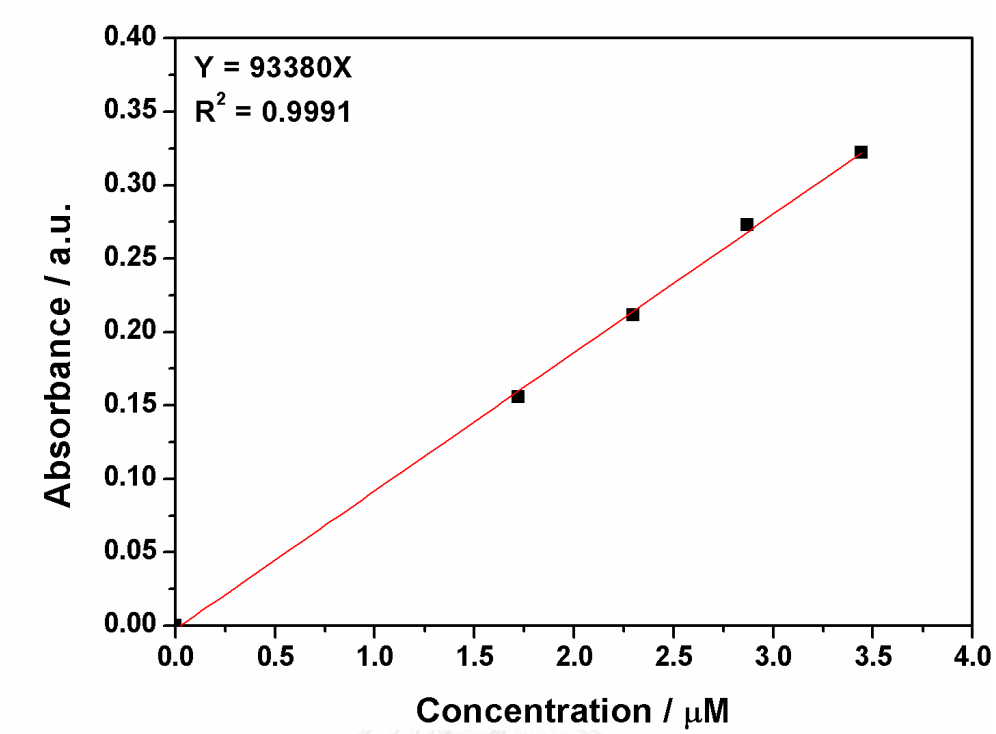

Figure B-7: Calibration curve of the 644 nm absorption for quantitative determination of compound **Ni-1** in toluene

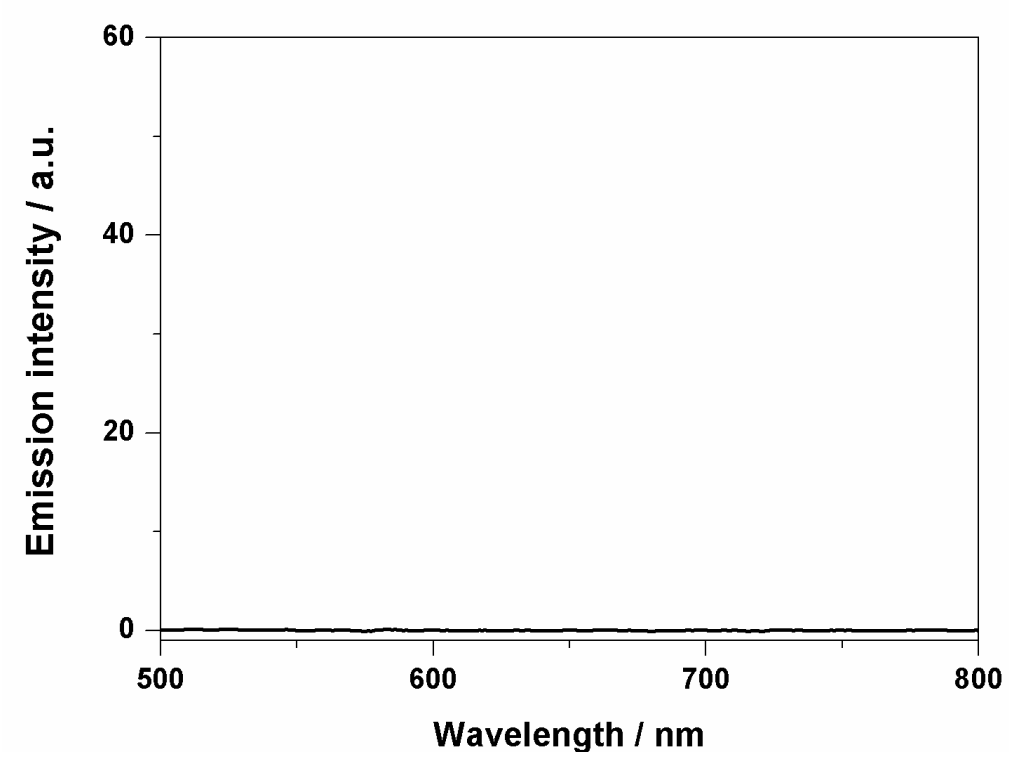

Figure B-8: Emission spectrum of compound **Ni-1** in toluene (λ_{ex} = 449 nm)

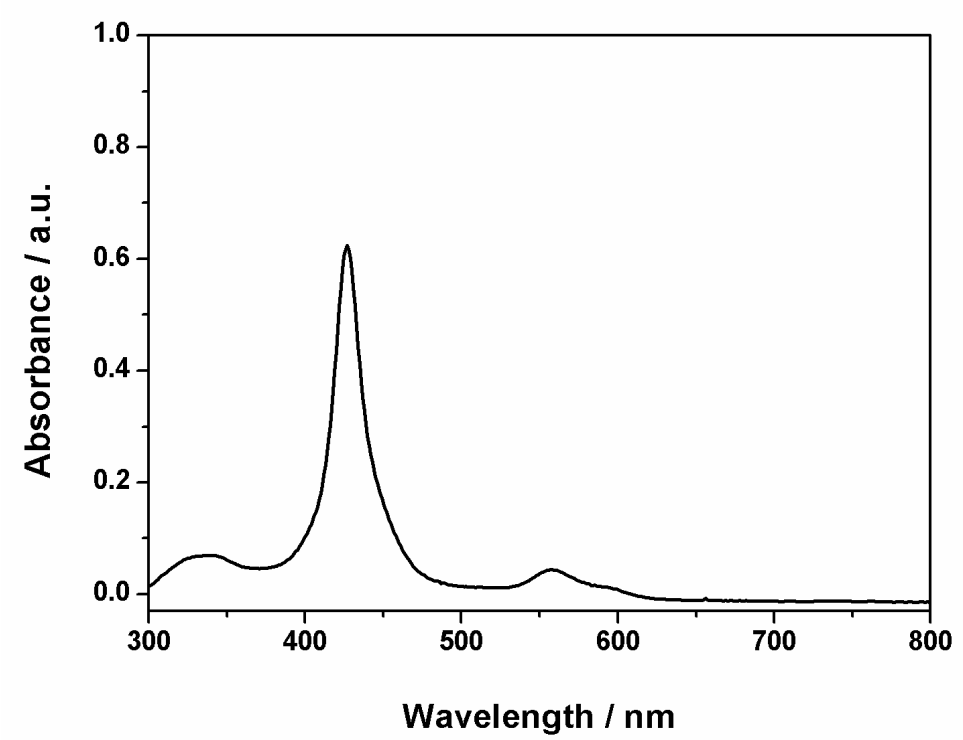

Figure B-9: Absorption spectrum of compound **Cu-4** in toluene

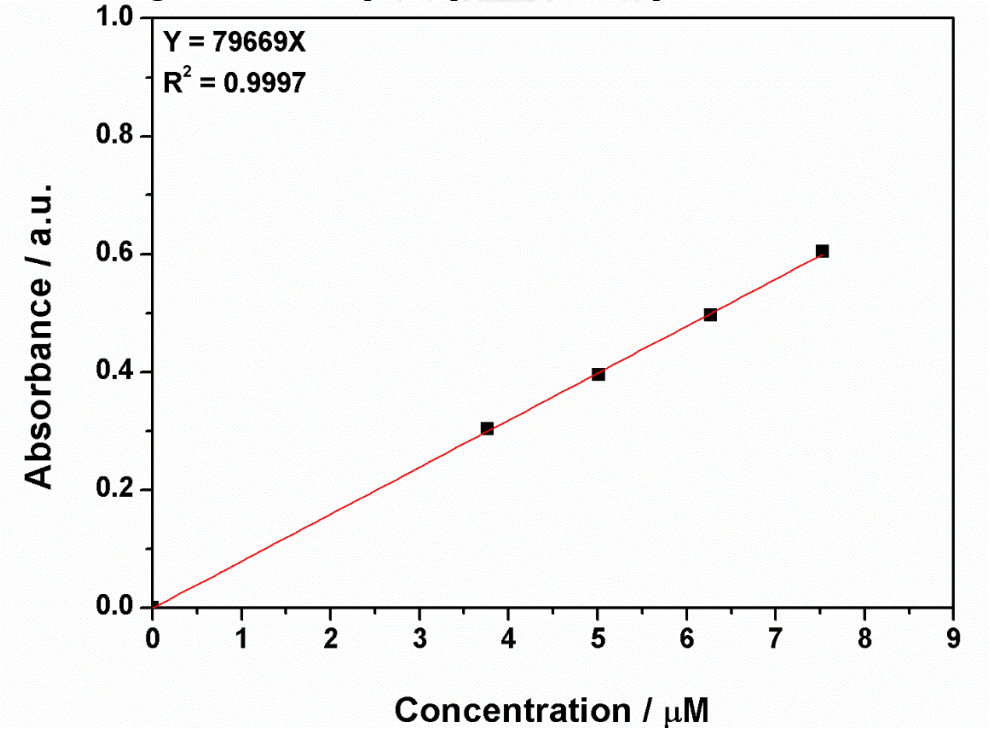

Figure B-10: Calibration curve of the 425 nm absorption
for quantitative determination of compound **Cu-4** in toluene

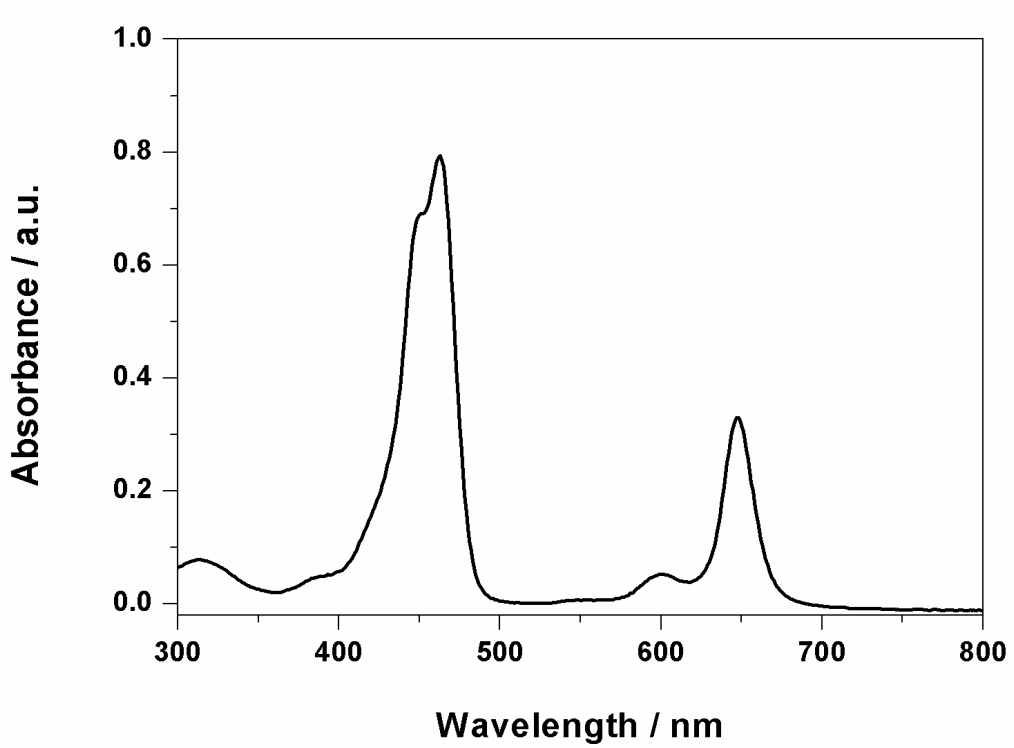

Figure B-11: Absorption spectrum of compound **Cu-1** in toluene

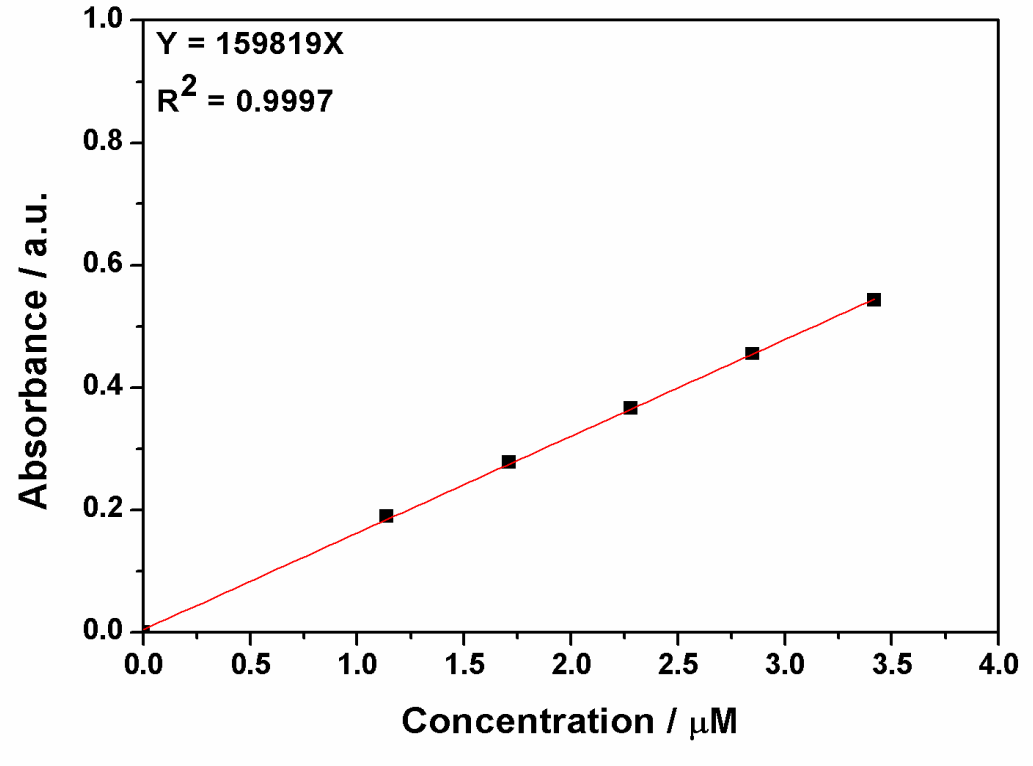

Figure B-12: Calibration curve of the 449 nm absorption for quantitative determination of compound **Cu-1** in toluene

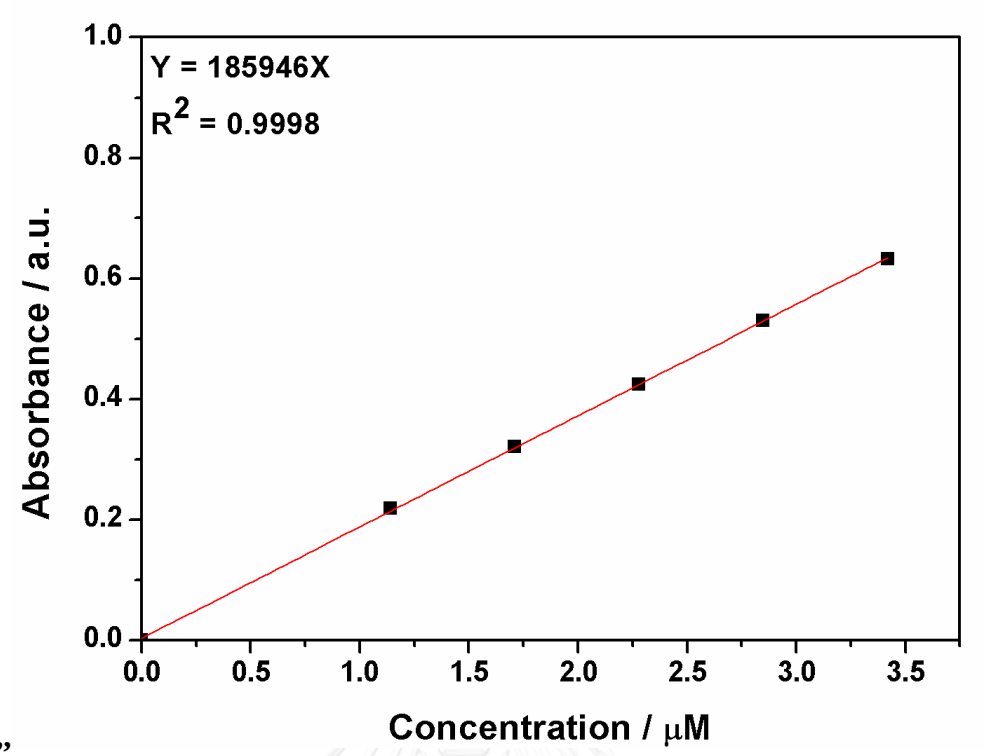

”

Figure B-13: Calibration curve of the 463 nm absorption for quantitative determination of compound **Cu-1** in toluene

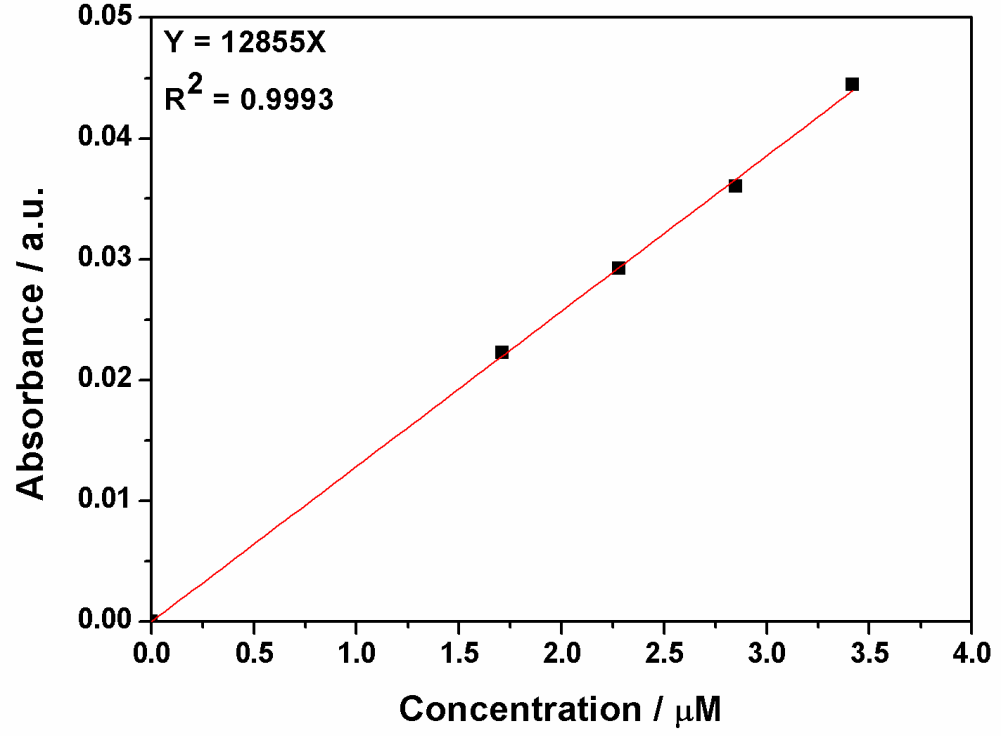

Figure B-14: Calibration curve of the 601 nm absorption for quantitative determination of compound **Cu-1** in toluene

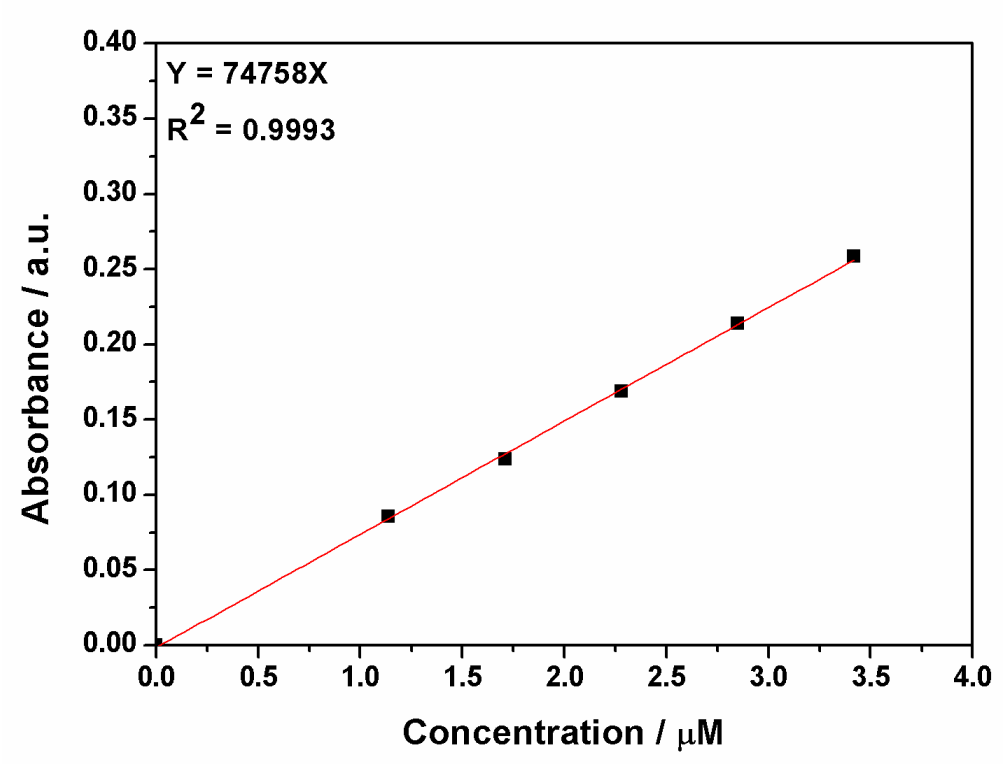

Figure B-15: Calibration curve of the 648 nm absorption for quantitative determination of compound **Cu-1** in toluene

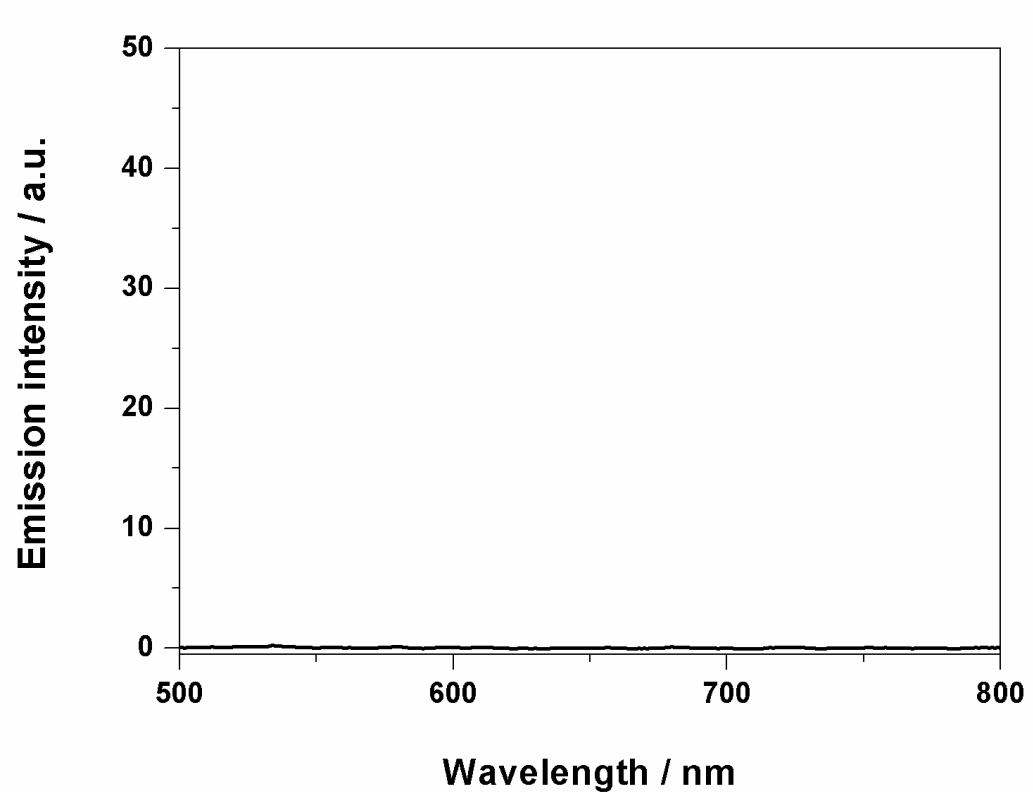

Figure B-16: Emission spectrum of compound **Cu-1** in toluene (λ_{ex} = 463 nm)

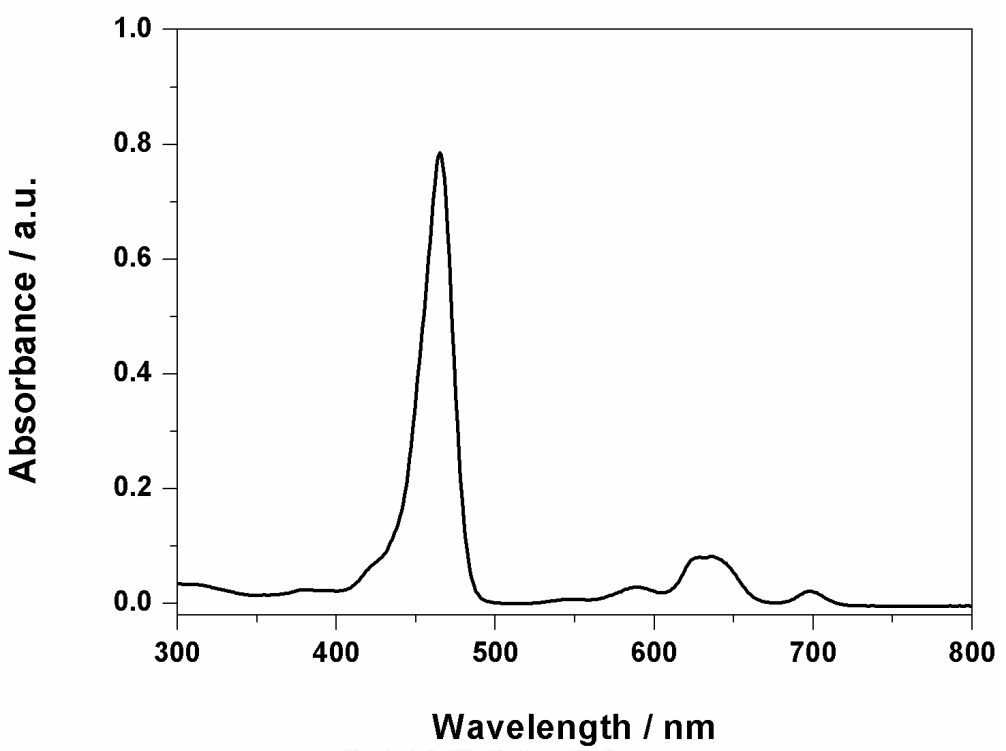

Figure B-17: Absorption spectrum of compound **1** in toluene

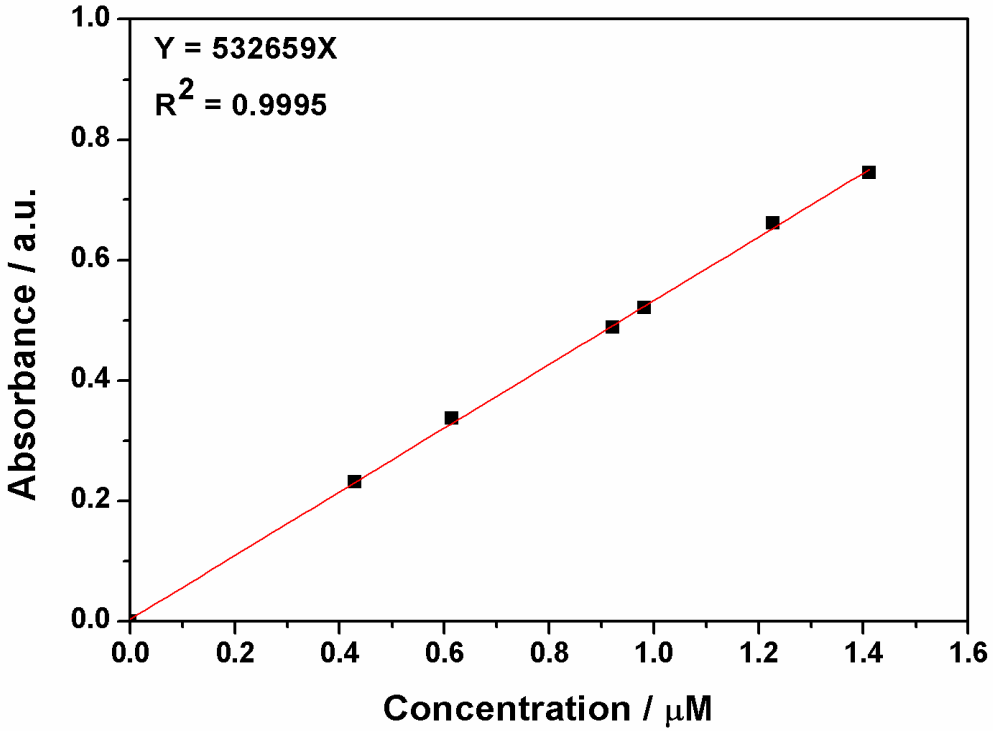

Figure B-18: Calibration curve of the 465 nm absorption for quantitative determination of compound **1** in toluene

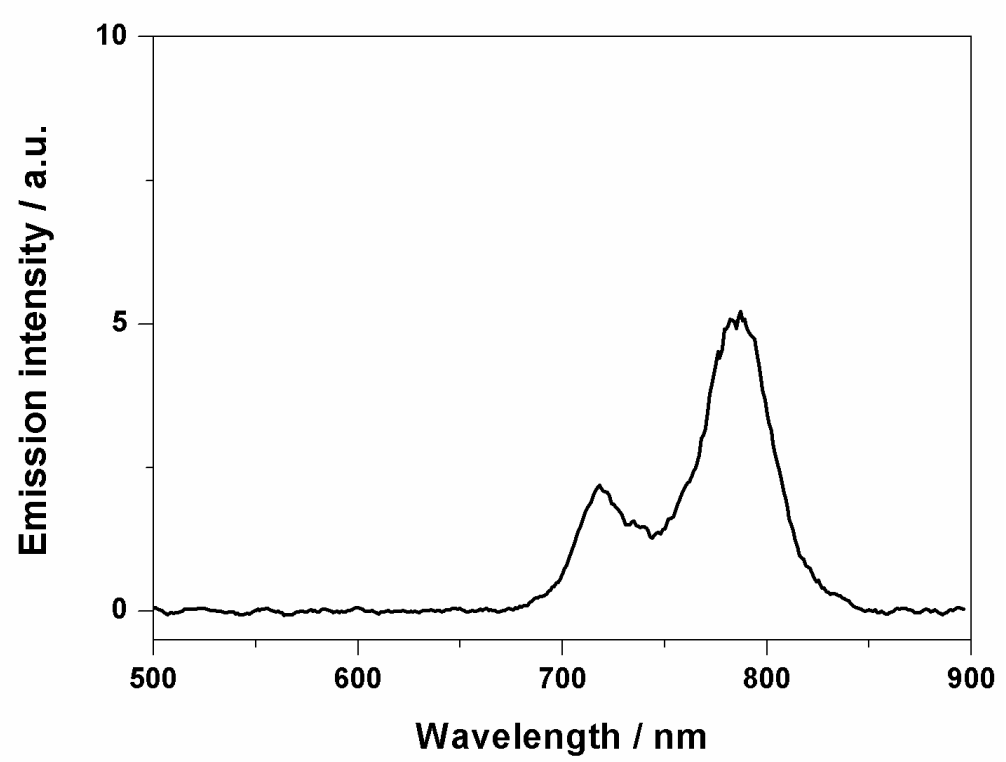

Figure B-19: Emission spectrum of compound **1** in toluene (λ_{ex} = 465 nm)

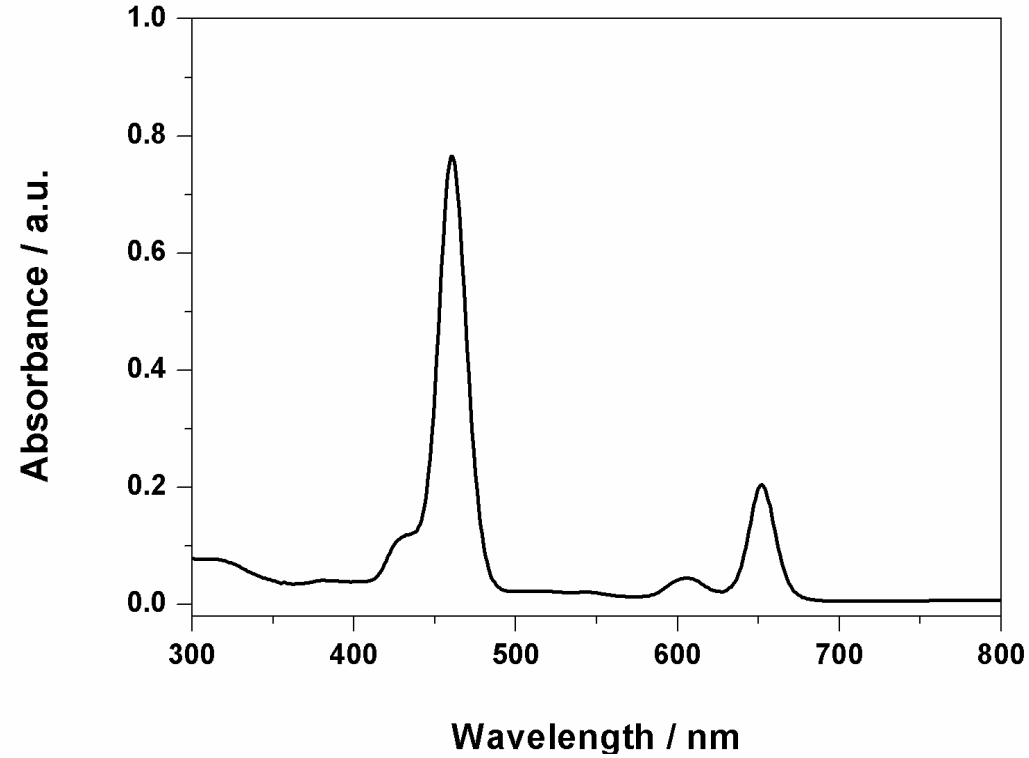

Figure B-20: Absorption spectrum of compound **Zn-1** in toluene

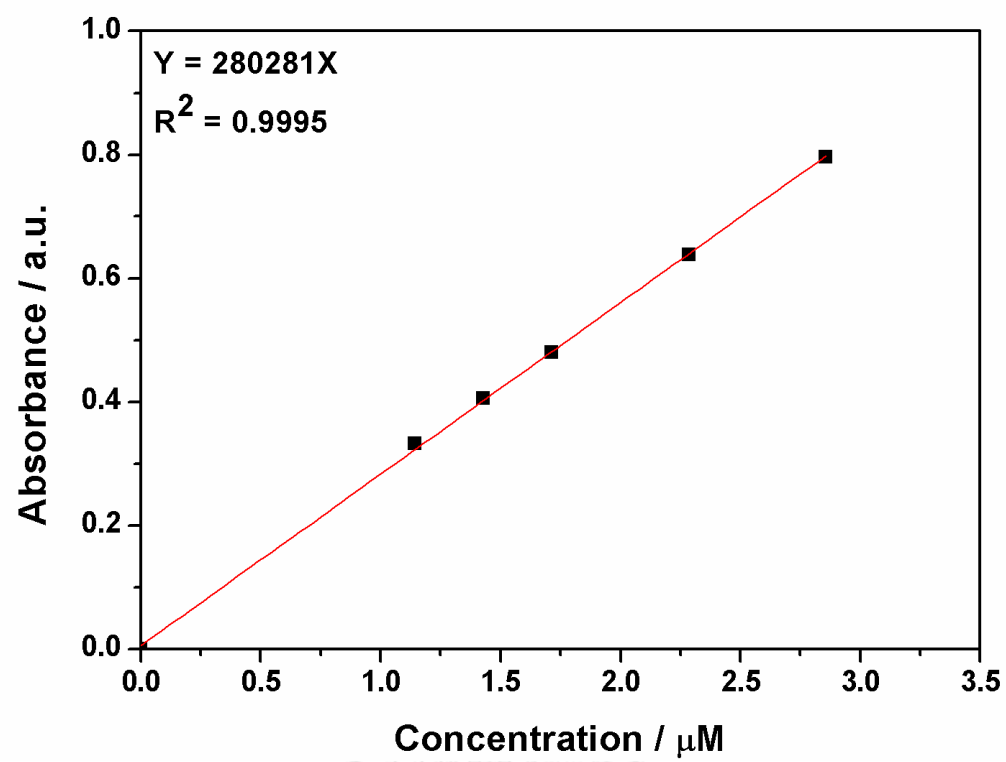

Figure B-21: Calibration curve of the 461 nm absorption or quantitative determination of compound **Zn-1** in toluene

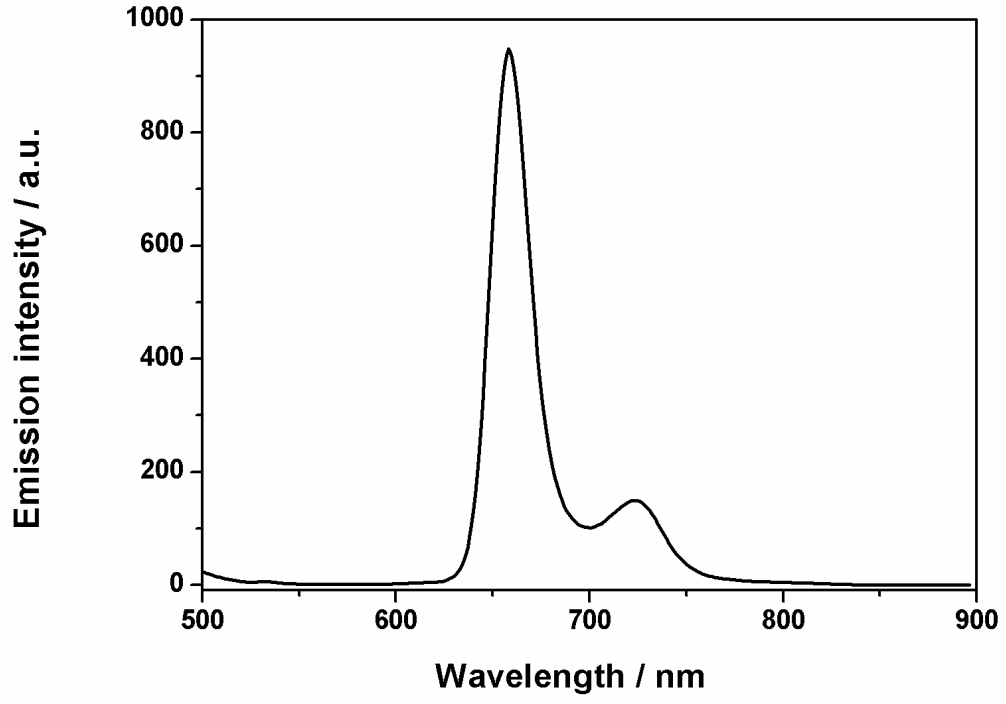

Figure B-22: Emission spectrum of compound **Zn-1** in toluene (λ_{ex} = 461 nm)

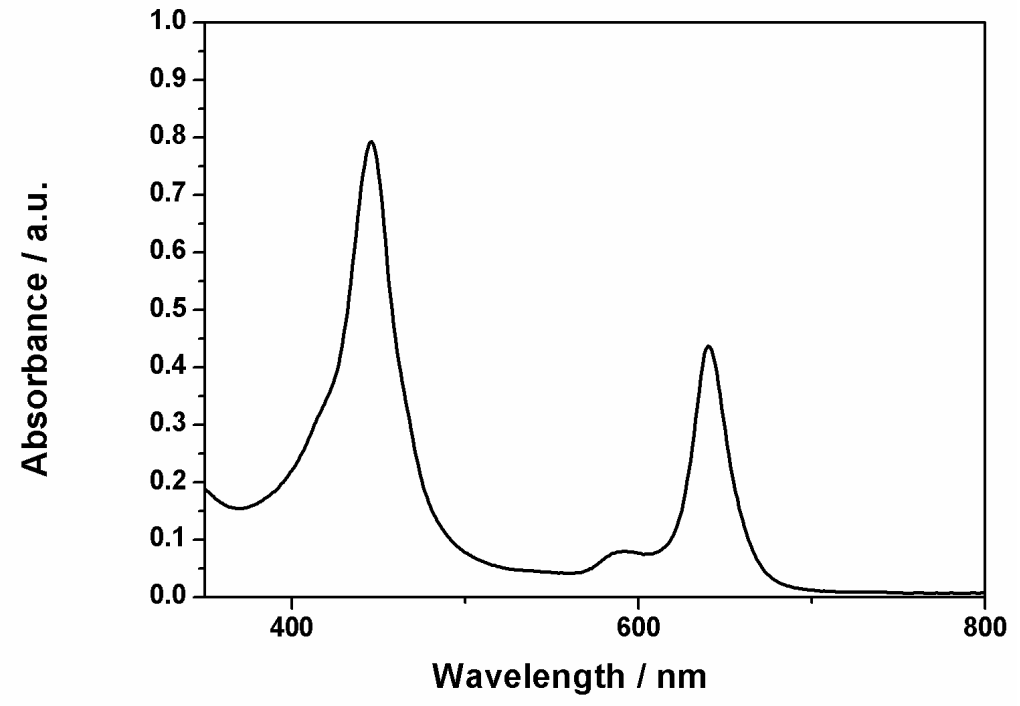

Figure B-23: Absorption spectrum of compound **Co-1** in toluene

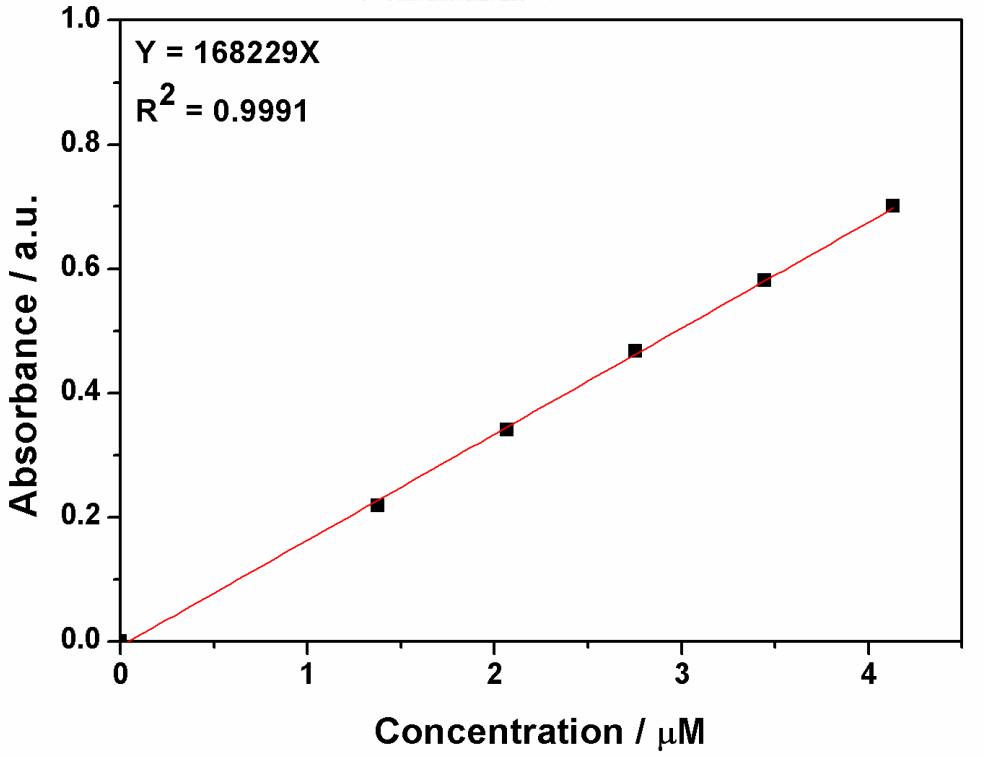

Figure B-24: Calibration curve of the 446 nm absorption for quantitative determination of compound **Co-1** in toluene

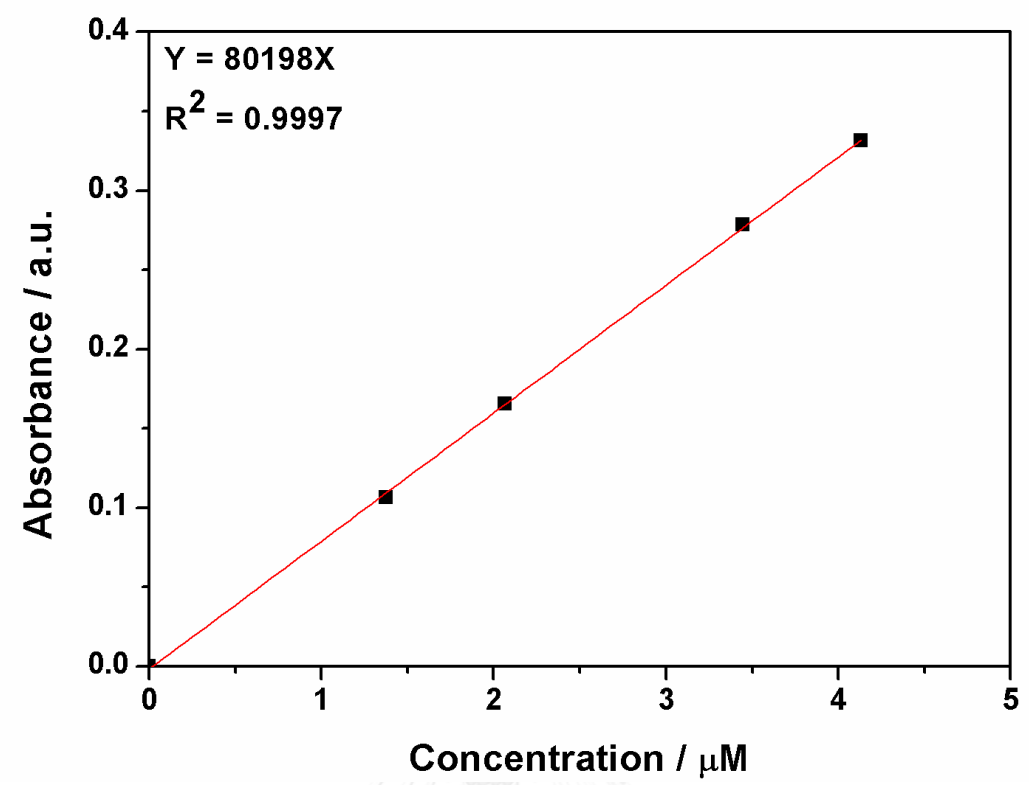

Figure B-25: Calibration curve of the 640 nm absorption for quantitative determination of compound **Co-1** in toluene

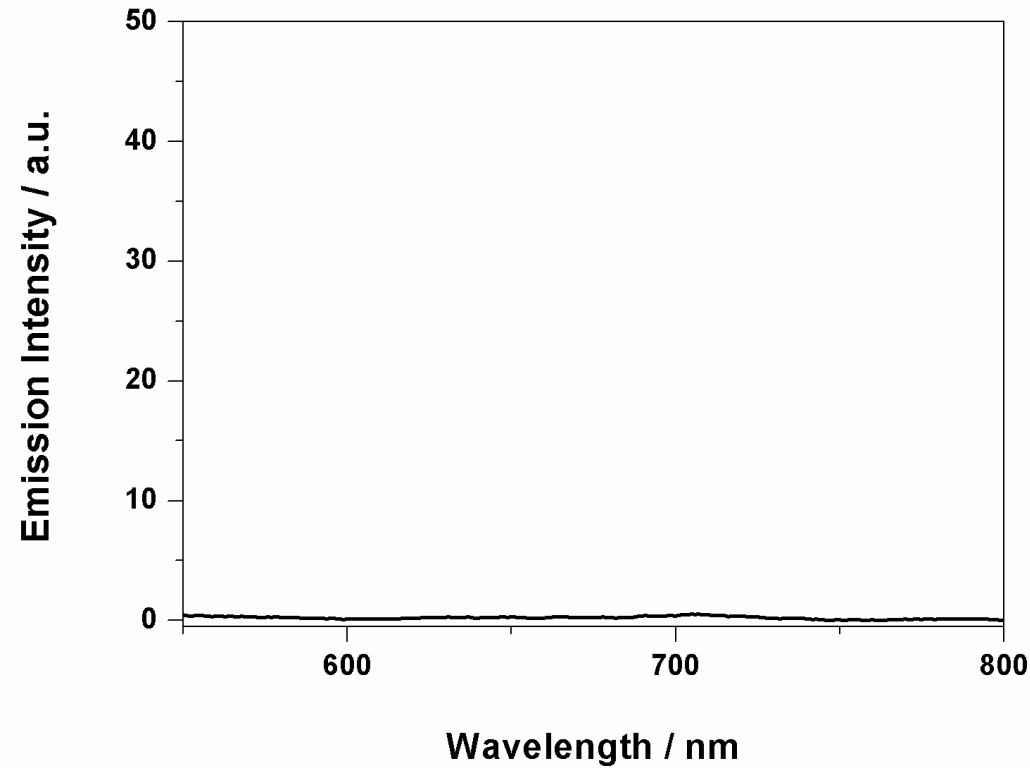

Figure B-26: Emission spectrum of compound **Co-1** in toluene (λ_{ex} = 446 nm)

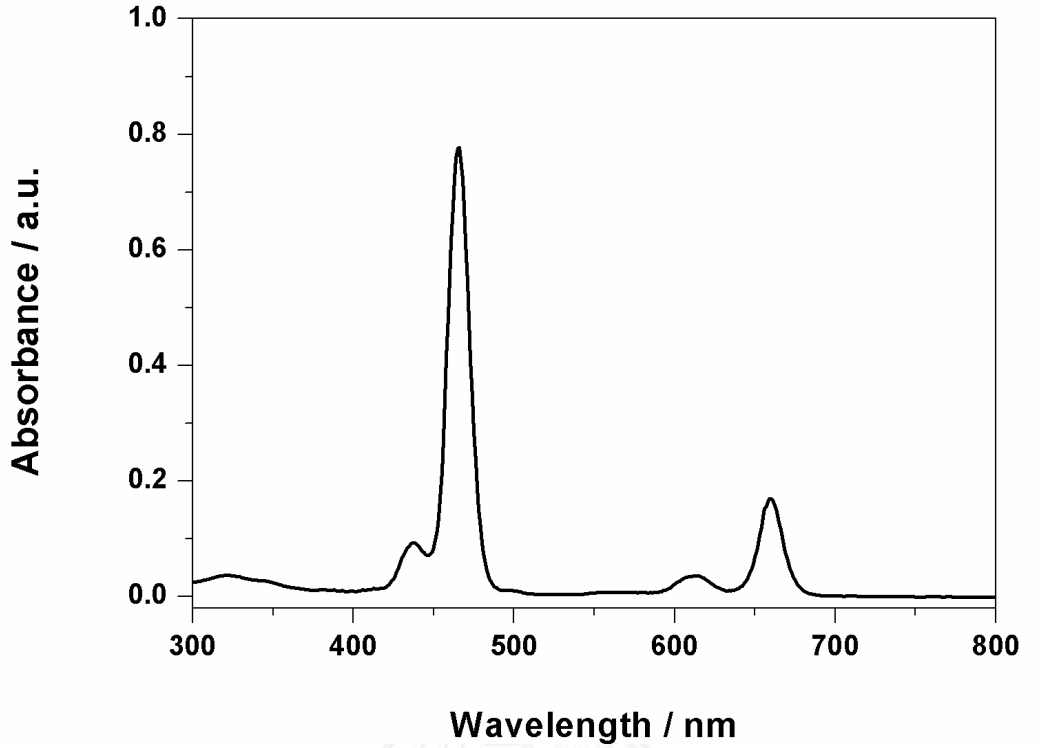

Figure B-27: Absorption spectrum of compound **$Sn(OH)_2$-1** in toluene

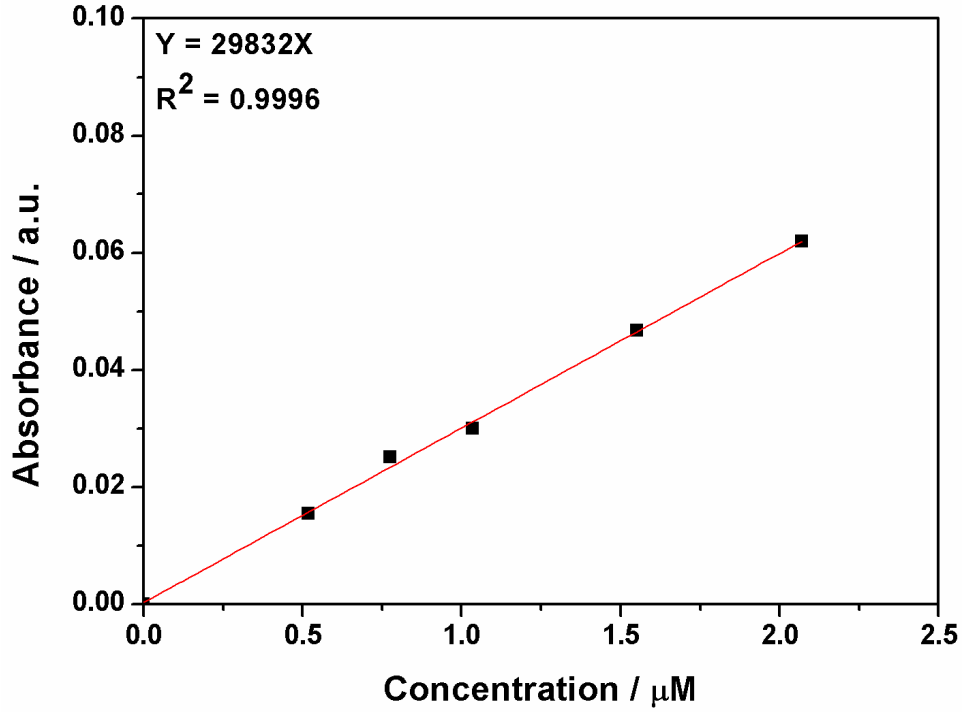

Figure B-28: Calibration curve of the 430 nm absorption for quantitative determination of compound **$Sn(OH)_2$-1** in toluene

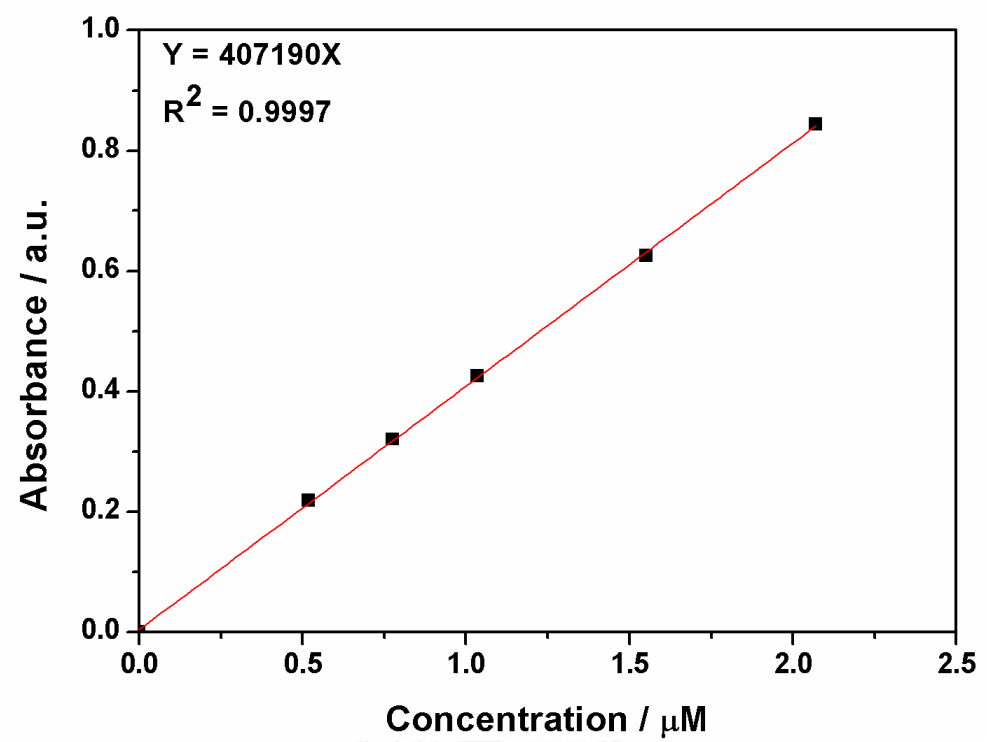

Figure B-29: Calibration curve for of the 466 nm absorption quantitative determination of compound **$Sn(OH)_2$-1** in toluene

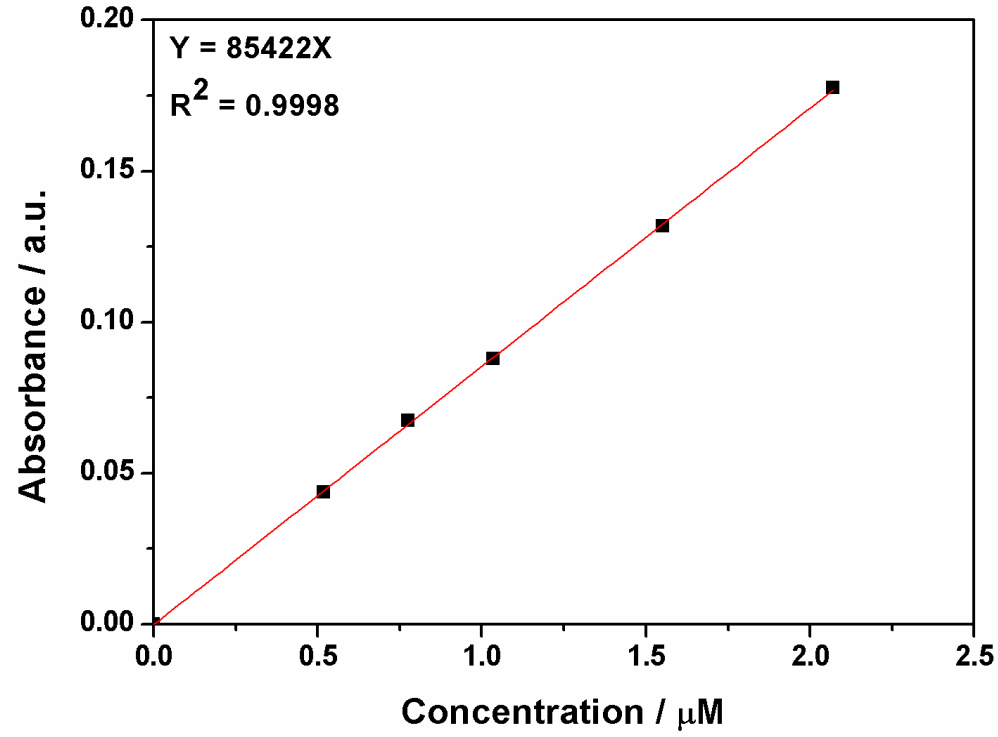

Figure B-30: Calibration curve of the 660 nm absorption for quantitative determination of compound **$Sn(OH)_2$-1** in toluene

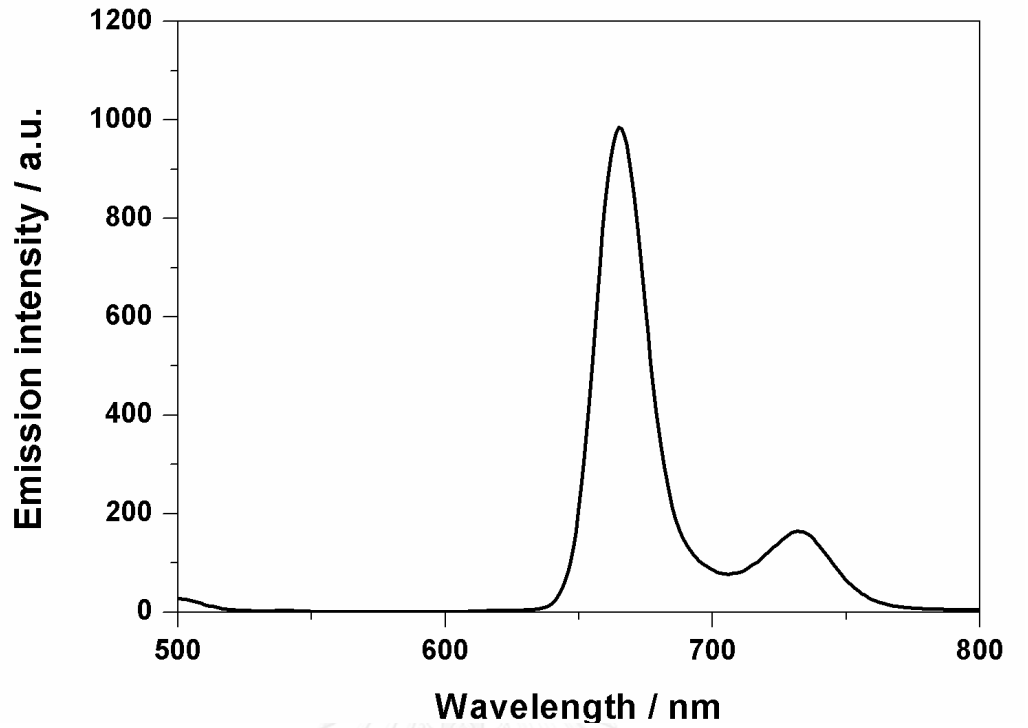

Figure B-31: Emission spectrum of compound **$Sn(OH)_2$-1** in toluene (λ_{ex} = 466 nm)

VITA

Miss Pichayada Jintanalert was born on June 10, 1988 in London, United Kingdom. She got a Bachelor's Degree of Applied Chemistry in Faculty of Science at Chulalongkorn University, Bangkok in 2009. After that, she was admitted into a Master Degree program in Chemistry, Faculty of Science, Chulalongkorn University, Bangkok in 2010. She had presented her research on "Development of Porphyrinic Compounds for Electrocatalytic Reduction of Carbon dioxide" The 29th National Graduate Research Conference, Mae Fah Luang University, 24-25 October 2013.